UNIVERSIDADE D
COIMBRA

Yaroslav Hryhoryev

Synthesis and Characterization of Palladium Porphyrins for the Construction of a TTA-UC System in a Solid Matrix

VOLUME 1

Dissertação no âmbito do Mestrado em Química Industrial- variante Desenvolvimento e Estratégia orientada pela Doutora Sara Martinho Almeida Pinto e pelo Doutor João Manuel Pina e apresentada ao Departamento de Química da Universidade de Coimbra.

September of 2023

“Like plants, so men also grow, some in the light, others in the shadows. There are many who need the shadows and not the light.”

C.G. Jung

Dedicated to my Family.

Acknowledgements

This thesis describes the culmination of two fruitful years of work that led to a path full of ups and downs that provided me with new experiences and knowledge. This path was not traversed alone, and the people that supported me during this journey and allowed me to grow were the ones that left the biggest mark, both in my work and in me as a person. They are my teachers, my mentors, and my friends.

I would like to start by expressing my most sincere gratitude to my supervisors Dra. Sara Martinho Almeida Pinto and Professor João Manuel Pina who, throughout this work, have not only supported my learning process but also allowed me to discover, for my own the experiences and hardships that chemistry has to offer, while at the same time allowing me to work on a topic that profoundly resonates with my visions. They gave me guidance whenever it was needed and where always the first to congratulate me when the research yielded successful results, through their way of working I learned the most, they are my mentors.

I would also like to express my deepest appreciations to Full Professor Mariette Pereira, for all the insight and scientific knowledge transmitted without which this work would not be possible. I would also like to show my appreciation by allowing me to partake in the Catalysis and Fine Chemistry group, one of the most challenging groups filled with wonderful people full of drive and competitiveness for the development of chemistry. Her teachings are an inspiration to all.

I want to express my gratitude to Prof. Mário Calvete for always providing me with outside-the-box ideas leading to innovative solutions in the laboratory work.

To all my colleagues and friends from the Catalysis and Fine Chemistry group I thank you with a full heart for all the assistance and knowledge that you provided me with. Also, for the great experiences and companionship in and out of the laboratory during these years.

I would like to express my appreciation to Pedro F. Cruz from the RMNlab for providing me with an NMR analysis of my samples.

I would like to thank and appreciate my groupmates from Macromolecules, Colloids, and Photochemistry group. With particular thanks to Full Professor Sérgio Melo for letting me use the cutting-edge spectroscopic apparatus in his laboratories. I also like to express my gratitude to Centro de Química de Coimbra for the FCT (I.P./MCTES) financed grant "Verão com Ciência 2022."

I would like to thank all my friends Zé Pedro, Rodrigo Antunes, Henrique Miguel, Pedro Silva, Hugo Bruno, Hugo Serrano for always being there in good and bad times, for the support, for your friendship and to our adventures. A special thanks to my friend Guilherme Serrão for the great years we spent in our academic life, to all our adventures, to the great talks and discussions about our progress, challenges, and aspirations, and for your friendship.

Finally, I would like to thank my family that always believed in me, in my goal and in my success. The support you showed me can´t be expressed by words the fait you had in me was my rock in the rough times and words you would say to me uplifted my spirits. A special thanks to my parents that taught me to chase happiness.

TABLE OF CONTENTS

I. Abbreviations

2-MeTHF	2-methyltetrahydrofuran
A	Annihilator (Acceptor) molecule
A_0	Ground State Annihilator (Acceptor) molecule
A_1^*	First Excited Singlet State Annihilator (Acceptor) molecule
A_3^*	First Excited Triplet State Annihilator (Acceptor) molecule
A_3^{**}	Higher Excited Triplet State Annihilator (Acceptor) molecule
A_5^*	First Excited Quintet State Annihilator (Acceptor) molecule
A^*A^*	Encounter complex (Two Acceptors in the Excited State)
Abs	Absorption
ACQ	Aggregation Caused Quenching
AIEgen	Aggregation Induced Emission Luminongen
BPEN	5,12-Bis(2-phenylethynyl)naphthacene
^{13}C NMR	Carbon Nuclear Magnetic Resonance
CI	Coulombic Interaction
d	Duplet (NMR signal)
D_0	Ground State Donor (Sensitizer) molecule
D_1^*	First Excited Singlet State Donor molecule
D_3^*	First Excited Triplet State Donor molecule
D_A	Acceptor transition Dipole
D_D	Donor's transition Dipole
DCM	Dichloromethane
DDQ	2,3-Dichloro-5,6-dicyano-1,4-benzoquinone
DMF	*N,N*-dimethylformamide
DPA	9,10-Diphenylanthracence
E_{T1} (E_{T2})	Energy of the First (Second) Excited Triplet State
E_{S1}	Energy of the First Excited Singlet State
ESI-TOF	Electrospray Ionization Time-of-Flight
FRET	Forster Resonance Energy Transfer
^{1}H NMR	Hydrogen (Proton) Nuclear Magnetic Resonance
HOMO	Highest Occupied Molecular Orbital

HRMS	High resolution mass spectrometer
IC	Internal Conversion
ISC	Intersystem Crossing
IUPAC	International Union of Pure and Applied Chemistry
LUMO	Lowest Unoccupied Molecular Orbital
m	Multiplet (NMR signal)
MW	Microwave
NIR	Near Infrared
OD	Optical Density
ppm	Parts per million
PdDTP-M	Palladium(II) 5,15-di(3,5-di-*tert*-butylphenyl)porphyrin
PDI	Photodynamic Inactivation
PDT	Photodynamic Therapy
$Pd(II)OAc_2$	Palladium(II) Diacetate
PdOEP	Palladium(II) Octaethylporphyrin
$PdPc(Obu)_8$	Palladium(II) Octabutoxyphthalocyanine
PdTAP	Palladium(II) Tetraanthroporphyrin
PdTPBP	Palladium(II) Tetrabenzophorphyrin
PdTPP	Palladium(II) Tetraphenylporphyrin
PtOEP	Platinum(II) Octaethylporphyrin
RET	Resonance Energy Transfer
RTTET	Reverse Triplet-Triplet Energy Transfer
s	Singlet (NMR signal)
S_0	Singlet Ground State
S_1	First Excited Singlet State
S_2	Second Excited Singlet State
t	Triplet (NMR signal)
T_1	First Electronic Triplet State
T_2	Second Electronic Triplet State
THF	Tetrahydrofuran
TIPS-AnS	(triisopropylsilyl)acetyleneanthracene 2-sulfonate
TLC	Thin Layer Chromatography

TMS	Tetrametilsilane
TPE	Tetraphenylethylene
TPP	5,10,15,20-Tetraphylphorphyrin
TTA-UC	Triplet-Triplet Annihilation Photon Upconversion
TTET	Triplet-Triplet Energy Transfer
UV-Vis	Ultraviolet-Visible Spectroscopy

II. Abstract

In the last few years, the development of solid-state systems with delayed fluorescence through triplet-triplet annihilation upconversion (TTA-UC) has become a very attractive research topic, with these types of systems emerging in different application areas such as solar energy gathering, optical sensing of oxygen, drug targeting, and bioimaging.

The development of systems that can be excited at the so-called NIR "imaging window" (650–1350 nm), where light has high tissue penetration and low auto-fluorescence, in order to achieve a better signal-to-noise ratio for bioimaging techniques, is of particular interest. The TTA-UC system are an "anti-Stokes" process and is particularly helpful in this scenario because it can upconvert excitation energy from the NIR region, resulting in an emission in a region at lower wavelengths that are easily detectable by current equipment. In the bioimaging field this photophysical process presents promising potential because the resulting emission is not hampered by the noise caused by tissue autofluorescence or by the excitation radiation. A sensitizer and an annihilator are two functional species that are required for the TTA-UC process to occur. As sensitizers, two palladium (II) porphyrins, **1Pd** and **3Pd**, exhibiting room temperature phosphorescence with long lifetimes of the triplet state, were synthesized through the nitrobenzene method, fallowing with the complexation with Pd(II)OAc_2, and their characteristics were evaluated in solution. **3Pd** was functionalized with electron-donating groups in the meso-positions to red-shift its absorption closer to the NIR region. Tetraphenylethylene (TPE), a known aggregation-induced emission luminogen (AIEgen), was chosen as the annihilator, enhancing the TTA-UC system's emissive capabilities in the solid state. Pure sensitizer and annihilator-containing cellulose acetate polymer blend films were also prepared, and their spectroscopic properties were investigated. For the investigated sensitizers:annihilator (Pd(II)porphyrin:TPE) pairs in cellulose acetate films it was successfully observed the TPE delayed fluorescence promoted by triplet-triplet annihilation upconversion. Overall, this work has contributed to the development of innovative TTA-UC organic

systems that could be employed as a solid-state optical probe for bioimaging, with absorption and emission capabilities to allow for its use in with conventional detectors.

Key-words: TTA-UC, Bioimaging, solid-state, Pd(II)Porphyrins, TPE

III. Resumo

Nos últimos anos, o desenvolvimento de sistemas no estado sólido com fluorescência retardada através da conversão ascendente de fotões por aniquilação tripleto-tripleto (TTA-UC) tornou-se um tópico de pesquisa de elevado interesse. Estes, têm sido estudados para diferentes aplicações como por exemplo em células solares, como sensores de oxigénio e para bioimagem.

O desenvolvimento de sistemas que podem ser excitados no IV (Infra-vermelho) próximo (650–1350 nm), onde a luz tem alta penetração nos tecidos, resultando em baixa auto-fluorescência, a fim de alcançar uma melhor relação sinal-ruído para técnicas de bioimagem é de particular interesse. O sistema TTA-UC é um processo "anti-Stokes" sendo particularmente útil neste cenário devido a sua capacidade de promover conversão ascendente de fotões de baixa energia, da região IV próximo, em fotões de maior energia emitidos, a comprimentos de onda mais baixos, permitindo a sua deteção recorrendo aos equipamentos atualmente usados. A técnica de bioimagem ganha grande sensibilidade porque a emissão resultante não é obstruída pelo ruído causado pela auto-fluorescência dos tecidos ou pela radiação de excitação. Um sensibilizador e um aniquilador são duas espécies funcionais essenciais ao processo de TTA-UC. Como sensibilizadores, duas *meso*-tetrafenilporfirinas de paládio(II), **1Pd** e **3Pd**, que apresentam fosforescência à temperatura ambiente com longos tempos de vidas do primeiro estado tripleto excitado, foram sintetizadas pelo método nitrobenzeno e complexadas com Pd(II)OAc_2, e as suas características fotofísicas avaliadas em solução. A **3Pd** foi funcionalizada com grupos dadores de eletrões nas posições *meso*-fenílicas para produzir um red-shift para uma região mais próxima do NIR. O tetrafeniletileno (TPE) é um luminogênio de emissão induzido por agregação (AIEgen) e foi escolhido como o aniquilador. Filmes polímericos de acetato de celulose contendo apenas o sensibilizador ou aniquilador foram preparados e as suas propriedades espectroscópicas foram avaliadas. Para os pares sensibilizadores:aniquilador (Pd(II)porfirina:TPE) investigados em filmes de acetato de celulose foi observado com sucesso a fluorescência retardada do TPE promovida pela conversão ascendente por aniquilação tripleto-tripleto. No geral, este trabalho contribuiu para o desenvolvimento de sistemas orgânicos TTA-UC inovadores que poderiam ser

utilizados como uma sonda óptica no estado sólido para bioimagem, com capacidades de absorção e emissão que possibilitam o seu uso com detectores convencionais.

Palavras-chave: TTA-UC, Bioimagem, estado sólido, Porfírinas de Paládio, TPE

IV. Nomenclature

Tetrapyrrolic macrocycles can now be categorized using either the Fischer[a)] nomenclature or the IUPAC (International Union of Pure and Applied Chemistry) nomenclature. The tetrapyrrolic conjugated macrocycle was named porphyrin by Fischer[a)], who also gave the peripheral locations the name of β-positions and the tetrapyrrolic methylene bridges as the *meso*-positions. The pyrrolic positions, according to this source, are numbered from 1 to 8, while the *meso*-positions are denoted by Greek letters and the pyrrole rings are known as A, B, C, and D (seen in red). On the other hand, all carbons are numbered from 1 to 20 in accordance with the IUPAC's requirements for tetrapyrrolic macrocycles, and the nitrogen of the pyrrole groups are numbered from 21 to 24.[b-d)] Scheme A shows both methods of representation of the porphyrin's nomenclature.

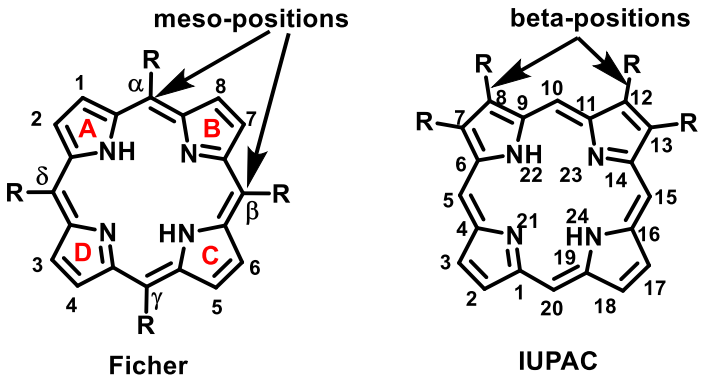

Scheme A – Nomenclature for the Ficher (left) and the IUPAC (right) nomenclature.

---

a) Fischer, H.; Orth, H. *Die Chemie des Pyrrols*; Akademische Verlagsgesellschaft: Leipzig, **1934**.

b) Moss, G. P. Nomenclature of Tetrapyrroles (Recommendations 1986). *Pure Appl. Chem.* **1987**, *59* (6), 779–832.

c) Nomenclature of Organic Chemistry. *Royal Society of Chemistry*. **2013**, 552-647

d) The IUPAC Compendium of Chemical Terminology: The Gold Book, 4th ed.; Gold, V., Ed.; International Union of Pure and Applied Chemistry (IUPAC): Research Triangle Park, NC, **2019**.

1. Introduction

In recent years non-linear optical photophysical systems have shown to have high potential for application in various domains such as medicinal imagiology,[1–6] solar energy gathering[7], drug-targeting,[8,9] oxygen sensing[4,10]. One of the non-linear optical photophysical systems that gained considerable attention for this purpose is photon up-conversion through sensitized triplet-triplet annihilation (TTA-UC). This process was recorded for the first time in the 1960s by *Parker* and *Hatchard*[11] by studying the behavior of molecules like pyrene[12] and anthracene and its derivatives[13–16]. This work was done in solution, using purely organic compounds. Afterwards *Baluschev's*[17] research team developed the first film based TTA-UC system that used a metal-organic complex as the sensitizer or acceptor (they used different metal bearing octaethylporphyrins) and an organic annihilator or emitter (polyfluorene), resulting in a room temperature anti-Stokes up-conversion fluorescence system displaying green to blue upconversion. Following this first article, there has been a significant increase in research conducted in this field and reports of extremely effective TTA-UC systems based on metal-organic complexes.[18,19] Comparing the upconversion emission observed in solution and in solid state systems from the literature[20–28] it becomes evident that the liquid system tend to have higher upconversion yield when compared to the solid state. In solution, the organic molecules that constitute the system can diffuse and form collisional pockets (colliding with one another in solution) leading the components to close proximity allowing the transfer of energy from one molecule to another. In this case the likelihood for two components to efficiently interact with one another is much higher since the molecules can move freely in the solvent allowing for the formation of a great number of dynamic encounters. In contrast in the solid state the molecules are trapped in place resulting in the fewer and static encounters (since molecular motion is restricted one molecule will only interact with molecules in its local vicinity), meaning that as the molecules that constitute the system are in predetermined place from the conception of the solid system leading to lower up-conversion yields. Some examples of solid-state systems were already reported and

can overcome the limitations imposed by the lack of mobility of the components system leading to efficient solid-state emissions comparable to the solution systems with the same components.[29–31] The construction of solid state systems that ensure efficient packing of the components will minimize the formation of trap states (states where the excitation leads to loss of energy through nonradiative decay) reducing the energy loss achieving higher upconversion yields.[28–30]

To construct an efficient TTA-UC system its components need to be carefully selected considering several factors such as the absorption regions of both the annihilator and the sensitizer, their energy levels, the lifetimes of the triplet excited states and the efficiency to populate the triplet state through intersystem crossing (ISC). These features can be modulated, changing the structure of the compounds to ensure the best conditions for an efficient triplet energy transfer between the components to yield an efficient upconversion emission. Nowadays the research is heavily focused on the development of efficient solid state TTA-UC systems for application on different domains.[7,8,30,32,33] The solid-state systems of less complexity are highly sought after given their practical nature, their higher shelf life, and reduced non-radiative deactivation of the triplet state by the solvent when compared to a liquid system.[28,34]

1.1. TTA-UC system's

Triplet-triplet annihilation photon upconversion is an energy conversion process where low energy photons are upconverted to higher energy photons through the use of a molecular energy transfer system (the overall processes are depicted in Scheme 1.1). The TTA-UC system is comprised of two molecules: the sensitizer or donor (D) and the annihilator or acceptor (A). The first step in the upconversion process is the absorption of low-energy photons by the donor molecule, which is excited to a higher electronic state before decaying swiftly to the first singlet excited state (D_1*). The second step consists in the deactivation of the excited donor to the lower lying first excited triplet state (D_3^*) by intersystem crossing (ISC). In the third step, the donor in the triplet excited state will transfer its energy through triplet-triplet energy transfer (TTET) to a ground-state acceptor

molecule (A_0). This energy transfer will result in the simultaneous excitation of the acceptor to the triplet state (A_3^*) and the decay of the donor molecule to the ground state (D_0). In the fourth step, triplet-triplet annihilation (TTA) occurs between two acceptor molecules, both of them in the triplet excited state (A_3^*), resulting in the transfer of the combined energy of the two excited states to one of the molecules (A_1^*), while the other returns to the ground state. Finally, in the fifth step radiative deactivation of the excited acceptor molecule to the ground state occurs, and the resulting emission is called upconversion emission (Scheme 1).

$$D_0 + h\nu(excitation) \xrightarrow{Excitation} D_1^* \qquad 1^{st}\text{ step}$$

$$D_1^* \xrightarrow{ISC} D_3^* \qquad 2^{nd}\text{ step}$$

$$D_3^* + A_0 \xrightarrow{TTET} D_0 + A_3^* \qquad 3^{rd}\text{ step}$$

$$A_3^* + A_3^* \xrightarrow{TTA} A_1^* + A_0 \qquad 4^{th}\text{ step}$$

$$A_1^* \rightarrow A_0 + h\nu(\text{upconversion}) \qquad 5^{th}\text{ step}$$

Scheme 1.1 – Required reaction steps to obtain an upconversion emission.

The second, third and fourth steps in Scheme 1.1 are essential to attain upconversion since the TTET, TTA, and ISC will be the processes that will be critical to the TTA-UC system's rate and efficiency. Focusing more on the application in bio-imaging[1–6,35,36] and drug-targeting[8,9] where the development of these emitters systems has a big appeal since these materials can be excited in the so-called NIR "imaging window" (650-1350nm), where the tissue absorbance and autofluorescence are minimal and light emission is possible to observe in regions that are easily detected by existing equipment.[37–41] One of the features that is crucial to improve in bioimaging methods is the signal-to-noise ratio, which is typically impeded by tissue autofluorescence. TTA-UC system, as an anti-Stokes process, overcomes this limitation, resulting in biomedical imaging with outstanding sensitivity[42]. Since anti-Stokes shifts are uncommon, light at the wavelengths under investigation is expected to originate, solely, from TTA-based process. Furthermore, the longer wavelengths used for the excitation increases the tissue penetration. TTA-UC is desirable for practical applications because, in contrast to other

upconversion methods that frequently involve the use of lasers, it can upconvert light from low-power, incoherent excitation sources.[38]

Despite the various benefits of such systems and their advantages in the application of bioimaging, there are still pitfalls that need to be addressed. One of the main pitfalls in the use of such systems in biological media is the quenching produced by oxygen.[33,43,44] There are various ways to protect the TTA-UC or limit its exposure to oxygen to enhance the system's emissive capabilities. One of the main ways of dealing with the oxygen influence on the system is by sealing or encapsulating the system components in a solid matrix (e.g.: polymer[28], organogel matrix[18,30,45] or nano-capsules[1,3,5,35]) that can limit the oxygen diffusion or quench totally.

Qian Liu et al[3] developed a green to blue upconversion system based on PEG stabilized-silica nanoparticles that were loaded with octaethylporphyrin palladium complex (as sensitizer) and 9,10-diphenylanthracene (as the acceptor). These nanoparticles worked as imaging probes for in vivo and in vitro bioimaging. The nanoparticles had an upconversion efficiency of 4.5% in aqueous solution, with a high signal-to-noise ratio given that the system didn´t exhibit any background fluorescence upon excitation with a low-power density excitation. This work is an example of a TTA-UC system that successfully devised a bioimaging probe that can operate at low power excitation with great sensitivity.

In Table 1.1 more examples of several TTA-UC systems used in solution and in the solid-state with different immobilization matrixes are presented. Although oxygen quenching can be reduced when the TTA-UC components are immobilized in a solid matrix like silica nanoparticles, polymer films, liposomes or gels, the system's efficiency can still be constrained resulting in small upconversion emissions. The efficiency across the multiple solid matrixes formed is expected to be different since the system's components are physically entrapped inside of the nanoparticles during their making. This means that each nanoparticle will have a varied organization and concentration of components within, making the TTA-UC more or less efficient than in solution.

From table 1.1 it becomes evident that in solid state the upconversion emission are smaller than in solution or in the liquid state given the effect that the

Table 1.1 – Summary of TTA-UC sensitizer and annihilator pairs used in solution and in different matrix in the solid-state.(a) in the presence of oxygen; (b) in the liquid state or in solution; (c) could not be quantified; (PdOEP) Pd(II)Octaethylporphyrin; (PdPc$(OBu)_8$) Pd(II)octabutoxyphthalocyanine; (PdTPBP) Pd(II)Tetrabenzophorphyrin; (Pt(OEP)) Pt(II)Octaethylporphyrin; (PdDTP-M) Pd(II) 5,15-di(3,5-di-*tert*-butylphenyl)porphyrin; (PdTAP-Familly)-mixture of diverse π-extended porphyrins; (TIPS-AnS) TIPS-anthracene 2-sulfonate.

Sensitizer	**Annihilator**	**Matrix**	**Φ_{UC} (%)**	**reference**
PdOEP	Perylene	Polymer nanocaps	-[c]	2
PdPc$(OBu)_8$	BPEN	nanoparticles	0 to 2.13[a]	4
PdTPBP	2,5,8,11-tetra (tertbutyl)perylene	Polymer based liposome	0.2[a] (0.54 at 37°C)	42
PdTPBP	Super Yellow	Polymer film	6	46
PtOEP	Anthracene	Polymer	0.35[a]	47
PtOEP	DPA	Gel	3.5[a]	45
PtOEP	DPA-derivative	Self-assembly	30[a,b]	32
PdDTP-M	DPA	solution	6.2[b]	48
PdTAP-Familly	Rubreno	solution	2.2[b]	49
PdTPBP	TIPS-AnS	Gelatin biofilms	8.5[a]	21

molecular motion has in the formation of effective encounters between the molecules.

Indeed, chromophores that are usually used in solution TTA-UC systems, in the solid state may produce aggregates where quenching of its fluorescence is likely to occur. Phenomenon associated with trap state formation such as sensitizer self-quenching resulting from pure sensitizer aggregates can limit the energy transfer to the accepter hindering the upconversion emission of the system. So, it is of high

interest to develop emissive systems that don´t suffer from these restrictive phenomena. We envision the development of a D/A pair immobilized in solid state matrix that could perform the desired outcome of an upconverted emission unbothered by aggregation caused quenching (ACQ) and with reduced trap state formation.

1.2. Porphyrins as sensitizers

In the last two decades there has been a growing interest in the development of TTA-UC system's employing sensitizers that would emit at room temperature with adequate long lifetimes of the first excited triplet state T_1.

Molecules complexed with heavy atoms have enhanced ISC efficiency given the influence that the heavy atom has on the spin-orbit coupling transitions that are in the basis of population of triplet states. So, it is not uncommon to find systems that apply the heavy atom effect in the development of efficient phosphorescent systems using a metal to form metalorganic chelates with the chromophore[24,50,51] or using solvents that are rich in heavy atoms like halogens.[52,53]

Porphyrins are tetrapyrrolic macrocycles that have been extensively studied as sensitizers/photosensitizes for several applications, namely PDT, PDI, catalysis and bioimaging.[54–58] Obtained from the condensation/cyclization of four aldehydes with four pyrrole units.[59,60] These tetrapyrrolic macrocycles have various characteristics such as a specific absorption profile with Soret and Q-bands and great emissive capabilities originating from its large conjugated π-system in addition, porphyrins also have high molar absorptivity coefficients, between 400 and 420nm. Porphyrins are very versatile molecules that can be structurally modulated to improve features such as solubility, region of absorption/emission, molar absorption coefficients as well as lifetimes, and energy of its excited states.

Despite their many benefits porphyrins have certain drawbacks when it comes to aggregation. Their large conjugated π-system tends to form aggregates at higher concentration promoting the formation of excited state trap states leading to an increase in nonradiative decay.[23] This effect can be minimized by enhancing the solubility of the sensitizer that would limit the formation of these trap states. The

introduction of alkyl chains in the macrocycle enhances the solubility of the porphyrin in nonpolar solvents. Also, from such a modification the interaction between the porphyrins and the hydrophobic annihilators molecules in TTA-UC systems could be enhanced.[32]

By modifying the porphyrins structure its spectral features can be tuned to produce good sensitizer candidates for TTA-UC systems. A good sensitizer candidate requires an efficient ISC to effectively populate the low energy T_1 state that is in the base of the energy transfer process (TTET) between the various sensitizer/annihilator pair. The T_1 state is required to be long lasting to ensure that it has enough time to interact with the donor molecules enhancing the probability of energy transfer between the pair. The energy gap between the sensitizer/annihilator pair also affects the upconversion emission and needs to be adequate. If the energy gap is too large the energy loss between sensitizer/annihilator pair will be also large reducing the upconversion yield (since other deactivation routes such as through IC could promote the deactivation of the sensitizer excited state). If the energy gap is too short despite the small energetic losses the reverse triplet-triplet energy transfer (RTTET) may occur, resulting in an overall decrease in the upconversion emission. The bandgap of the sensitizer and annihilator are also important to ensure that the emission of the annihilator isn´t reabsorbed by the sensitizer.

For the TTA-UC system to be better suited for biological imaging modification to the porphyrins can be made ensuring that the porphyrin gets closer to the so-called NIR "imaging window". From the literature[22,61,62] different modification can be made to achieve a red-shift in the porphyrins on such example is the extension the conjugated π-system. Palladium (II) meso-tetraaryl-tetraanthro[2,3]porphyrin is an example of one such conjugated system, although frequently this entails a drawn-out and difficult synthetic process.[49] As a consequence, the first excited singlet and the first excited triplet states lower their energy.

Additionally, the introduction of electron donating groups in the porphyrin ring can also slightly red-shift its spectra. This shift, although much smaller than the one produced by extending the pi-conjugation, doesn't drastically impact the T_1 energy and lifetime maintaining the valuable characteristics of the porphyrin. *Pınar*

Sen et al[63] developed a palladium porphyrins derivative bearing *para*-alkoxy groups in the phenyl substituents.

In porphyrins another way to produce a "red-shift" in its absorption is to employ aggregates. It is noted that porphyrins may undergo a specific type of aggregation when in high polarity solvents these aggregates are known as J-aggregates and are characterized by having a red-shifted spectral profile compared to the monomeric form of the porphyrin. Such aggregates may prove to be trap states, as referred earlier, but if the annihilator and sensitizer are found locally an upconversion emission in the aggregate can occur.[64]

Li Li et al[25] developed one such TTA-UC system that exhibited solid state upconversion emission from AIE nanocrystals dopped with porphyrin. The structurally well-organized nanocrystals of 9,10-distyrylanthracene exhibited emission when palladium benzoporphyrin was introduced into the crystalline structure leading to the conclusion that even in the solid state given a well-organized structure the production of trap states can be minimized.

Free-base porphyrins without heavy atoms have a reduced capability of promoting the availability of the T_1 state, since the ISC process is a spin-forbidden process. When the porphyrins are complexed with a heavy metal, such as palladium, platinum or zinc through chelation, it's ISC rate is enhanced with the first two metals being able to exhibit the best ISC efficiency.[65] From the literature is also evident that Pd(II)/Pt(II) porphyrin complexes exhibit room-temperature phosphorescence and long lifetimes of triplet state.[66,67] Long lived triplet lifetimes ensure a higher time window for the TTET process to occur while room temperature phosphorescence ensures that the nonradiative decay from the triplet state is a sufficiently slow process to minimize the energy loss and depopulation of the T_1 state. With these characteristics palladium porphyrins are envisioned to minimize the energy loss from the competitive processes of nonradiative deactivation ensuring a higher probability for the energy to be transferred to the acceptor molecule.

1.3. Annihilators

For the production of a TTA-UC system it is crucial that the annihilator has good efficiency. Following the sensitizer's absorption of a photon, and population of its first singlet excited state, a subsequent decay occurs, through ISC, into the triplet state of the sensitizer. Then TTET needs to occur annihilator receives the triplet energy of the sensitizer's triplet state getting excited in the process. After this energy transfer, the annihilator must be able to fuse with another annihilator molecule by TTA, converting energy from two triplet states into a single higher-energy singlet state annihilator and a ground state annihilator. After this process the annihilator is expected to emit a higher energy photon yielding a fluorescence emission of higher energy.[22,23,27]

In order to get the good upconversion efficiency, the annihilator should adhere to the following criteria: 1) the triplet energy of the annihilator must be slightly lower than of the sensitizer, guaranteeing an effective energy transfer between the components with less probability of reverse TTET (occurs when the sensitizer and annihilator have a very small energy gap between their triplet states); 2) the first excited singlet state would be efficiently populated by the TTA process if the first excited triplet state of the annihilator has an energy larger than half that of the first singlet state; 3) the annihilator molecule must have a high fluorescence emission quantum yield; 4) the energy of two annihilator molecules in triplet state must not be higher than the energy of the first quintet state or the second triplet state, these state are considered to be parasitic states and may reduce the overall efficiency of the system.

These criteria are very important and should be considered when constructing a TTA-UC system. In general, the annihilator used in such systems are organic aromatic hydrocarbon molecules, sometimes modified to fit the systems design. TTA-UC system described in Table 1.1 shows distinct annihilators for each system.

9,10-diphenylanthracene, DPA, is the most widely used annihilator and is derived from the anthracene molecule with two phenyl substituents, it has strong absorption at 268, 357, 377, and 396 nm in solution and has an emission at 468nm

(blue emission).[68] It's a great annihilator to use in combination with Pd(II)/Pt(II) octaethylporphyrins and was extensively studied in the literature as well as its derivatives.[69–74] Other compounds that are used as annihilators such as perylene[2,75,76], pyrene[77,78], BPEA[19] and rubrene[79–81] have also seen results in the construction of TTA-UC systems.

In this work the TPE was chosen to be the annihilator for the system. The AIE capabilities of a molecule mean that it doesn't emit in solution but does in solid or aggregate states. This phenomenon occurs when certain molecular motions are restricted in the molecule, limiting its nonradiative decay pathways leading to emission. TPE has a strong absorption in the UV region (250 to 350 nm) and will emit between the 400 to 550 nm range.[82] This emission range falls in between the sensitizers absorption limiting the reabsorption. From the literature[83,84] the triplet lifetimes and the approximated triplet energies for the TPE where accessed. TPE has long triplet lifetimes rounding the 180ns range under atmospheric air and its triplet state as its peak neat 453 nm.[84] Having these characteristics it validates three conditions to be an efficient annihilator for a TTA-UC system: 1) the triplet state having smaller energy than the triplet state of the sensitizer (porphyrin) leading to an exothermic driving force that allows the transfer of energy from the sensitizer to the annihilator pair, 2) the emission of the TPE is in a region where reabsorption by the sensitizer is limited and 3) the sum of the energy of two TPE molecules in their triplet state would exceed half of the energy it's singlet excited state. These reasons as well as the solid-state emission of the TPE make it a suitable chromophore to act as an annihilator in the TTA-UC.

1.4. Energy transfer

Since TTA-UC delayed fluorescence emission depends on the efficiency of TTET and TTA (which are bimolecular energy transfer processes) these need to be understood. Bimolecular energy transfer can occur via two different pathways, radiative and nonradiative, but always with a spectral overlap between the emission (of the donor) and the absorption (of the acceptor) and always from a molecule in the excited state to a molecule in the ground state since the driving force behind this

energy transfer will be the exothermic nature of the process. The simplest way for energy to be transferred from a donor molecule to an acceptor is through radiative transfer also known as trivial transfer. This process is a radiative in nature meaning that the excited state species will decay to the ground state and in the process will emit a photon that can be absorbed by a second molecule in the ground state promoting its excitation, as follows:

$$D_1^* \rightarrow D_1 + h\nu \qquad \text{(Fluorescence)}$$

$$A_1 + h\nu \rightarrow A_1^* \quad \text{or} \quad D_1 + h\nu \rightarrow D_1^* \qquad \text{(Absorption)}$$

This energy transfer is dependent on the spectral overlap and the concentration of the species. Radiative transfer doesn´t require any interaction between the D/A pair. The concentration of D/A, in solution, is a factor that limits the radiative energy transfer in two ways. First, an increased number of chromophore molecules causes a direct increase in the quantity of photons emitted, having a bigger number of photons available increases the likelihood that one of them will be absorbed by radiative energy transfer. Second, an excessive concentration can prove harmful for the system because too many chromophores may dampen the excitation and cause an inner filter effect, which results in inhomogeneous emissions that result ultimately in the distortion or disappearance of the emission spectra on which the system is dependent. Low concentrations are required to mitigate the inner filter effect and as a result low intensity emission will produce less photon diminishing the probability of energy transfer. The spectral overlap is essential for the radiative energy transfer, since the resulting emitted photons need to be in adequate energy range to be absorbed by the accepter resulting in its excitation.

In the case of nonradiative energy transfer two molecules need to interact with one another to allow the transfer of energy. These interactions are Coulombic interaction, also known as Förster resonance energy transfer (FRET) and/or interaction resulting from orbital overlap between the two molecules, also known as the Dexter electron exchange mechanism. At long distances, 80–100 Å, the transfer of energy occurs solely through dipole-dipole coupling interactions

between the transition dipoles (D_D and D_A) associated with the transition from (D*) to (D) and (A) to (A*), as can be seen in Figure 1.1. At short range, the two forms of interaction occur: the Coulombic interaction results from short-distance multipolar interactions, while the orbital overlap allows for the transfer of energy through the Dexter mechanism of electron exchange, as seen in Figure 1.2.

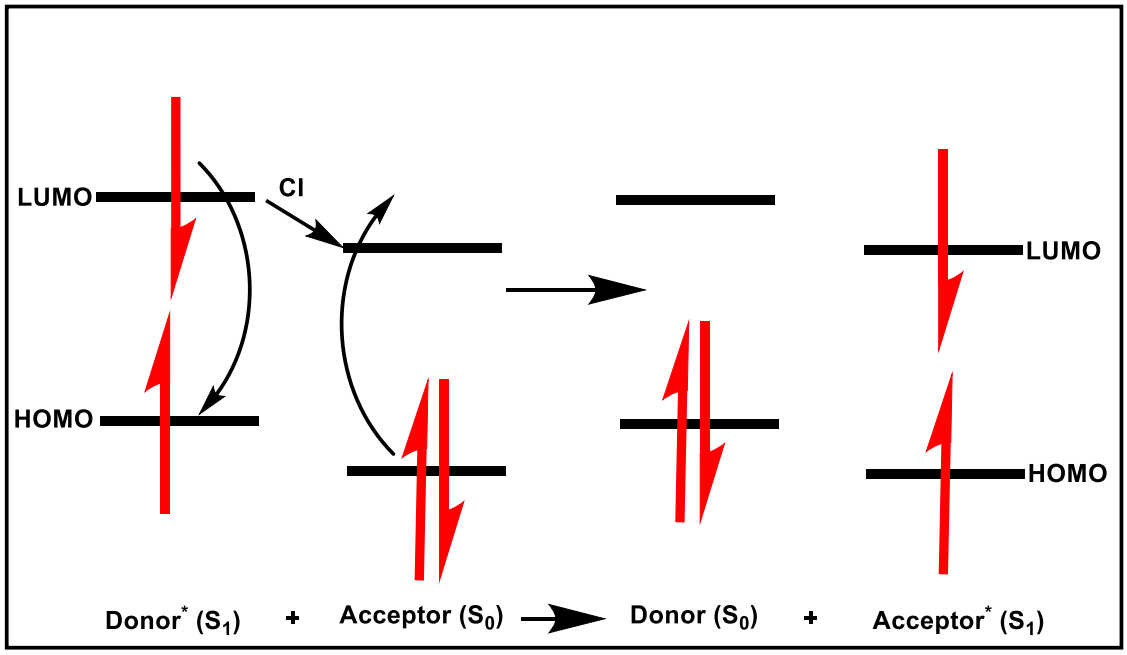

Figure 1.1 - Schematic representation of the resonance energy transfer (RET) mechanism from a donor in S_1 excited-state to the acceptor in S_0 through Coulombic Interaction (CI).

If the energy transitions between the states are allowed (e.g.: singlet-singlet energy transfer) both Coulombic interaction and Dexter mechanism contribute to the transfer of energy despite the Coulombic interactions being the predominant mechanism even at short distances. When transitions are forbidden only energy transfer due to orbital overlap is possible since these transitions have small transition dipole moments, making the prevalent mechanism the Dexter electron exchange.

The Dexter energy transfer is a process that relies on the overlap of the electronic clouds (wavefunctions) of the molecules, that occurs at short distances (<10 Å) or during collisions. In Figure 1.2 B) the TTET process is shown, where one electron in the LUMO orbital of the (D) migrates to the LUMO orbital of the (A), at the same time that another electron migrates from the HOMO orbital of (A) to the

HOMO orbital of (D). The rate of the energy transfer using the Dexter mechanism, k_{Dexter}, can be obtained from the following equation 1.1:

$$k_{Dexter} = K \times J \times e^{\frac{-2r_{AD}}{L}} \qquad \text{Equation 1.1}$$

where K is an experimental factor that relates to the magnitude of the orbital interactions that are responsible for the exchange of electrons; r_{AD} is the distance between the D/A pair and is the rate depends exponentially on it; L is the sum of the of the van der Waals radii; J corresponds to the integral of the spectral overlap between the donor's fluorescence emission spectrum with the acceptor's absorption spectrum normalized for the extinction coefficient of the acceptor molecule, ε_A:

$$J = \int_0^\infty F_D(\lambda)\varepsilon_A(\lambda)\, d\lambda \qquad \text{Equation 1.2}$$

here the $F_D(\lambda)$ corresponds to the fluorescence emission of the donor in a specific wavelength (λ) and $\varepsilon_A(\lambda)$ is the molar excitation coefficient of the acceptor molecule in the same wavelength (λ). From these equations it becomes clear that the two factors governing the rate of Dexter mechanism are the distance and the spectral overlap between the D/A pair.

The spectral overlap, J, is used to ascertain the energy similarities between the emission energy of the donor with the absorption energy of the acceptor. This makes it possible to determine the likelihood of energy transfer based on the degree of the overlap of the two spectra. Even after having a great spectral overlap the process will exponentially depend on the distance between the two species, r_{AD}, resulting in the mechanism only being efficient at short distances (5-10 Å). In liquid medium the molecules move freely and can collide with one another increasing the probability of efficient energy transfer between them. In this case the efficiency is limited by the rate of the diffusion-controlled bimolecular collisions of the D/A pair. On the other hand, in solid or rigid matrix these molecular motions are restricted resulting in an overall decrease in efficiency. This decrease in efficiency is linked to the limitations of the spatial arrangement of the molecules in the solid matrix, since the position of the molecules are fixed in space, the number of encounter complexes

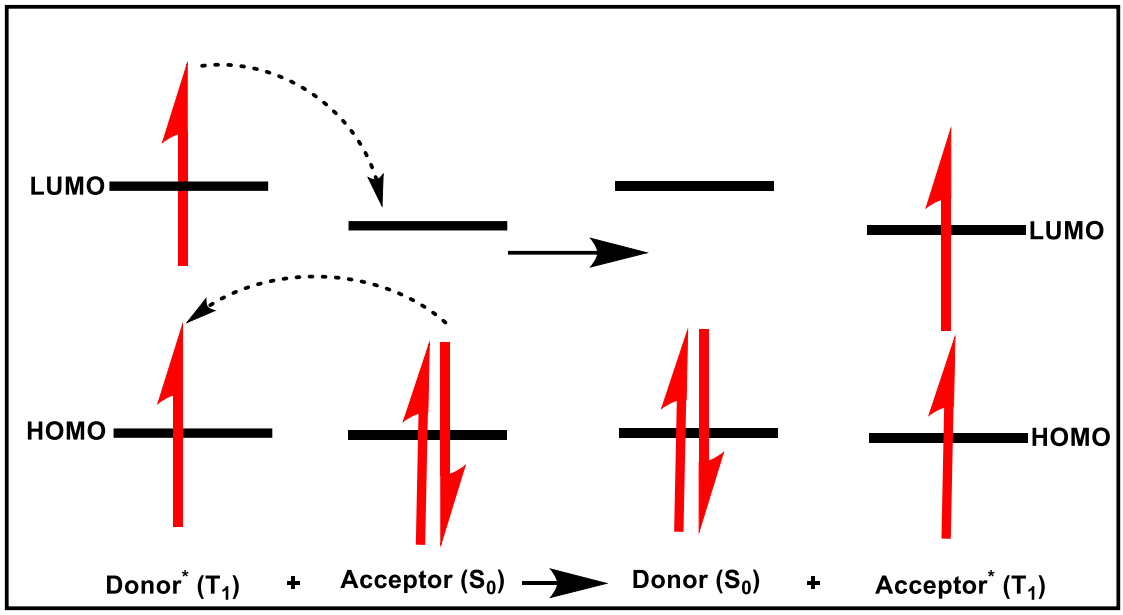

Figure 1.2 – Schematic representation of the Dexter energy transfer process.

in the solid-matrix will be kept in the same and in smaller number when compared to solution where the number of encounters is being controlled by diffusion.

Given a successful energy transfer through TTET between the D/A pair results in the population of the first triplet excited state of the acceptor. The acceptor molecules are in the triplet state which means they have a total of three forms of combining its electrons since they are unpaired, them being $T_{-}(\downarrow\downarrow)$, $T_0(\downarrow\uparrow)$, and $T_{+}(\uparrow\uparrow)$. Through TTA these acceptor molecules will interact with each other forming encounter complexes (A^*A^*), as seen in Figure 1.3. The combination of two triplet state molecules will result in a total of 3 × 3 = 9 different forms of combining the two states. Of the 9 possible combinations the encounter complex will have three possible spin configurations singlet, triplet, and quintet. Five of the combinations will produce a quintet state, three of the combinations will produce a triplet state and only one configuration will yield a singlet state. Equation 1.3 show the 3 possible spin configurations for the encounter complex and the dissociation results for the singlet and triplet state:

$$A_3^*A_3^* = \begin{bmatrix} |AA|^1 \\ |AA|^3 \\ |AA|^5 \end{bmatrix} \rightarrow \begin{matrix} A_1^* + A_0\ (1^{st}\ case) \\ A_3^* + A_0\ (2^{nd}\ case) \\ A_5^* + A_0\ (3^{rd}\ case) \end{matrix} \qquad \text{Equation 1.3}$$

After the formation of the encounter complex between two acceptors the transfer of their combined excited state energy ($2 \times E_{T1}$) to one of the molecules is possible. If the energy transfer didn't occur the complex would dissociate back to their original triplet state molecules. To efficiently transfer energy between the species that comprise the encounter complex their combined energy needs to be of equal or greater than the energy of their higher states. According to Wigner's rules for an energy transfer to be allowed there needs to be conservation of the spin value, so the spin of the encounter complex will be conserved during the dissociation. The first case shown in Equation 1.3 depicts the case where the encounter complex formed is a singlet.

The spin of the encounter complex is maintained but the spin of the two individual excited states is inverted, resulting ultimately in one of the species going to the first excited singlet state (A_1^*) and the other to the ground state. This process is possible only if the following energy relation is meet:

$$2 \times E_{T1} \geq E_{S1} \qquad \text{Equation 1.4}$$

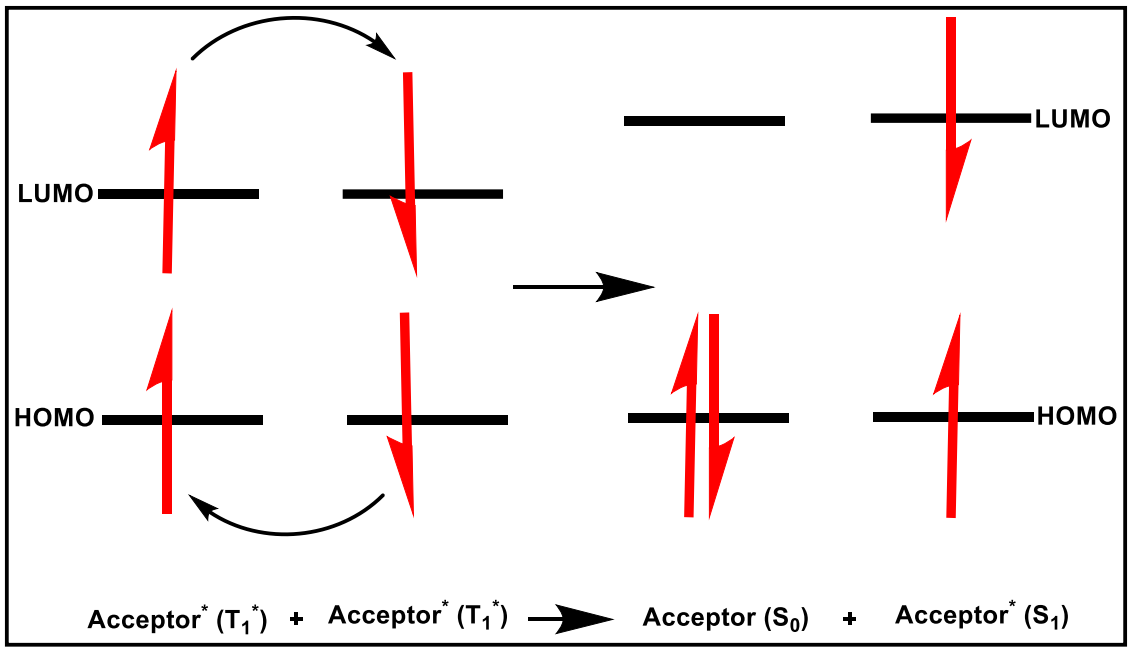

Figure 1.3 – Schematic representation of the TTA process between two acceptor molecules in their triplet excited state through the Dexter exchange mechanism.

where E_{T1} is the energy of the first excited triplet state of the acceptor, and E_{S1} is the energy of the first excited singlet state.

In the second case shown in Equation 1.3, the resulting encounter complex is in its triplet state and from its dissociation results one excited specie at a higher triplet state (A_3^{**}) while the other specie returns to its ground state (A_0).
This second process only occurs if the following energy relation is meet:

$$2 \times E_{T1} \geq E_{T2} \qquad \text{Equation 1.5}$$

where the E_{T2} is the energy of the second excited triplet state.

The third case has a lower probability of occurring since the energetic availability of the quintuplet state is generally inaccessible. The second and third cases the excited state obtained are considered parasitic states or trap states since their transition to the ground state is expected to take the nonradiative route, thus, they will reduce the overall upconversion emission during the TTA process. The best energetic condition for the first triplet excited state for the annihilator, to avoid the population these trap states is seen in the Equation 1.6.

$$E_{T2} \geq 2 \times E_{T1} \geq E_{S1} \qquad \text{Equation 1.6}$$

This would be the ideal energy conditions for the annihilator molecule. Ensuring that no energy would be lost during the annihilation process by population of trap state.

1.5. Objective

In this work we describe the construction of a solid state TTA-UC system comprised of a cellulose acetate based polymeric blend with immobilized sensitizer and annihilator molecules. For the TTA-UC system, palladium(II) porphyrins **1Pd** Palladium (II) 5,10,15,20-tetraphenylporphyrinato and **3Pd** Palladium (II) 5-(4-hidroxyphenyl)-10,15,20-(4-((2-ethylhexyl)oxy)phenyl)porphyrinato were synthesized to act as the systems sensitizers and as the annihilator

tetraphenylethylene (TPE) was chosen for its AIE (aggregation induced emission) capabilities. TPE with its increased emission in the solid state and its adequate spectral characteristics allowed it to be used as an annihilator for this TTA-UC systems. The system was trapped in a matrix of cellulose acetate this encapsulation in the solid-state lead to the formation of polymeric films with great clarity allowing for the spectroscopic characteristics of the system to be studied.

The primary goal of this work was to develop a TTA-UC system that had good emissive capabilities in the solid-state with efficient upconversion of excitation radiation close to the NIR, that could potentially be applied in bioimaging or in the development of optical sensor. Combining sensitizers that tend to form aggregates in the solid state such as porphyrins with annihilators that have strong emission in the solid/aggregated state for the formation of a TTA-UC system were the formation of aggregates was as beneficial factor rather than a negative one. Since the majority of solid-state TTA-UC systems are plagued by the formation of trap states, some made of pure sensitizer others of pure annihilator regions were upconversion is limited. This system was envisioned to overcome the drawbacks of conventional organic dyes, that suffer from fluorescence quenching in the solid state as a result of ACQ, while at the same time achieving with the porphyrin's formation of red-shifted aggregates, we believe that it is possible for the system to access shorter wavelengths and be capable of upconverting light closer to the "near-IR" while at the same time promoting an anti-Stokes shift emission by upconversion to lower wavelengths, limiting tissue auto-fluorescence, and consequently enhancing the signal-to-noise ratio of the bioimaging technique. The scheme 1.4 illustrates a schematic representation of the TTA-UC material developed in this work.

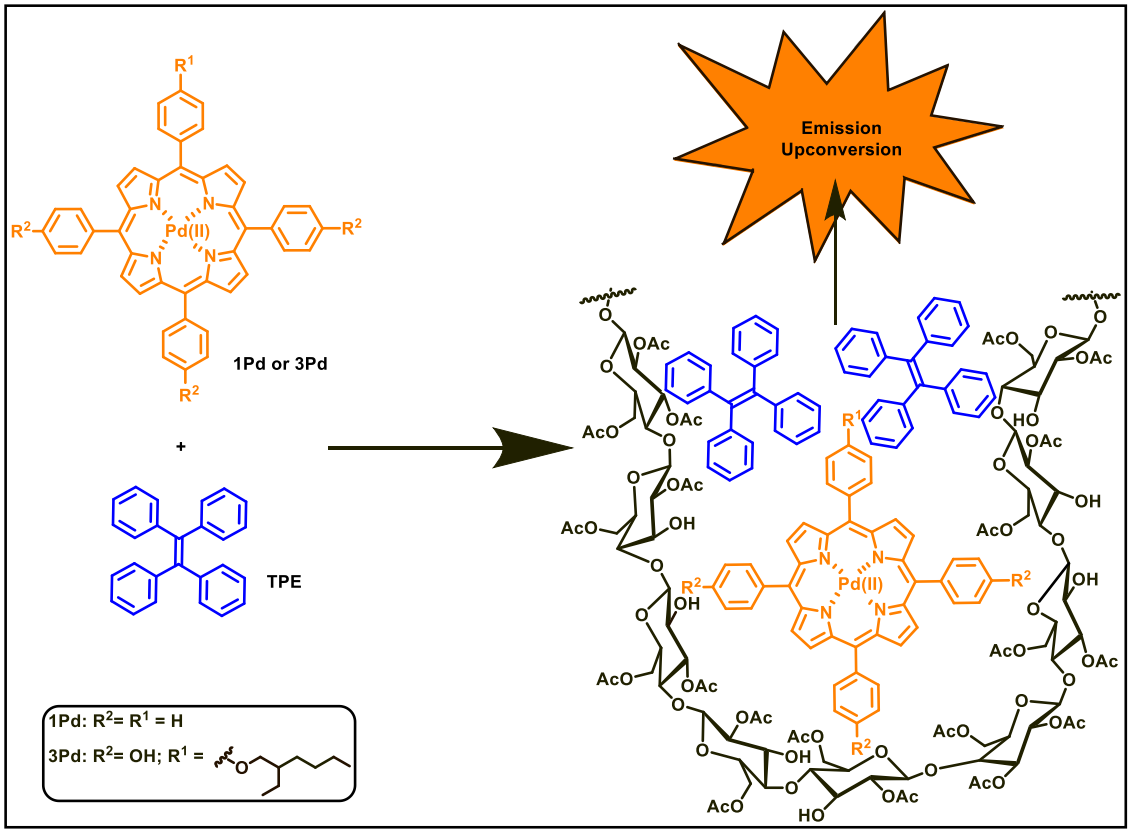

Figure 1.4 – Schematic representation of cellulose acetate polymer films with the TTA-UC system's components immobilized in its matrix.

1.6. References

(1) Wohnhaas, C.; Baluschev, S.; Turshatov, Triplet–Triplet Annihilation Upconversion Based Nanocapsules for Bioimaging Under Excitation by Red and Deep-Red Light. *Macromol. Biosci.* **2013**, *13* (10), 1422–1430.

(2) Wohnhaas, C.; Baluschev, S.; Landfester, K. Annihilation Upconversion in Cells by Embedding the Dye System in Polymeric Nanocapsules. *Macromol. Biosci.* **2011**, *11* (6), 772–778.

(3) Liu, Q.; Blue-Emissive Upconversion Nanoparticles for Low-Power-Excited Bioimaging in Vivo. *J. Am. Chem. Soc.* **2012**, *134* (11), 5390–5397.

(4) Li, F. Highly Photostable Near-IR-Excitation Upconversion Nanocapsules Based on Triplet–Triplet Annihilation for in Vivo Bioimaging Application. *ACS Appl. Mater. Interfaces* **2018**, *10* (12), 9883–9888.

(5) Kwon, O. S.; Artzi, N.; Kim, J.-H. Dual-Color Emissive Upconversion Nanocapsules for Differential Cancer Bioimaging In Vivo. *ACS Nano* **2016**, *10* (1), 1512–1521.

(6) Huang, L.; Han, G. Designing next Generation of Photon Upconversion: Recent Advances in Organic Triplet-Triplet Annihilation Upconversion Nanoparticles. *Biomaterials* **2019**, *201*, 77–86.

(7) Naimovičius, L.; Bharmoria, P.; Moth-Poulsen, K. Triplet–Triplet Annihilation Mediated Photon Upconversion Solar Energy Systems. *Mater. Chem. Front.* **2023**, *7* (12), 2297–2315.

(8) Liu, Q.; Kohane, D. S. Enhanced Precision of Nanoparticle Phototargeting in Vivo at a Safe Irradiance. *Nano Lett.* **2016**, *16* (7), 4516–4520.

(9) Li, Y.; Wang, W. Phototriggered Targeting of Nanocarriers for Drug Delivery. *Nano Res.* **2018**, *11* (10), 5424–5438.

(10) Filatov, M. A.; Baluschev, S.; Landfester, K. Protection of Densely Populated Excited Triplet State Ensembles against Deactivation by Molecular Oxygen. *Chem. Soc. Rev.* **2016**, *45* (17), 4668–4689.

(11) Proceedings of the Chemical Society. *Proc. Chem. Soc.* **1962**, No. December, 386–387.

(12) Parker, C. A.; Hatchard, C. G. Delayed Fluorescence of Pyrene in Ethanol. *Trans. Faraday Soc.* **1963**, *59* (0), 284–295.

(13) Parker, C. A.; Hatchard, C. G. Triplet-Singlet Emission in Fluid Solutions. Phosphorescence of Eosin. *Trans. Faraday Soc.* **1961**, *57* (0), 1894–1904.

(14) Parker, C. A.; Bowen, E. J. Sensitized P-Type Delayed Fluorescence. *Proc. R. Soc. Lond. Ser. Math. Phys. Sci.* **1997**, *276* (1364), 125–135.

(15) Parker, C. A.; Joyce, T. A. Delayed Fluorescence of Anthracene and Some Substituted Anthracenes. *Chem. Commun. Lond.* **1967**, No. 15, 744–745.

(16) Parker, C. A.; Hatchard, C. G.; Bowen, E. J. Delayed Fluorescence from Solutions of Anthracene and Phenanthrene. *Proc. R. Soc. Lond. Ser. Math. Phys. Sci.* **1997**, *269* (1339), 574–584.

(17) Keivanidis, P. e.; Baluschev, S. Up-Conversion Photoluminescence in Polyfluorene Doped with Metal(II)–Octaethyl Porphyrins. *Adv. Mater.* **2003**, *15* (24), 2095–2098.

(18) Sasaki, Y.; Ajioka, I.; Yanai, N.; Kimizuka, N. Near-Infrared Optogenetic Genome Engineering Based on Photon-Upconversion Hydrogels. *Angew. Chem. Int. Ed.* **2019**, *58* (49), 17827–17833.

(19) Baluschev, S.; A General Approach for Non-Coherently Excited Annihilation up-Conversion: Transforming the Solar-Spectrum. *New J. Phys.* **2008**, *10* (1), 013007.
(20) Turshatov, A.; Howard, I. A.; Richards, B. S. Room-Temperature High-Efficiency Solid-State Triplet–Triplet Annihilation Up-Conversion in Amorphous Poly(Olefin Sulfone)s. *ACS Appl. Mater. Interfaces* **2017**, *9* (9), 8280–8286.
(21) Bharmoria, P.; Moth-Poulsen, K. Recyclable Optical Bioplastics Platform for Solid State Red Light Harvesting via Triplet–Triplet Annihilation Photon Upconversion. *J. Mater. Chem. A* **2022**, *10* (40), 21279–21290.
(22) To, W.; Che, Che C.-M. A Robust Palladium(II)–Porphyrin Complex as Catalyst for Visible Light Induced Oxidative C-H Functionalization. *Chem. – Eur. J.* **2013**, *19* (18), 5654–5664.
(23) Edhborg, F.; Olesund, A.; Albinsson, B. Best Practice in Determining Key Photophysical Parameters in Triplet–Triplet Annihilation Photon Upconversion. *Photochem. Photobiol. Sci.* **2022**, *21* (7), 1143–1158.
(24) Azenha, E. G.; Arnaut, L. G. Heavy-Atom Effects on Metalloporphyrins and Polyhalogenated Porphyrins. *Chem. Phys.* **2002**, *280* (1), 177–190.
(25) Li, L.; Zeng, Y.; Li, Y. Light-Harvesting Organic Nanocrystals Capable of Photon Upconversion. *ChemSusChem* **2017**, *10* (22), 4610–4615.
(26) Singh, A.; Johnson, L. W. Phosphorescence Spectra and Triplet State Lifetimes of Palladium Octaethylporphyrin, Palladium Octaethylchlorin and Palladium 2,3-Dimethyloctaethylisobacteriochlorin at 77 K. *Spectrochim. Acta. A. Mol. Biomol. Spectrosc.* **2003**, *59* (5), 905–908.
(27) Seo, S. E.; Kim, H.; Kim, J.-H.; Kwon, O. S. Recent Advances in Materials for and Applications of Triplet–Triplet Annihilation-Based Upconversion. *J. Mater. Chem. C* **2022**, *10* (12), 4483–4496.
(28) Gray, V.; Moth-Poulsen, K.; Albinsson, B.; Abrahamsson, M. Towards Efficient Solid-State Triplet–Triplet Annihilation Based Photon Upconversion: Supramolecular, Macromolecular and Self-Assembled Systems. *Coord. Chem. Rev.* **2018**, *362*, 54–71.
(29) Enomoto, R.; Murakami, Y. Van Der Waals Solid Solution Crystals for Highly Efficient In-Air Photon Upconversion under Subsolar Irradiance. *Mater. Horiz.* **2021**, *8* (12), 3449–3456.
(30) Wei, L.; Wu, W. Triplet–Triplet Annihilation Upconversion in LAPONITE®/PVP Nanocomposites: Absolute Quantum Yields of up to 23.8% in the Solid State and Application to Anti-Counterfeiting. *Mater. Horiz.* **2022**, *9* (12), 3048–3056.
(31) Chen, C.-H.; Chiu, T.-L.; Bardeen, C. J.; Lee, J.-H. Efficient Solid-State Triplet-Triplet Annihilation up-Conversion Electroluminescence Device by Incorporating Intermolecular Intersystem-Crossing Dark Sensitizer. *Chem. Eng. J.* **2022**, *427*, 130889. https://doi.org/10.1016/j.cej.2021.130889.
(32) Ogawa, T.; Yanai, N.; Monguzzi, A.; Kimizuka, N. Highly Efficient Photon Upconversion in Self-Assembled Light-Harvesting Molecular Systems. *Sci. Rep.* **2015**, *5* (1), 10882.
(33) Ongun, M. Z.; Ertekin, K.; Hirel, C. Improvement of the O2 Detection: Substituent's Effect on Pd(II) Meso-Tetraphenylporphyrin Probes. *Sens. Actuators B Chem.* **2019**, *288*, 316–324.

(34) Helsenbeck, S. J.; Haustein, C. Solvent Effects in Room Temperature Phosphorescence. **1988**, 4, 95
(35) Liu, Q.; Yin, B.; Li, F. A General Strategy for Biocompatible, High-Effective Upconversion Nanocapsules Based on Triplet–Triplet Annihilation. *J. Am. Chem. Soc.* **2013**, *135* (13), 5029–5037.
(36) Vepris, O.; Cruz, L. J. Optically Coupled PtOEP and DPA Molecules Encapsulated into PLGA-Nanoparticles for Cancer Bioimaging. *Biomedicines* **2022**, *10* (5), 1070.
(37) Pereira, N. A. M.; Pinho e Melo, T. M. V. D. [8π+2π] Cycloaddition of Meso-Tetra- and 5,15-Diarylporphyrins: Synthesis and Photophysical Characterization of Stable Chlorins and Bacteriochlorins. *Eur. J. Org. Chem.* **2011**, *2011* (20–21), 3970–3979.
(38) Ravetz, B. D.; Congreve, D. N.; Rovis, T.; Campos, L. M. Photoredox Catalysis Using Infrared Light via Triplet Fusion Upconversion. *Nature* **2019**, *565* (7739), 343–346.
(39) Pereira, N. A. M.; Pinho e Melo, T. M. V. D. Novel 4,5,6,7-Tetrahydropyrazolo[1,5-a]Pyridine Fused Chlorins as Very Active Photodynamic Agents for Melanoma Cells. *Eur. J. Med. Chem.* **2015**, *103*, 374–380.
(40) Pereira, N. A. M.; Pinho e Melo, T. M. V. D. Novel Approach to Chlorins and Bacteriochlorins: [8π+2π] Cycloaddition of Diazafulvenium Methides with Porphyrins. *Eur. J. Org. Chem.* **2010**, *2010* (34), 6539–6543.
(41) Pereira, N. A. M.; Melo, T. M. V. D. P. e. Novel Fluorinated Ring-Fused Chlorins as Promising PDT Agents against Melanoma and Esophagus Cancer. *RSC Med. Chem.* **2021**, *12* (4), 615.
(42) Askes, S.; Bonnet, S. Imaging Upconverting Polymersomes in Cancer Cells: Biocompatible Antioxidants Brighten Triplet-Triplet Annihilation Upconversion. *Small* **2016**, *12*.
(43) J. Stich, M. I.; S. Wolfbeis, O. Multiple Fluorescent Chemical Sensing and Imaging. *Chem. Soc. Rev.* **2010**, *39* (8), 3102–3114.
(44) Fercher A.; Papkovsky D. B. Intracellular O2 Sensing Probe Based on Cell-Penetrating Phosphorescent Nanoparticles. *ACS Nano* **2011**, *5* (7), 5499–5508.
(45) Duan, P.; *Photon Upconversion in Supramolecular Gel Matrixes: Spontaneous Accumulation of Light-Harvesting Donor–Acceptor Arrays in Nanofibers and Acquired Air Stability*. J. Am. Chem. Soc. **2015**, 137, 5, 1887–1894
(46) Jankus, V. Energy Upconversion via Triplet Fusion in Super Yellow PPV Films Doped with Palladium Tetraphenyltetrabenzoporphyrin: A Comprehensive Investigation of Exciton Dynamics. *Adv. Funct. Mater.* **2013**, *23* (3), 384–393.
(47) Yu, X.; Ayres, N.; Zhang, P. Triplet–Triplet Annihilation Upconversion from Rationally Designed Polymeric Emitters with Tunable Inter-Chromophore Distances. *Chem. Commun.* **2015**, *51* (3), 588–591.
(48) Xun, Z.; Zeng, Y.; Li, Y. Pd-Porphyrin Oligomers Sensitized for Green-to-Blue Photon Upconversion: The More the Better? *Chem. - Eur. J.* **2016**, *22* (25), 8654–8662.
(49) Filatov, M.; Ilieva, I.; Landfester, K.; Baluschev, S. *Exploring the IR-Limit of the Triplet-Triplet Annihilation Upconversion: Tetraaryltetraanthra [2, 3] Porphyrin-Family*; **2013**.
(50) Elbjeirami, O.; Rawashdeh-Omary, M. A.; Omary, M. A. Phosphorescence Sensitization via Heavy-Atom Effects in D10 Complexes. *Res. Chem. Intermed.* **2011**, *37* (7), 691–703.

(51) Obata, M.; Hirohara, S.; Tanaka, R.; Kinoshita, I.; Ohkubo, K.; Fukuzumi, S.; Tanihara, M.; Yano, S. In Vitro Heavy-Atom Effect of Palladium(II) and Platinum(II) Complexes of Pyrrolidine-Fused Chlorin in Photodynamic Therapy. *J. Med. Chem.* **2009**, *52* (9), 2747–2753.
(52) De Luca, G.; Pollicino, G.; Romeo, A.; Scolaro, L. M. Sensing Behavior of Tetrakis(4-Sulfonatophenyl)Porphyrin Thin Films. *Chem. Mater.* **2006**, *18* (8), 2005–2007.
(53) Romanova, Z. S.; Deshayes, K.; Piotrowiak, P. Remote Intermolecular "Heavy-Atom Effect": Spin−Orbit Coupling Across the Wall of a Hemicarcerand. *J. Am. Chem. Soc.* **2001**, *123* (10), 2444–2445.
(54) Sen, P.; Soy, R.; Mgidlana, S.; Mack, J.; Nyokong, T. Light-Driven Antimicrobial Therapy of Palladium Porphyrins and Their Chitosan Immobilization Derivatives and Their Photophysical-Chemical Properties. *Dyes Pigments* **2022**, *203*, 110313.
(55) Berg, K.; Selbo, P. K.; Weyergang, A.; Dietze, A.; Prasmickaite, L.; Bonsted, A.; Engesaeter, B. Ø.; Angell-Petersen, E.; Warloe, T.; Frandsen, N.; Høgset, A. Porphyrin-Related Photosensitizers for Cancer Imaging and Therapeutic Applications. *J. Microsc.* **2005**, *218* (2), 133–147.
(56) Lang, H.; Rueffer, T. *Applications of Porphyrinoids as Functional Materials*; Royal Society of Chemistry, **2021**.
(57) Monnereau, C.; Ramos, P. H.; Deutman, A. B. C.; Elemans, J. A. A. W.; Nolte, R. J. M.; Rowan, A. E. Porphyrin Macrocyclic Catalysts for the Processive Oxidation of Polymer Substrates. *J. Am. Chem. Soc.* **2010**, *132* (5), 1529–1531.
(58) Barona-Castaño, J. C.; Carmona-Vargas, C. C.; Brocksom, T. J.; de Oliveira, K. T. Porphyrins as Catalysts in Scalable Organic Reactions. *Molecules* **2016**, *21* (3), 310.
(59) Buchler, J. W. Synthesis and Properties of Metalloporphyrins. In *The Porphyrins*; Dolphin, D., Ed.; Academic Press, **1978**; pp 389–483.
(60) Falk, J. E. *Porphyrins and Metalloporphyrins: A New Edition Based on the Original Volume by J. E. Falk*; Elsevier Scientific Publishing Company, **1975**.
(61) A. Filatov, M.; Heinrich, E.; Landfester, K.; Baluschev, S. Meso - Tetraphenylporphyrin with a Pi-System Extended by Fusion with Anthraquinone. *Org. Biomol. Chem.* **2015**, *13* (25), 6977–6983.
(62) Graham, K. R.; Schanze, K. S.; Xue, J.; Reynolds, J. R. Extended Conjugation Platinum(II) Porphyrins for Use in Near-Infrared Emitting Organic Light Emitting Diodes. *Chem. Mater.* **2011**, *23* (24), 5305–5312.
(63) Şen, P.; Bretonnière, Y. Photophysical Properties and Study of the Singlet Oxygen Generation of Tetraphenylporphyrinato Palladium(II) Complexes. *J. Porphyr. Phthalocyanines* **2013**, *17* (10), 964–971.
(64) Nagai, A.; Siegwart, D. J. Tumor Imaging Based on Photon Upconversion of Pt(II) Porphyrin Rhodamine Co-Modified NIR Excitable Cellulose Enhanced by Aggregation. *ACS Biomater. Sci. Eng.* **2015**, *1* (12), 1206–1210.
(65) Lamoen, D.; Parrinello, M. Geometry and Electronic Structure of Porphyrins and Porphyrazines. *Chem. Phys. Lett.* **1996**, *248* (5), 309–315.
(66) Spellane, P. J.; Gouterman M. Porphyrins. 40. Electronic spectra and four-orbital energies of free-base, zinc, copper, and palladium tetrakis(perfluorophenyl)porphyrins. *Inorg. Chem.* **1980**, 19, 386-391
(67) Allison J. B.; Becker R. S. Effect of Metal Atom Perturbations on the Luminescent Spectra of Porphyrins. J. Chem. Phys. **1960**, 32, 1410–1417

(68) Gray V.; Moth-Poulsen K. Photophysical Characterization of the 9,10-Disubstituted Anthracene Chromophore and Its Applications in Triplet–Triplet Annihilation Photon Upconversion. *J. Mater. Chem. C* **2015**, *3* (42), 11111–11121
(69) Liu, X. Structure, Optical, and Thermal Properties of 9, 10-Diphenylanthracene Crystals. *Crystals* **2019**, *9* (10), 512.
(70) Dzebo D.; Albinsson B. Intramolecular Triplet–Triplet Annihilation Upconversion in 9,10-Diphenylanthracene Oligomers and Dendrimers. *J. Phys. Chem. C* **2016**, *120* (41), 23397–23406. https://doi.org/10.1021/acs.jpcc.6b07920.
(71) Haefele, A.; Castellano, F. N. Getting to the (Square) Root of the Problem: How to Make Noncoherent Pumped Upconversion Linear. *J. Phys. Chem. Lett.* **2012**, *3* (3), 299–303.
(72) Sato, R. Theoretical Analyses of Triplet–Triplet Annihilation Process of 9,10-Diphenylanthracene in Solution. *Chem. Lett.* **2017**, *46* (6), 873–875.
(73) Gao, C.; A. Smith, T.; H. Wong, W. W. Triplet Fusion Upconversion Using Sterically Protected 9,10-Diphenylanthracene as the Emitter. *Phys. Chem. Chem. Phys.* **2020**, *22* (11), 6300–6307.
(74) Mendonsa, A. A.; Cash, K. J. Triplet–Triplet Annihilation Upconversion-Based Oxygen Sensors to Overcome the Limitation of Autofluorescence. *ACS Sens.* **2023**.
(75) Liu, S.; Li, X. Applying Triplet-Triplet Annihilation Upconversion in Degradation of Oxidized Lignin Model with Good Selectivity. *Chem. Eng. J.* **2022**, *431*, 133377.
(76) Moiseev, A. G.; Perepichka, D. F. Protecting the Triplet Excited State in Sterically Congested Platinum Porphyrin. *Dalton Trans.* **2014**, *43* (6), 2676–2683.
(77) Kiseleva, N.; S. Richards, B.; Turshatov, A. BODIPY–Pyrene Donor–Acceptor Sensitizers for Triplet–Triplet Annihilation Upconversion: The Impact of the BODIPY-Core on Upconversion Efficiency. *Phys. Chem. Chem. Phys.* **2022**, *24* (6), 3568–3578.
(78) Lee H.-L.; Kim J.-H. Visible-to-UV Triplet-Triplet Annihilation Upconversion from a Thermally Activated Delayed Fluorescence/Pyrene Pair in an Air-Saturated Solution. *Korean J. Chem. Eng.* **2019**, *36* (11), 1791–1798.
(79) Singh-Rachford, T. N.; Castellano, F. N. Pd(II) Phthalocyanine-Sensitized Triplet−Triplet Annihilation from Rubrene. *J. Phys. Chem. A* **2008**, *112* (16), 3550–3556.
(80) Deng, F.; Schanze, K. S.; Castellano, F. N. Near-IR Phosphorescent Metalloporphyrin as a Photochemical Upconversion Sensitizer. *Chem. Commun.* **2013**, *49* (67), 7406–7408.
(81) MacQueen, R. W.; Schmidt, T. W. Action Spectrum Experiment for the Measurement of Incoherent Photon Upconversion Efficiency under Sun-like Excitation. *RSC Adv.* **2014**, *4* (95), 52749–52756.
(82) Xiong, J.-B.; Zheng, Y.-S. Enantioselective Recognition for Many Different Kinds of Chiral Guests by One Chiral Receptor Based on Tetraphenylethylene Cyclohexylbisurea. *J. Org. Chem.* **2016**, *81* (9), 3720–3726.
(83) Xu, S.; Yuan, Y.; Cai, X.; Liu, B. Tuning the Singlet-Triplet Energy Gap: A Unique Approach to Efficient Photosensitizers with Aggregation-Induced Emission (AIE) Characteristics. *Chem. Sci.* **2015**, *6* (10), 5824–5830.

(84) Goerner, H. Triplet states of phenylethylenes in solution. Energies, lifetimes, and absorption spectra of 1,1-diphenyl-, triphenyl-, and tetraphenylethylene triplets. . *Phys. Chem*. **1982**, 86,2028-2035

2. Synthesis of porphyrins and metalloporphyrins

The main goal of the work described in the current thesis was the development of an efficient solid-state TTA-UC system with potential for the application as a bioimaging probe.[1–5] To achieve this goal, we started by synthesizing a porphyrin that could act as a sensitizer, an essential component of the envisioned system. Porphyrins are known to have great stability, sensitivity, selectivity, and can be structurally modified to suit a specificity of a given system for these reasons we chose the aforementioned macrocycle as the sensitizer. The porphyrins have great absorption and emission on the visible region of the electromagnetic spectrum and can undergo efficient ISC (intersystem crossing), when modified, to populate the triplet state, making them an essential component of the TTA-UC system as the photon acceptor molecule.[4,6–8]

There are several methods for the synthesis of porphyrins. The first synthetic methodology was proposed by *Rothemund* and involved an one-pot reaction, between an aldehyde and pyrrole dissolved in a pyridine and methanol mixture under anaerobic conditions.[9–11] The reaction was carried out in a glass sealed container for 24 up to 48 hours under 90 to 220°C, yielding small amounts of porphyrin mixed with variable amounts of chlorin.[9–11] A long time has passed since the initial findings of *Rothemund* and a lot of new progress in the synthesis of porphyrins were made, giving rise to new synthesis methods some derived from the work of *Rothemund*, such as the *Adler-Longo.*[12–14] The *Adler-Longo* approach consists of an one-pot acid catalyzed reaction between an aldehyde and pyrrole under aerobic conditions. In this methodology, first the acid is heated to its reflux temperature followed by the addition of aldehyde. Thereafter, the pyrrole is added to initiate the condensation with the protonated aldehyde in the mixture, which is then refluxed for 30 min. After the reaction time has ended, the crude mixture is cooled to room temperature, and the product is precipitated with methanol and dried under vacuum, obtaining 20-40% of porphyrin yield. Contrary to *Rothemund* method, *Adler* utilized the presence of atmospheric oxygen to oxidize the products of the condensation/cyclization doubling the reaction yield when compared to the *Rothemund's* method.[11,12,14] The use of atmospheric oxygen as an oxidant meant that

the oxidation step was dependent on the oxygen diffusion in the reaction medium, leading to slow kinetics and incomplete oxidation, resulting in the product being a mixture of porphyrin and chlorin. The *Adler-Longo* approach has the advantage of using an acid to catalyze the condensation/cyclization step, ensuring a faster reaction kinetics for the reaction between the aldehyde and the pyrrole resulting in a reduced reaction time to 30min compared to the *Rothemund* methodology (48h).[11,14]

Gonsalves and Pereira made a great leap in the synthesis of porphyrins by splitting the two steps in the synthesis of *meso*-tetraalkylporphyrins in the condensation/cyclization and oxidations steps. More so, they used a quinone (DDQ) to oxidize the porphyrinogen, the intermediary between the two step.[15] Sometime after, the development of a one-step one-pot method for the synthesis of porphyrins was achieved by *Gonsalves and Pereira*, the nitrobenzene method.[16–18] In this procedure, one or more aldehydes are dissolved in a mixture of acetic or propionic acid with nitrobenzene and then heated to 140°C. Then, the pyrrole is added, and the reaction is kept at 140°C for approximately one hour. In the end of the reaction, the product may be precipitated from the medium, in the majority of cases, by using methanol or other appropriate solvent that ensures precipitation of the porphyrin from the medium. When the product doesn't precipitate from the addition of a solvent, extensive purification is required. In this case, where additional purification is required, first the solvent is removed under reduced pressure and the obtained crude solid-mixture is applied in a silica-gel chromatographic column. With an adequate eluent it's possible to separate the desired compounds from the unwanted byproducts.

In this methodology by employing an organic oxidant (nitrobenzene) instead of using atmospheric oxygen, the reaction favors the production of pure porphyrins without chlorin contamination. Furthermore, when employing this methodology in the synthesis of symmetric porphyrins (using only one aldehyde) the majority of the obtained porphyrins can be precipitated pure from the medium avoiding extensive purification processes.

Lindsey et. al. developed a two-step porphyrin synthesis method under mild temperature conditions, during both the condensation and oxidation steps, to obtain

a high yield and high purity end product using a broad variety of aldehydes in small molar concentrations (0.01M). The first step involves the condensation of pyrrole with the aldehyde, using chloroform or dichloromethane as solvent, in a closed vessel under nitrogen atmosphere with the presence of trifluoroacetic acid or a mixture of boron trifluoride and diethyl ether at room temperature. The second step is the oxidation of the porphyrinogen to the desired porphyrin using organic oxidants, like p-chloranil or DDQ.[19–21] Typically, using this methodology the porphyrins are obtained in 30 to 40% yields.[20]

The *Lindsey* methodology has the advantage of using mild reaction temperatures, broadening the type of substituted benzaldehydes that could be used in the reaction. Another advantage comes from the use of an organic oxidant in the second step. The oxidant not only enhances the kinetics of the reaction, reducing the reaction time, but also reduces the chances of an incomplete oxidative dehydrogenation of the porphyrinogen, providing a crude product free of chlorin. Despite these advantages, the *Lindsey* methodology also has its shortcomings. First, the necessity to employ lush quantities of organic solvents (e.g., chloroform or dichloromethane) during the condensation step. Second, the use of costly organic oxidants, such as *p*-chloranil or DDQ, increases the overall cost of the methodology.

Macdonald et al. developed a two-step methodology for porphyrin synthesis that consisted in the [2+2] condensation of dipyrrylmethanes in acidic media.[22–25] First, the dipyrrylmethanes are heated to 100°C in an acidic solution (e.g.: formic, acetic, or p-toluenesulfonic acid) containing hydrogen bromide resulting in the formation of porphodimethene as an intermediary. Second, to the resulting porphodimethene sodium or zinc acetate is added in the presence of atmospheric oxygen, or occasionally using DDQ as an organic oxidant, resulting in the desired porphyrins being obtained as a mixture of isomers.[23,25] The formation of isomers arises from two factors, the first is the substituents in the alfa and beta positions of dipyrromethanes that influence the type of isomers that can be formed, the second is the acidic media impact on dipyrrylmethanes that may lead to acidolytic cleavage of the dipyrrylmethanes, resulting in scrambling and isomer production. Another version of the *Macdonald* methodology is the [3+1] condensation, where tripyrranes and pyrrole are used instead of dipyrromethanes under the same acidic conditions

followed by the same oxidation step.[25,26] This methodology produces high yields of porphyrin (around 20-65% depending on dipyrromethanes), is more versatile, and has milder reaction conditions than *Rothemund* or *Adler-Longo* methods.[23] However, the methodology also has its disadvantages, since it requires the synthesis and purification of dipyrromethanes if they are not commercially available, and the reaction produces a mixture of isomers, requiring chromatography to obtain high-purity compounds and reducing the overall yield if only one of the isomers is the goal.

Considering the several methods described above, the nitrobenzene (one-step) method remains one of the most widely used for the synthesis of meso-aryl porphyrins.[16–18,27] The research for more sustainable strategies based on this method has led to the appearance of new methodologies in recent years, like e the nitrobenzene-microwave method,[28] the nitrobenzene/NaY method[18,29] and the microwave water method[30].

The nitrobenzene-microwave method, developed by *Pinero et al.* scales the nitrobenzene method for the synthesis of *meso*-arylporphyrins to microwave conditions, changing the conventional irradiation method to microwave irradiation.[28] From this change microwave irradiation improves the heating efficiency of the reaction mixture by heating the mixture directly. Employing this methodology in the synthesis of porphyrins improved, in the majority of cases, the reaction yield and reduced, in all cases, the reaction time from hours to minutes.

Calvete et al. introduced a modification to the nitrobenzene method by employing the porous NaY aluminosilicate zeolite for porphyrin synthesis.[18,29,31] The NaY works as a Lewis acid and co-catalyst to the acetic acid, providing an increase in the reaction yield for the synthesis of symmetric and non-symmetric *meso*-arylporphyrins bearing different substituents in the *meso*-aryl positions.[29,31] The yields of the reaction were enhanced in the reaction with benzaldehydes bearing one or two *ortho*-fluorinated substituents, as well as for the perfluorinated *meso*-aryl porphyrin. This method is also characterized by a low ecological impact as well as a high cost-effectiveness compared to the standard methods for porphyrin synthesis that tend to be more expensive and difficult to produce.[29,31]

Calvete, Pereira et al. developed a new methodology for the synthesis of meso-substituted porphyrins under microwave irradiation using water as solvent.[30] Under harsh microwave conditions, of heat and pressure, water changes its properties, such as the dielectric constant and the value of the ionic product. Under microwave irradiation, water functions as a solvent, acid catalyst, and oxidant all at the same time, allowing the synthesis of meso-substituted porphyrins in high yields at extremely high concentrations (50 M).[30]

In this work we have synthesized symmetric and non-symmetric *meso*-substituted porphyrins via the one-pot nitrobenzene methodology under batch and microwave conditions.[16,17,27,28] This methodology was selected for its simplicity, as a one-pot single-step reaction obtaining porphyrins in relatively adequate yields, without chlorin contamination.

2.1 Synthesis of 5,10,15,20-tetraphenylporphyrin

This work started with the synthesis of 5,10,15,20-tetraphenylporphyrin (1) as can be seen in Scheme 2.1**.** This porphyrin was synthesized to act as a reference in spectroscopic studies. Both free-base and the corresponding Pd(II) porphyrin have been extensively studied and are well suited to be used as reference.[32,33] So, a reaction mixture containing benzaldehyde and nitrobenzene/glacial acetic acid (1:2 in v:v) was prepared, heated to 140°C, and the pyrrole was then added dropwise. After approximately 1 hour of reaction time, the crude mixture was cooled to room temperature and methanol was added to promote precipitation. The obtained purple crystalline powder was filtered and after drying under vacuum to remove any traces of solvents, 5,10,15,20-tetraphenylporphyrin was obtained in 8% yield. The same porphyrin was also synthesized by the nitrobenzene method under microwave irradiation.[28] This process was employed to reduce the reaction time as well as to enhance the reaction yield. The reagents were introduced in a proper microwave vessel and the reaction was carried out for 5 min. After confirming, by TLC, the formation of porphyrin (1), methanol was added to the medium to promote the precipitation of the porphyrin, giving porphyrin (1) in 20% yield. Porphyrin (1)

was characterized by proton NMR in $CDCl_3$, the signals chemical shift, integration patterns, and multiplicity where in agreement with the literature.[34]

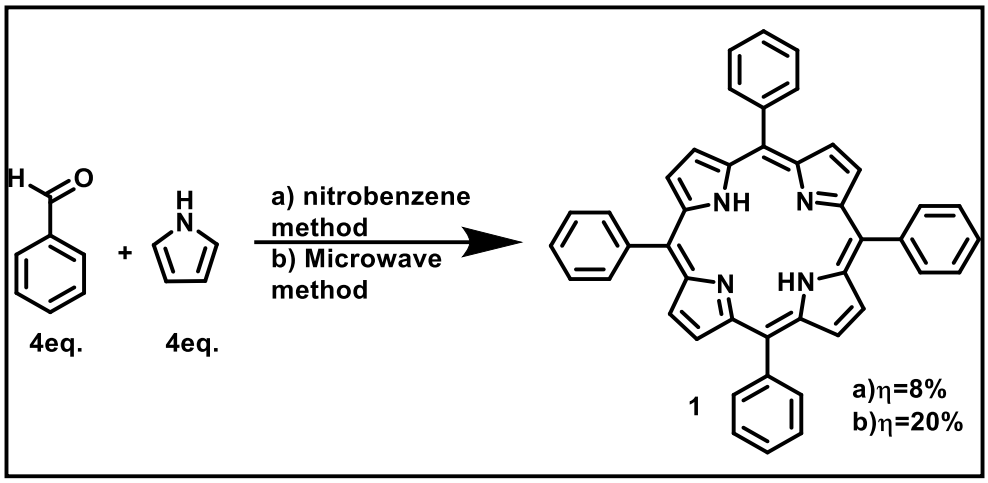

Scheme 2.1 – Synthesis of 5,10,15,20-tetraphenylporphyrin (1);(a) the nitrobenzene method; (b) microwave nitrobenzene method.

2.2 Synthesis of 5-(4-hidroxyphenyl)-10,15,20-(4-((2-ethylhexyl)oxy)phenyl) porphyrin

To develop an efficient sensitizer for a TTA-UC system several features need to be taken in to account: (1) the photosensitizer needs to have a good absorption with minimal overlap between the sensitizer and annihilator; (2) have an efficient ISC process to promote a great population of the triplet excited states in the molecule; (3) provide an efficient energy transfer between the sensitizer and annihilator. First it was decided to proceed with synthesis of a non-symmetric *meso*-substituted porphyrin with one 4-hydroxyphenyl group, that could be the anchor point for potential further functionalization of the porphyrin, combined with three 4-((2-ethylhexyl)oxy)phenyl groups. These alkoxy groups increase solubility in organic solvents and also may influence the formation of J-aggregates in polar solvents.[35] Also, from the introduction of electron donating atoms, such as an oxygen in the *para*-position of the phenyl may allow for the porphyrins spectral properties to shift closer to the NIR region.[36,37]

Initially we started by the synthesis of 4-((2-ethylhexyl)oxy)benzaldehyde through the *Williamson* ether synthesis, as seen in Scheme 2.2[38,39] First, 4-hydroxybenzaldehyde was dissolved in acetonitrile and an excess of K_2CO_3 was

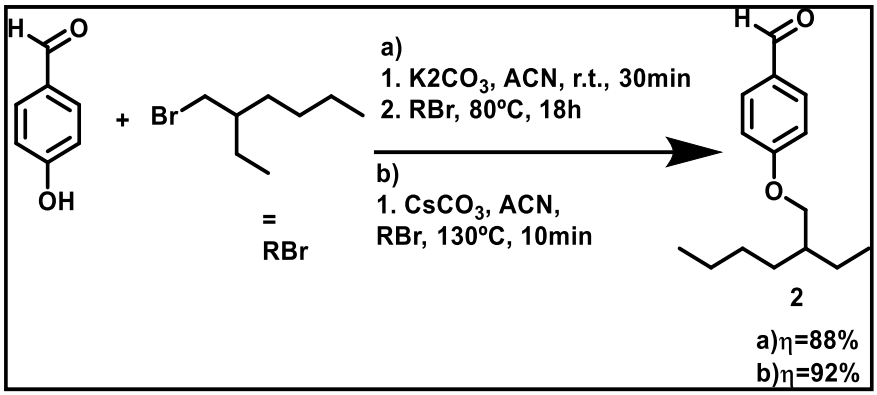

Scheme 2.2 – Synthesis of 4-((2-Ethylhexyl)oxy)benzaldehyde (2); (a) the nitrobenzene method and (b) through the microwave nitrobenzene method with the respective yields of reaction.

added, the reaction was left stirring for 30 min at room temperature. Afterwards, a small excess of 1-bromo-2-ethylhexane was added to the mixture and the reaction was heated to 80°C and left stirring for 18h. Following the reaction with TLC we observed that after the 18h all the 4-hydroxybenzaldehyde was consumed, so we considered the reaction complete.

The remaining solid was filtered and the acetonitrile was evaporated, then the crude product was purified by column chromatography giving pure aldehyde (2) in 88% yield, as seen in Scheme 2.1, point a). The reaction mechanism for the Williamson ether synthesis is depicted in scheme 2.3. It starts with the formation of the required phenolate after deprotonation of the hydroxyl group of the 4-hydroxybenzaldehyde by the carbonate base. This step is essential to produce a stronger nucleophile and is made first to ensure the reduction of any byproduct that may be formed by direct reaction between the haloalkane and the base. Following the phenolate formation the nucleophilic group attacks the electrophilic carbon that is bonded to the halogen promoting a S_N2 nucleophilic substitution.

The synthesis of the aldehyde was also performed using microwave irradiation in order to reduce the reaction time. So, we started by using the same temperature used in the conventional heating, with P=200W, (Table 2.1, entry B). The reaction was followed by TLC, and after 10 min of heating the product formation was not observed. The reaction was then left for one additional hour, but again no

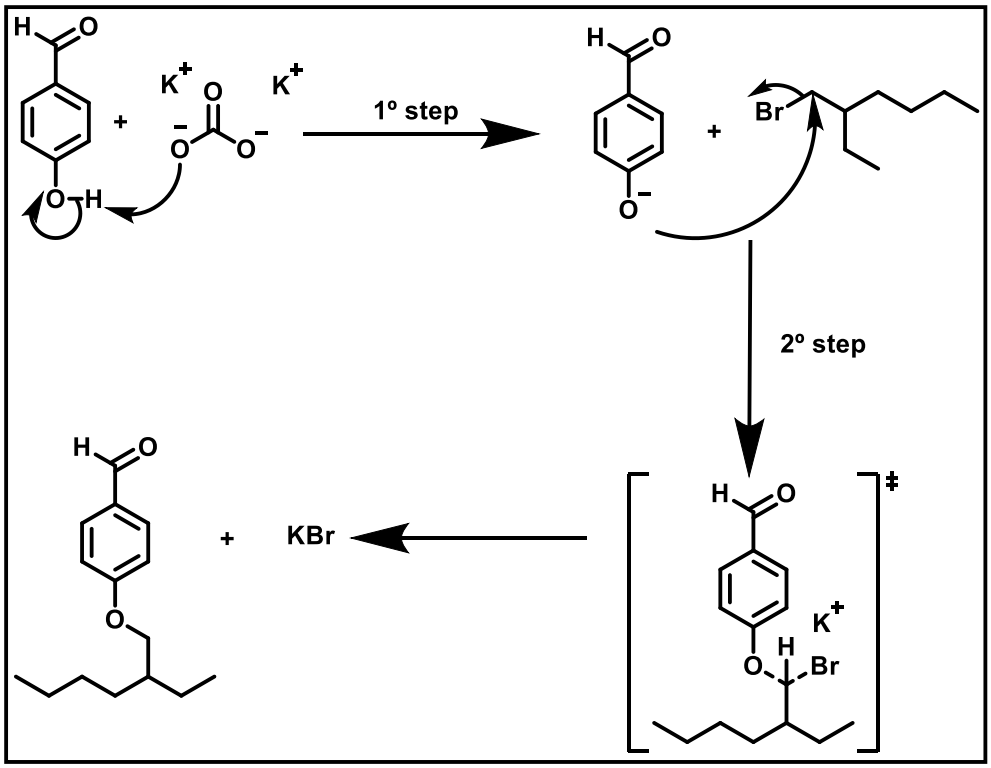

Scheme 2.3 – Mechanistic representation of the reaction of the Williamson ether synthesis of 4-((2-*e*thylhexyl)oxy)benzaldehyde (2).

change was observed. The issue was traced back to the limited solubility of the K_2CO_3 in acetonitrile, which caused a restriction in the reaction since the phenolate was not produced, and under the reaction time and heat condition the reaction didn´t proceed.[40] In continuation with the study, instead of increasing the reaction temperature that may favor the E_2 instead of the nucleophilic substitution[38,41] We choose to use a different base (Cs_2CO_3) that had a better solubility in acetonitrile giving the effect of the cesium ion in this carbonate.[42–44] The reaction was carried out under the same conditions as with the previous base, and after 20 min, the phenolate had formed, but the reaction conditions were still lacking as no product had been formed. As the Cs_2CO_3 was easily dissolved in the reaction mixture and even the formation of the phenolate was observed the problem was not purely dependent on the lack of solubility of the base, so the reaction was irradiated for an additional 60 minutes, but still no product was seen to form.

Then the solvent itself was evaluated, since the dielectric constant and the dielectric loss of acetonitrile tend to decrease with temperature reducing the amount of microwave radiation that the solvent can convert to heat.[45–47]

So less efficient heat production provides the need to increase temperatures to obtain a desirable kinetics for the reaction and reduce the time of reaction. As expected by providing a higher temperature condition, of 130°C, the reaction occurs in almost quantitative conversion yield ($\eta = 92\%$) after only 10 min of reaction time, as seen in Scheme 2.2. A reaction with K_2CO_3 at 130 °C was also accessed yielding small quantities of aldehyde with most of the starting materials still present in the reaction mixture, this means that in these conditions the reaction could occur but with slower kinetics compared to the Cs_2CO_3 which has, almost a quantitative yield after only 10 min. Afterwards, the 4-((2-*e*thylhexyl)oxy)benzaldehyde was purified with the same conditions that were used in the batch reactions.

The obtained aldehyde (2) was characterized by proton and carbon NMR. Figure 2.1 is the ^{1}H NMR of aldehyde (2) and Table 2.2 contains the observed signals.

Table 2.1. – Comparison between the conventional and microwave heating methods.

Entry	Solvent	Base	Type of Heating	T (°C)	Time (min)
A	ACN	K_2CO_3	Conventional	80	1080
B	ACN	K_2CO_3	Microwave	80	80
C	ACN	Cs_2CO_3	Microwave	80	80
D	ACN	K_2CO_3	Microwave	130	10
E	ACN	Cs_2CO_3	Microwave	130	10

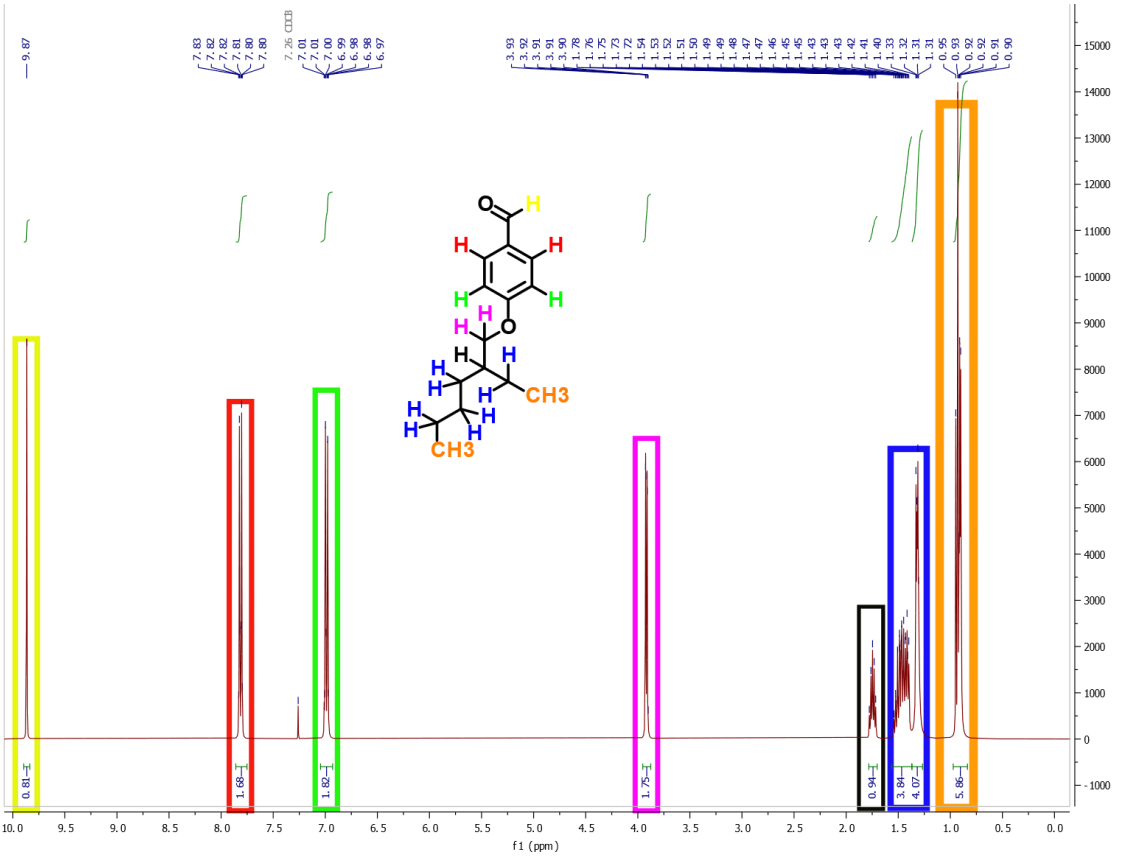

Figure 2.1 - Proton NMR spectrum of 4-(2-ethylhexyloxy)benzaldehyde (2) in $CDCl_3$ (7.26ppm).

In order to attribute a signal to a proton or group of protons with the same chemical environment, the signals are classified according to their chemical shifts, multiplicity, and the number of protons integrated under each signal. Given the deshielding induced by the carbonyl group, the aldehyde's proton (in yellow) appears first. Followed by two aromatic signals (red and green) corresponding to *orto*-protons and *meta*-protons, respectively, given that the deshielding effect of the carbonyl group is greater than that of the oxygen. The next signal (seen in violet) corresponds to the alkyl protons near the electronegative oxygen atom. The remaining alkyl signals appear in the following order -CH (seen in black) then -CH_2(seen in blue) followed by -CH_3 (seen in orange).

Table 2.2 – ^{1}H NMR data of compound (2) in $CDCl_3$; (a) in relation to the aldehyde group of the compound (2); (b) – two overlapping triplets.

Chemical shift (δ, ppm)	**Signal multiplicity**	**Integration**	**Characterization**
9.87	singlet	1 proton	Aldehydes proton
7.83 to 7.80	multiplet	2 protons	*orto*-benzylic[a]
7.01 to 6.97	multiplet	2 protons	*meta*-benzylic[a]
3.92	duplet	2 protons	$-OCH_2$
1.78 to 1.72	multiplet	1 proton	-CH
1.54 to 1.31	multiplet	8 protons	Alkylic $-CH_2$
0.95 to 0.90	triplet[b]	6 protons	$-CH_3$

In Figure 2.2 it is depicted the ^{13}C NMR of aldehyde (2) and in Table 2.3 are the respective peak characterization for the observed signal.

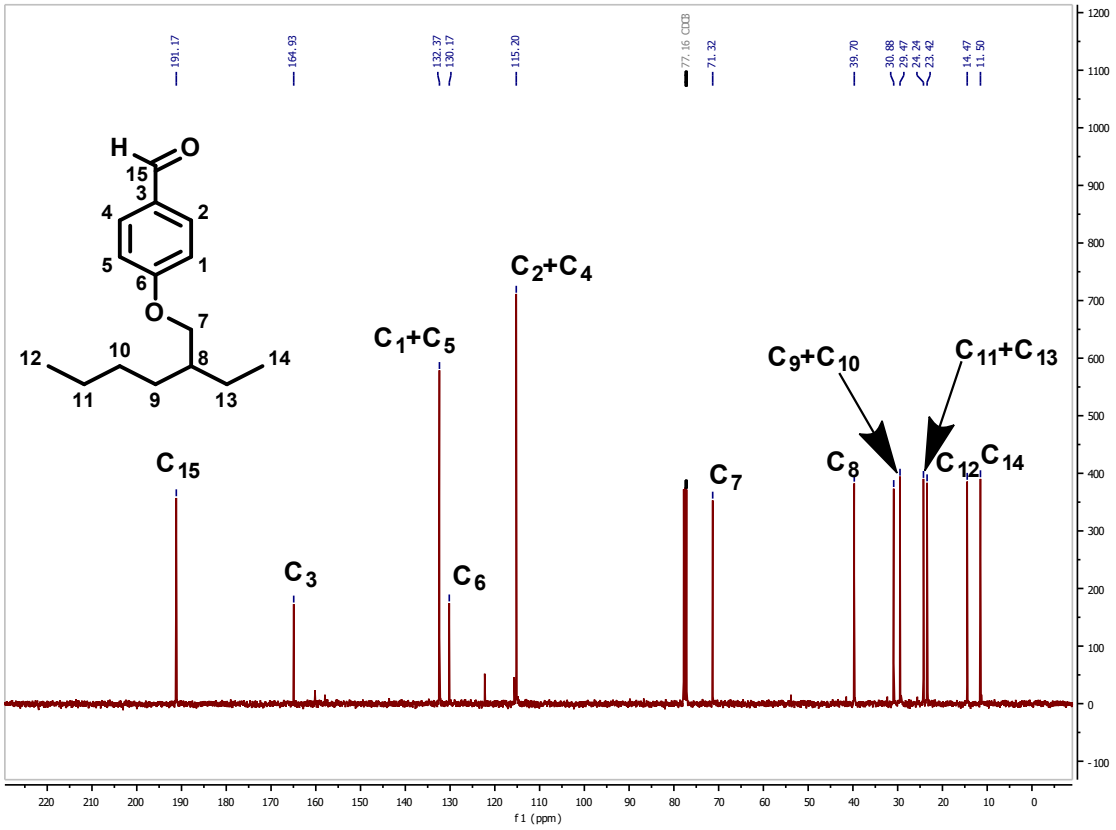

Figure 2.2 – ^{13}C NMR spectrum of 4-((2-ethylhexyl)oxy) benzaldehyde (2) in CDCl3 (77.16ppm).

Table 2.3 – ^{13}C NMR data of compound (2) in $CDCl_3$; (a) – carbons with the same chemical environment.

Chemical shift (δ, ppm)	Characterization
191.17	C15
164.93	C3
132.37	C1 and C5[a]
130.17	C6
115.20	C2 and C4[a]
71.32	C7
39.70	C8
30.88	C9
29.47	C10
24.24	C13
23.42	C11
14.47	C12
11.50	C14

This attribution is given based on the electronic density of each group (CH_3 has the highest electron density decreasing with the number of C-H bonds). After the successful production of 4-((2-ethylhexyl)oxy)benzaldehyde (2), we progressed with the synthesis of the 5-(4-hydroxyphenyl)-10,15,20-(4-((2-ethylhexyl)oxy)phenyl)porphyrin (3). To obtain the desired porphyrin we dissolved, in acetic acid and nitrobenzene mixture, 1:3 molar ratio of 4-hydroxybenzaldehyde and 4-((2-ethylhexyl)oxy)benzaldehyde (2), followed by the addition of 4 molar equivalents of pyrrole. Afterward the reaction was heated to 140°C and left under rigorous stirring for approximately 1h. Since two aldehydes in different molar amounts were used, the formation of several porphyrins is expected. Contrarily to TPP, previously referred, it was not possible to precipitate the desired porphyrin from the reaction media. Therefor the solvents were evaporated via reduced pressure distillation, and the reaction mixture was purified by silica gel column chromatography in order to separate/purify the obtained porphyrins. In this case, the application of the crude mixture was made without solvent in order to increase the efficiency of the separation. The column was eluted firstly with n-hexane, to remove any residue of nitrobenzene, followed with gradient increase in polarity by adding dichloromethane. Starting with a mixture of 10:1 (n-hexane:DCM) till pure DCM was employed. With this elution we obtained the pure

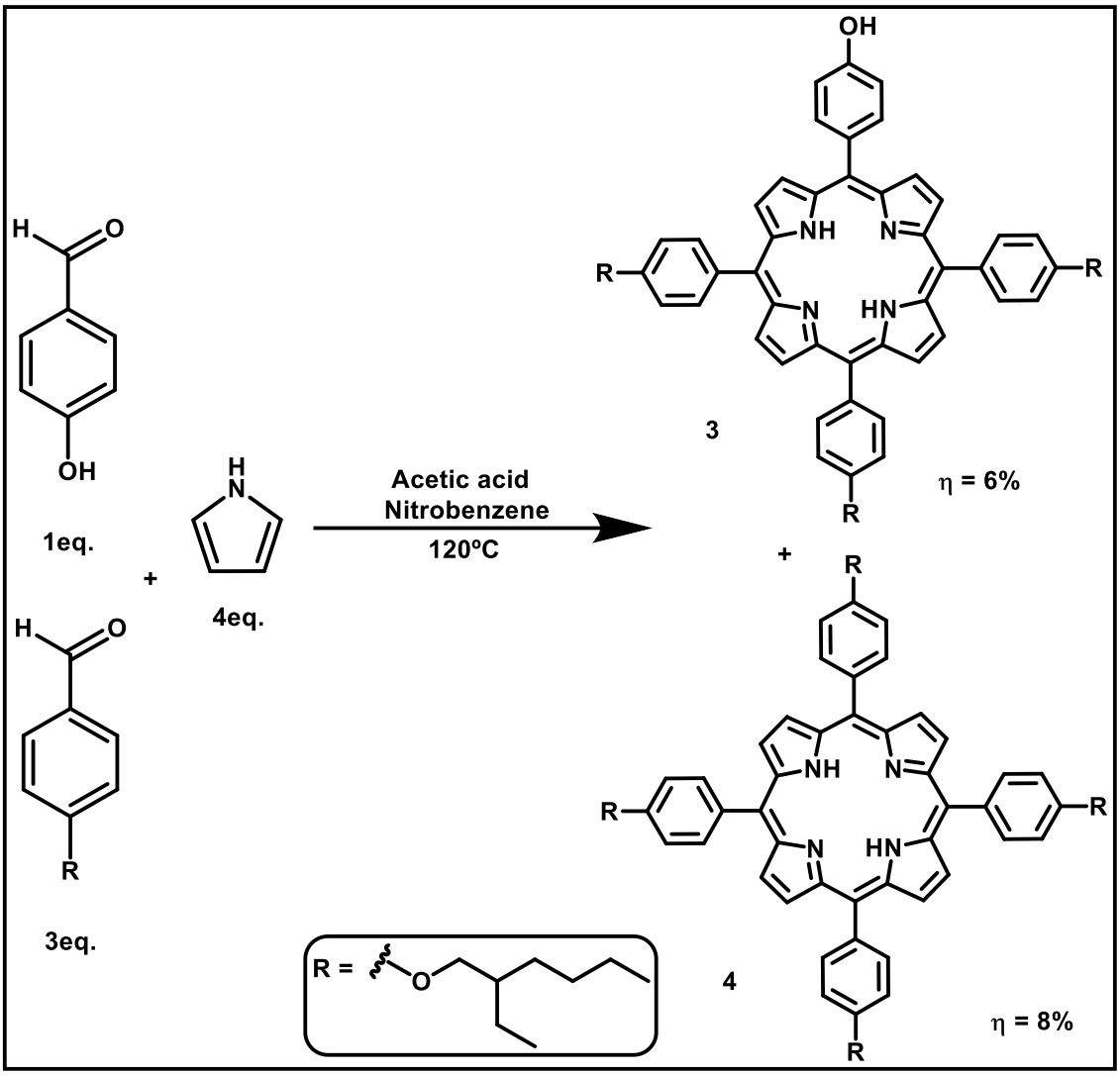

Scheme 2.4 – Nitrobenzene method for the porphyrin synthesis of porphyrins (3) and (4).

fraction of porphyrin (4). By continuing the increase in the eluent's polarity with the addition of MeOH we obtained the porphyrin (3). Following the purification of porphyrin (3) and (4), we proceeded with their characterization. Figure 2.4 shows the proton NMR spectra of compound (3) in $CDCl_3$, and Table 2.4 represents spectral data of the signals and the corresponding attributed protons to each signal. The asymmetry of porphyrin (3) promotes a small change in the chemical environment in the surrounding area of the benzylic *para*-positions, which splits the signals of the aromatic and beta-pyrrolic protons that otherwise would be equivalent such as in porphyrin (4).

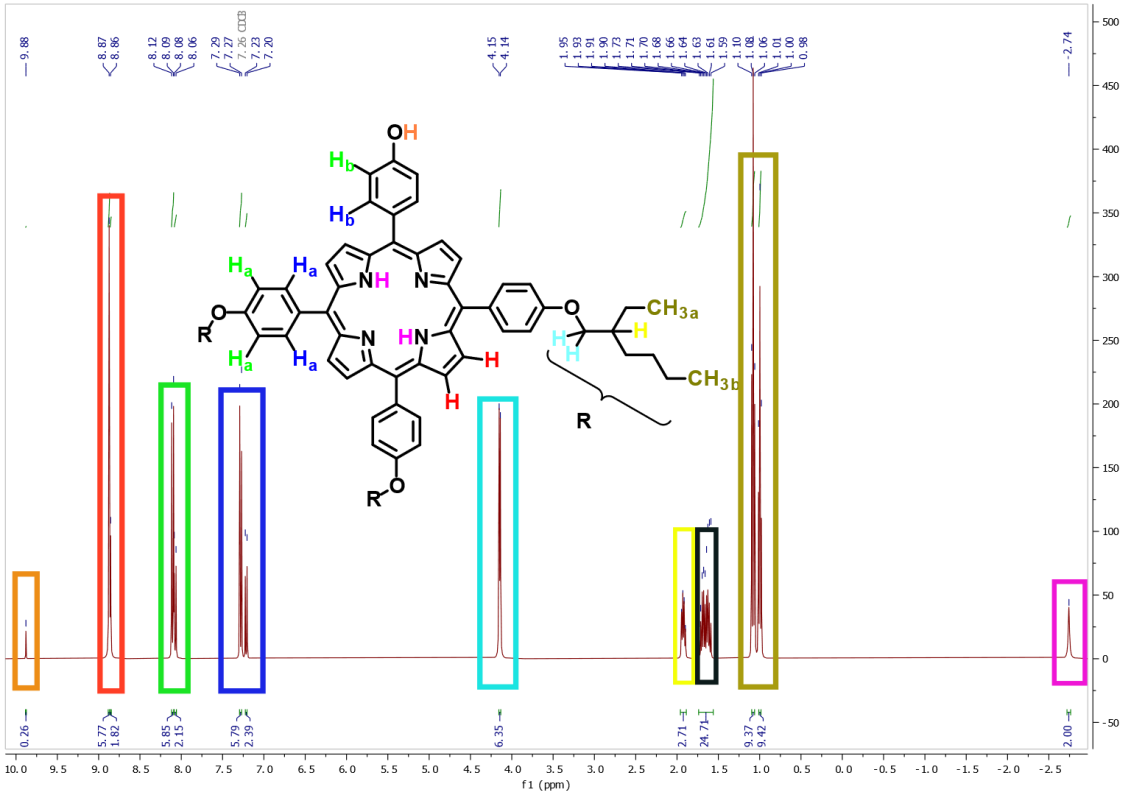

Fig. 2.3 – Proton NMR spectrum of porphyrin (3) in $CDCl_3$ (7.26ppm).

When starting downfield the first signal is a broad singlet with one proton which is attributed to the hydrogen of the hydroxyl group (seen in orange). The next signal at 8.87 to 8.86 ppm is a broad multiplet corresponding to a total of 8 protons attributed to the beta-pyrrolic protons of the porphyrin (seen in red). The next signals at 8.12 to 8.06 are two multiplet that are attributed to the meta-position protons of the phenylic group. The first, with an integration of 6, corresponds to the H_a of the phenyl groups that have the alkylic chain. The second one, with an integration of 2 corresponds to the H_b of the other phenyl group (as seen in green). The next signal at 7.29 ppm and 7.20 ppm, in a similar manner to the last one, is comprised of two duplets with an integration of 6 and 2 protons, respectively, corresponding to the *orto*-position phenyl protons (seen in dark blue). The next signal at 415 and 414 ppm is a doublet with 6 integrated protons, the signal appears downfield in the alkylic area of the spectrum resulting from the deshielding done by a nearby electronegative atom such as oxygen and has only one adjacent proton meaning this signal corresponds to the $-OCH_2$ groups (seen in cyan).

Table 2.4 – ^{1}H NMR data of compound (3) in $CDCl_3$; (a) – H_a protons of the alkoxy *para*-substituted phenyl; (b) – H_b protons of the hydroxyl substituted phenyl.

Chemical shift (δ, ppm)	**Signal multiplicity**	**Integration**	**Characterization**
9.88	singlet	1 proton	-OH
8.87 to 8.86	multiplet	8 protons	β–pyrrolic
8.12 to 8.09	multiplet	6 protons	*meta*-phenylic[a]
8.08 to 8.06	multiplet	2 protons	*meta*-phenylic[b]
7.29 to 7.27	multiplet	6 protons	*orto*-phenylic[a]
7.23 to 7.20	multiplet	2 protons	*orto*-phenylic[b]
4.15 to 4.14	duplet	6 protons	$-OCH_2$
1.95 to 1.90	multiplet	3 protons	-CH
1.73 to 1.59	multiplet	24 protons	Alkylic $-CH_2$
1.10 to 1.06	triplet	9 protons	$-CH_3$(a)
1.01 to 0.98	triplet	9 protons	$-CH_3$(b)

The multiplet at 1.95 to 1.90 ppm with 3 protons corresponds to the -CH group (seen in yellow). The next signal is a mixture of various multiplet signals from the overlap of multiple similar $-CH_2$ signals, with a combined integration of 24 protons, representing all the remaining alkylic protons of the $-CH_2$ groups. The next two signals at 1.10 and 0.98 ppm are two triplets, appearing in close proximity, each with an integration of approximately 9 protons, each characterizing a different $-CH_3$ group. The last signal at -2.74 ppm corresponds to the porphyrin's core protons, which suffer from a high degree of shielding from the delocalized electrons of the porphyrin's π-conjugated system.

2.3. Synthesis of Metalloporphyrins

Following the goal of producing a good photosensitizer, with adequate features to be used in a TTA-UC system, we choose to introduce a transition metal from the d^{10} group (e.g., palladium(II)) in the porphyrin core. Inserting such metal in the porphyrin core produces changes in the electronic structure of the porphyrin macrocycle consequently altering its photophysical characteristics. More so,

palladium(II) with an electronic configuration of [Kr] $5s^0 4d^8$ has 8 valence electrons producing a strong spin-orbit coupling with the porphyrin ring resulting in beneficial changes to the excited-state dynamics of the system namely by enhancing the inter system crossing (ISC) kinetics, ultimately resulting in attaining a higher population of triplet states and enhanced TTA-UC efficiency in regard to the free-base porphyrin.[48–50]

From the literature, it was evident that different kinds of methods exist for the metalation of porphyrins.[51–57] The benchmark method for this synthesis of palladium porphyrins is the benzonitrile method[52,58,59] which employs different palladium salts dissolved in benzonitrile to produce the corresponding porphyrin. Although this method has a relatively good yield it has some drawbacks. The main one is the high boiling point of the benzonitrile (b.p.= 190.7 °C) which makes the purification of the product extensive and compels the use of harsh reaction temperatures that may reduce the overall yield by enabling decomposition of palladium acetate, so other methods were sought.[60]

A modified version of the DMF method was employed.[51,61] Contrary to the standard DMF method[53,57] where the porphyrin and the metal salt were dissolved in DMF and then refluxed, in the modified version 2,6-lutidine is added to the mixture.[51,62,63] As a weak nucleophilic base, 2,6-lutidine will work as a weak coordination ligand that will facilitate the metalation of the porphyrin. The synthesis of palladium(II)tetraphenylporphyrin, **1Pd**, in a round bottom flask one molar equivalent of porphyrin was dissolved in previously dried DMF, and a few drops of 2,6-lutidine were added. then a molar excess of palladium acetate was added to the mixture. The reaction was left stirring at 120°C for 24h and was followed by TLC, UV-Vis, and fluorescence excitation. With this methodology and after purification, the obtained palladium(II) porphyrin was always obtained with a contamination of free base porphyrin (assessed by the analysis of the fluorescence excitation spectrum, see Figure 6.2 and 6.3 in Chapter 6)

To overcome this contamination problem, we performed a new palladium metalation but using a method that we called acetonitrile method.[63–65] In this case we started by dissolving the porphyrin in a mixture of dry chloroform and freshly distilled acetonitrile (80:20; v:v), then an excess of 4 equivalents of palladium

acetate were added and the reaction was left under reflux, with stirring. After 30min almost all of the porphyrin was converted into the palladium(II) complex and only a small amount of free-base porphyrin remained. After an additional 30min, all the free-base porphyrin was consumed, and the end of the reaction was determined by TLC, by UV spectroscopy with the observation of the disappearance of two Q bands, as the complexation of the porphyrin with a metal produces a change in orbital energy, originating degenerate orbitals, and finally by taking fluorescent emission and excitation spectra from the samples to determine the presence of any traces amounts of free-base porphyrin.

The purification of the crude mixture was done by silica gel column chromatography, using a mixture of n-hexane and DCM as eluent and the purity of the product was assessed by comparing the excitation and absorption spectra (seen in Figure 6.2 and 6.3 in Chapter 6). With this methodology it was possible to obtain Pd(II) porphyrin without free-base porphyrin contamination. Comparing the two methodologies we concluded that only the latter produced **1Pd** with high purity, and this methodology was selected to proceed with for all the Pd complexations performed.

From the DMF modified method, it was noted that a lot of metallic residues were formed at the end of the reaction. Palladium acetate is known to react with water, even when in small quantities, yielding unwanted intermediaries such as palladium hydroxide.[66–68]. When dissolved in a solvent with a high dipole moment (3.86 for DMF)[66] the palladium acetate tends to split to its monomeric form at room temperature making it more susceptible to moisture present in the solvent, resulting in a ligand competition, between the porphyrin and the water, for the palladium ion making the metalation of the porphyrin inefficient. Also, in the temperature conditions of the DMF modified method, a parallel reaction can occur, namely β-hydride elimination that is catalyzed by palladium acetate, resulting in the reduction of palladium(II) acetate to the metallic form of palladium(0).[60,69,70]

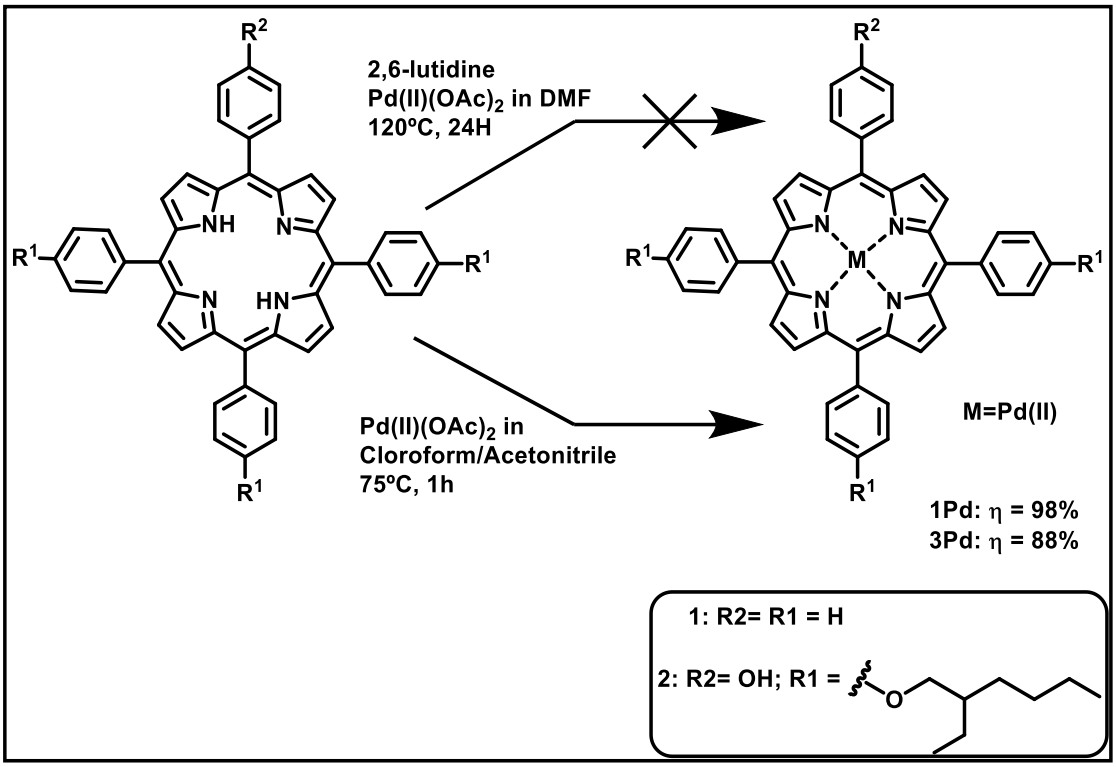

Scheme 2.5 – Synthesis of metalloporphyrins using (top) the modified DMF method and (below) acetonitrile method. The yields of the reaction after purification for the acetonitrile method.

Palladium acetate can also be found in three different crystalline structures $Pd_3(OAc)_6$, $Pd_3(OAc)_5(NO_2)$, and $[Pd(OAc)_2]_n$, the last two being byproducts from the industrial synthesis of palladium acetate firstly reported by *Wilkinson*[71]. From the synthesis of palladium acetate, each one of the palladium acetate derivatives will have its characteristics. The palladium acetate in its polymeric form, $[Pd(OAc)_2]_n$, will not be soluble and will not form metal complexes which if present in the commercially available compound will reduce the amount of palladium capable of undergoing metalation reaction. $Pd_3(OAc)_5(NO_2)$ despite being capable of producing metal organic complexes may affect the yield of the reaction depending on if the ligand is acetate or NO_2^-, as the latter may prove to be difficult to remove. The palladium acetate used during this reaction may have a mixture of different amounts of these species and therefore the reaction kinetics as well as the yield may be affected.[68,72,73]

After all these occurring problems, purification through the chromatographic column was still tried but with no success as the compound remained contaminated

with unreacted free-base porphyrin, such contamination was detected by comparing the excitation spectra with the absorption spectra.

To overcome the above referred problems we decided to perform all the synthesis of the metalloporphyrin, using the acetonitrile method.[64,65,74] First, the choice of palladium salt used in the metalation is a decisive factor for the success of the metalation reaction. Generally, the salt used in the metalation reactions in the benzonitrile, DMF and DMF modified method is palladium chloride that is not particularly soluble in non-coordinating solvents and has a smaller reactivity than palladium acetate. This difference in reactivity comes from the ligands, as from ligand field theory the Cl^- ion is a monodentate ligand and in consequence the ligand only interact with the d-orbitals of the metal through σ-bonding and doesn't have π-anti bonding orbitals present that could donate electron density to the metal, contrary to chloride ion the CH_3OO^- ion has a carbonyl group which has π-bonding and π-anti bonding orbitals that can enhance the reactivity of the salt by allowing delocalization of electronic density from one oxygen to another, and in a similar manner promote the delocalization of the electronic density to the metal allowing it to promote metal-ligand interaction more easily.[75–77]

Second, the method employed in the metalation reaction should take to account the palladium salt used as the more reactive palladium acetate can promote the metalation of porphyrin at a lower temperature compared to palladium chloride but can also be reduce easily under solvent and temperature conditions at which palladium chloride is normally used. Palladium chloride not only uses higher temperatures but also needs to employ solvents such as benzonitrile, to promote as the first step a formation of adducts such as bis(benzonitrile)palladium dichloride, that can be employed *in situ* metalation reaction to make the palladium salt more susceptible to coordination with the porphyrin as well as to enhance its solubility in the reaction media.[52,59,78]

2.4. References

(1) Liu Q.; Yin, B.; Li, F. A General Strategy for Biocompatible, High-Effective Upconversion Nanocapsules Based on Triplet–Triplet Annihilation. *J. Am. Chem. Soc.* **2013**, *135* (13), 5029–5037.

(2) Liu Q.; Li, F. Blue-Emissive Upconversion Nanoparticles for Low-Power-Excited Bioimaging in Vivo. *J. Am. Chem. Soc.* **2012**, *134* (11), 5390–5397.

(3) Kwon, O. S.; Artzi, N.; Kim, J.-H. Dual-Color Emissive Upconversion Nanocapsules for Differential Cancer Bioimaging In Vivo. *ACS Nano* **2016**, *10* (1), 1512–1521.

(4) Liu Q.; Li, F. Highly Photostable Near-IR-Excitation Upconversion Nanocapsules Based on Triplet–Triplet Annihilation for in Vivo Bioimaging Application. *ACS Appl. Mater. Interfaces* **2018**, *10* (12), 9883–9888.

(5) Wohnhaas, C.; Baluschev, S.;Turshatov, A. Triplet–Triplet Annihilation Upconversion Based Nanocapsules for Bioimaging Under Excitation by Red and Deep-Red Light. *Macromol. Biosci.* **2013**, *13* (10), 1422–1430.

(6) Fercher, A.; Papkovsky, D. B. Intracellular O2 Sensing Probe Based on Cell-Penetrating Phosphorescent Nanoparticles. *ACS Nano* **2011**, *5* (7), 5499–5508.

(7) Koren K.; Borisov, S. M.; Stable Optical Oxygen Sensing Materials Based on Click-Coupling of Fluorinated Platinum(II) and Palladium(II) Porphyrins—A Convenient Way to Eliminate Dye Migration and Leaching. *Sens. Actuators B Chem.* **2012**, *169* (5), 173–181.

(8) Buchler J. W. 10 - Synthesis and Properties of Metalloporphyrins. In *The Porphyrins*; Dolphin, D., Ed.; Academic Press, **1978**; pp 389–483.

(9) Rothemund, P. FORMATION OF PORPHYRINS FROM PYRROLE AND ALDEHYDES. *J. Am. Chem. Soc.* **1935**, *57* (10), 2010–2011.

(10) Rothemund, P. A New Porphyrin Synthesis. The Synthesis of Porphin [1]. *J. Am. Chem. Soc.* **1936**, *58* (4), 625–627.

(11) Rothemund, P.; Menotti, A. R. Porphyrin Studies. IV.1 The Synthesis of α,β,γ,δ-Tetraphenylporphine. *J. Am. Chem. Soc.* **1941**, *63* (1), 267–270.

(12) Adler A. *Mechanistic Investigations of Porphyrin Syntheses. I. Preliminary Studies on ms-Tetraphenylporphin.* **1964,** 86, 3145-3149

(13) Goldmacher, J.; Barton, L. A. Liquid Crystals. I. Fluorinated Anils. *J. Org. Chem.* **1967**, *32* (2), 476–477.

(14) Adler, A. D.; Longo, F. R. *A* simplified synthesis for meso-tetraphenylporphine. *ACS Publications*. **1966,** 32, 476.

(15) Gonsalves, A. M. D. R.; Pereira, M. M. A New Look into the Rothemund Meso-Tetraalkyl and Tetraarylporphyrin Synthesis. *J. Heterocycl. Chem.* **1985**, *22* (3), 931–933.

(16) A. W. Johnstone, R.; M. Pereira, M.; M. d'A. Rocha Gonsalves, A.; C. Serra, A. Improved Syntheses of 5,10,15,20-Tetrakisaryl- and Tetrakisalkylporphyrins. *HETEROCYCLES* **1996**, *43* (7), 1423.

(17) Gonsalves, A. M. d'A R.; Varejão, J. M. T. B.; Pereira, M. M. Some New Aspects Related to the Synthesis of Meso-Substituted Porphyrins. *J. Heterocycl. Chem.* **1991**, *28* (3), 635–640.

(18) Pinto, S. M. A.; Pereira, M. M. Nitrobenzene Method: A Keystone in Meso-Substituted Halogenated Porphyrin Synthesis and Applications. *J. Porphyr. Phthalocyanines* **2019**, *23* (04n05), 329–346.
(19) Lindsey, J. S. Synthetic Routes to Meso-Patterned Porphyrins. *Acc. Chem. Res.* **2010**, *43* (2), 300–311.
(20) Lindsey, S.; Hsu, C.; Schreiman, C. SYNTHESIS OF TETRAPHRNYLPORPRYRINS UNDER VERY MILD CONDITIONS. *Tetrahedron Letters*, **1986,** 27, 41,pp 4969-4970.
(21) Wagner, R. W.; Lindsey, J. S. An Improved Synthesis of Tetramesitylporphyrin. *Tetrahedron Lett.* **1987**, *28* (27), 3069–3070.
(22) Lee, D. A.; Smith, K. M. Syntheses of Symmetrically Substituted 5-Alkyl- And5-Aryl-Dihydrodipyrrins and of Porphyrins and Bisporphyrins Therefrom. *J. Chem. Soc. Perkin 1* **1997**, No. 8, 1215–1228.
(23) Arsenault, G. P.; Bullock, E.; MacDonald, S. F. Pyrromethanes and Porphyrins Therefrom1. *J. Am. Chem. Soc.* **1960**, *82* (16), 4384–4389.
(24) Tarlton, E. J.; MacDonald, S. F.; Baltazzi, E. *Uroporphyrin 31*. ACS Publications.
(25) Lash, T. D. What's in a Name? The MacDonald Condensation. *J. Porphyr. Phthalocyanines* **2016**, *20* (08-11), 855–888.
(26) Lash, T. D. Porphyrin Synthesis by the "3+1" Approach: New Applications for an Old Methodology. *Chem. – Eur. J.* **1996**, *2* (10), 1197–1200.
(27) Henriques, C. A.; Pereira, M. M. Unsymmetrical Porphyrins: The Role of Meso-Substituents on Their Physical Properties. *J. Porphyr. Phthalocyanines* **2012**, *16* (03), 290–296.
(28) Nascimento, B. F. O.; Pineiro, M.; Rocha Gonsalves, A. M. d'A.; Ramos Silva, M.; Matos Beja, A.; Paixão, J. A. Microwave-Assisted Synthesis of Porphyrins and Metalloporphyrins: A Rapid and Efficient Synthetic Method. *J. Porphyr. Phthalocyanines* **2007**, *11* (02), 77–84.
(29) Calvete, M. J. F.; Pereira, M. M. A Cost-Efficient Method for Unsymmetrical Meso-Aryl Porphyrin Synthesis Using NaY Zeolite as an Inorganic Acid Catalyst. *Mol. J. Synth. Chem. Nat. Prod. Chem.* **2017**, *22* (5), 741.
(30) Henriques, C. A.; Pereira, M. M. Ecofriendly Porphyrin Synthesis by Using Water under Microwave Irradiation. *ChemSusChem* **2014**, *7* (10), 2821–2824.
(31) Silva, M.; Calvete, M. J. F.; Pereira, M. M. Size and Ability Do Matter! Influence of Acidity and Pore Size on the Synthesis of Hindered Halogenated Meso - Phenyl Porphyrins Catalysed by Porous Solid Oxides. *Chem. Commun.* **2014**, *50* (50), 6571–6573.
(32) Pineiro, M.; Arnaut, L. G.; Photoacoustic Measurements of Porphyrin Triplet-State Quantum Yields and Singlet-Oxygen Efficiencies. *Chem. - Eur. J.* **1998**, *4* (11), 2299–2307.
(33) Wilkinson, F.; Helman, W. P.; Ross, A. B. Quantum Yields for the Photosensitized Formation of the Lowest Electronically Excited Singlet State of Molecular Oxygen in Solution. *J. Phys. Chem. Ref. Data* **2009**, *22* (1), 113.
(34) Marsh, D. F.; Falvo, R. E.; Mink, L. M. Microscale Synthesis and 1H NMR Analysis of Tetraphenylporphyrins. *J. Chem. Educ.* **1999**, *76* (2), 237.
(35) Li, X.; Chen, Z.; Zou, G. Tuning J-Aggregates of Tetra(p-Hydroxyphenyl)Porphyrin by the Headgroups of Ionic Surfactants in Acidic Nonionic Micellar Solution. *J. Phys. Chem. B* **2007**, *111* (17), 4342–4348.

(36) Charisiadis, A.; Angaridis, P. A.; Coutsolelos, A. G.; Costa, R. D. Peripheral Substitution of Tetraphenyl Porphyrins: Fine-Tuning Self-Assembly for Enhanced Electroluminescence. *ChemPlusChem* **2018**, *83* (4), 254–265.
(37) Ha, J.-H.; Kim, Y.-R. Substitution Effect of Hydroxyl Group on Photophysical Properties of Tetraphenylporphyrin (H2TPP) and Germanium(IV) Tetraphenylporphyrin Dichloride (Ge(IV)TPPCl2). *J. Mol. Struct.* **2002**, *606* (1), 189–195.
(38) Wade, L. G.; Simek, J. W. Organic Chemistry, Ninth edition.; Pearson: Glenview, IL, **2017**.
(39) Williamson, A. XLV. Theory of Ætherification. *Lond. Edinb. Dublin Philos. Mag. J. Sci.* **1850**, *37* (251), 350–356.
(40) Steinmetz A. The Broad Scope of Cesium Salts in Organic Chemistry. **2016**, 3, 60487
(41) Clayden, J.; Greeves, N.; Warren, S. G. *Organic Chemistry*, 2nd ed.; Oxford University Press: Oxford ; New YorK, **2012**.
(42) Varala, R.; Rao, K. Cesium Salts in Organic Synthesis: A Review. *Curr. Org. Chem.* **2015**, *19*, 1–1.
(43) Dijkstra, G.; Kruizinga, W. H.; Kellogg, R. M. An Assessment of the Causes of the "Cesium Effect." *J. Org. Chem.* **1987**, *52* (19), 4230–4234.
(44) Cella, J. A.; Bacon, S. W. Preparation of Dialkyl Carbonates via the Phase-Transfer-Catalyzed Alkylation of Alkali Metal Carbonate and Bicarbonate Salts. *J. Org. Chem.* **1984**, *49* (6), 1122–1125.
(45) Gupta, M.; Paul, S.; Gupta, R. General Characteristics and Applications of Microwaves in Organic Synthesis. *Acta Chim Slov* **2009**.
(46) Gabriel, C.; Mingos, D. M. P. Dielectric Parameters Relevant to Microwave Dielectric Heating. *Chem. Soc. Rev.* **1998**, *27* (3), 213–224.
(47) Kappe, C. O. Controlled Microwave Heating in Modern Organic Synthesis. *Angew. Chem. Int. Ed.* **2004**, *43* (46), 6250–6284.
(48) Turro J. N. Modern Molecular Photochemistry of Organic Molecules. *The Benjamin/Cummings Publishing Company* **1978**
(49) Seo, S. E.; Kim, H.; Kim, J.-H.; Kwon, O. S. Recent Advances in Materials for and Applications of Triplet–Triplet Annihilation-Based Upconversion. *J. Mater. Chem. C* **2022**, *10* (12), 4483–4496.
(50) Singh, A.; Johnson, L. W. Phosphorescence Spectra and Triplet State Lifetimes of Palladium Octaethylporphyrin, Palladium Octaethylchlorin and Palladium 2,3-Dimethyloctaethylisobacteriochlorin at 77 K. *Spectrochim. Acta. A. Mol. Biomol. Spectrosc.* **2003**, *59* (5), 905–908.
(51) Droege, D. G.; Johnstone, T. C. Synthesis and Functionalization of Challenging *Meso*-Substituted Aryl Bis-Pocket Porphyrins Accessed via Suzuki-Miyaura Cross-Coupling. *J. Org. Chem.* **2022**, *87* (17), 11783–11795.
(52) Falk, J. E. *Porphyrins and Metalloporphyrins: A New Edition Based on the Original Volume by J. E. Falk*; Elsevier Scientific Publishing Company, **1975**.
(53) Adler, A. D.; Longo, F. R.; Kampas, F.; Kim, J. On the Preparation of Metalloporphyrins. *J. Inorg. Nucl. Chem.* **1970**, *32* (7), 2443–2445.
(54) Gomes, C.; Pineiro, M. Modern Methods for the Sustainable Synthesis of Metalloporphyrins. *Molecules* **2021**, *26* (21), 6652.

(55) Pinto, S. M. A.; Burrows, H. D.; Pereira, M. M. Metalloporphyrin Triads: Synthesis and Photochemical Characterization. *J. Photochem. Photobiol. Chem.* **2012**, *242*, 59–66.
(56) Herrmann, O.; Mehdi, S. H.; Corsini, A. Heterogeneous Metal-Insertion: A Novel Reaction with Porphyrins. *Can. J. Chem.* **1978**, *56* (8), 1084–1087.
(57) Buchler, J. W. 10 - Synthesis and Properties of Metalloporphyrins. In *The Porphyrins*; Dolphin, D., Ed.; Academic Press, **1978**; pp 389–483.
(58) Khalil, G.; Gouterman, M.; B. Synthesis and Spectroscopic Characterization of Ni, Zn, Pd and Pt Tetra(Pentafluorophenyl)Porpholactone with Comparisons to Mg, Zn, Y, Pd and Pt Metal Complexes of Tetra(Pentafluorophenyl)Porphine. *J. Porphyr. Phthalocyanines* **2002**, *06* (02), 135–145.
(59) Papkovsky, D. B.; Ponomarev, G. V.; Trettnak, W.; O'Leary, P. Phosphorescent Complexes of Porphyrin Ketones: Optical Properties and Application to Oxygen Sensing. Anal. Chem. **1995**, 67, 41 12-41 17
(60) Crabtree, R. H. Resolving Heterogeneity Problems and Impurity Artifacts in Operationally Homogeneous Transition Metal Catalysts. *Chem. Rev.* **2012**, *112* (3), 1536–1554.
(61) Pereira, M. M. Synthesis and Photophysical Properties of a Covalently Bonded Palladium *Meso* -Sulfophenylporphyrin-Poly(Vinyl Alcohol)Polymer with Potential Applications as an Oxygen Sensor. *J. Porphyr. Phthalocyanines* **2006**, *10* (02), 87–95.
(62) Chen, Y.; Gao, G.-Y.; Peter Zhang, X. Palladium-Mediated Synthesis of Novel Meso-Chiral Porphyrins: Cobalt-Catalyzed Cyclopropanation. *Tetrahedron Lett.* **2005**, *46* (30), 4965–4969.
(63) Lash, T. D. Metal Complexes of Carbaporphyrinoid Systems. *Chem. – Asian J.* **2014**, *9* (3), 682–705.
(64) Orzeł, Ł.; Waś, J.; Kania, A.; Susz, A.; Rutkowska-Zbik, D.; Staroń, J.; Witko, M.; Stochel, G.; Fiedor, L. Factors Controlling the Reactivity of Divalent Metal Ions towards Pheophytin a. *JBIC J. Biol. Inorg. Chem.* **2017**, *22* (6), 941–952.
(65) Volostnykh, M. V.; Borisov, S. M.; Konovalov, M. A.; Sinelshchikova, A. A.; Gorbunova, Y. G.; Tsivadze, A. Yu.; Meyer, M.; Stern, C.; Bessmertnykh-Lemeune, A. Platinum(II) and Palladium(II) Complexes with Electron-Deficient *Meso* -Diethoxyphosphorylporphyrins: Synthesis, Structure and Tuning of Photophysical Properties by Varying Peripheral Substituents. *Dalton Trans.* **2019**, *48* (24), 8882–8898.
(66) Carole, W. A.; Colacot, T. J. Understanding Palladium Acetate from a User Perspective. *Chem. - Eur. J.* **2016**, *22* (23), 7686–7695.
(67) Stoyanov, E. S. Ir Study of the Structure of Palladium(Ii) Acetate in Chloroform, Acetic Acid, and Their Mixtures in Solution and in Liquid-Solid Subsurface Layers. *J. Struct. Chem.* **2000**, *41* (3), 440–445.
(68) Bakhmutov, V. I.; Murillo, C. A. Non-Trivial Behavior of Palladium(II) Acetate. *Dalton Trans.* **2005**, No. 11, 1989. https://doi.org/10.1039/b502122g.
(69) Mueller, J. A.; Sigman, M. S. Elucidating the Significance of β-Hydride Elimination and the Dynamic Role of Acid/Base Chemistry in a Palladium-Catalyzed Aerobic Oxidation of Alcohols. *J. Am. Chem. Soc.* **2004**, *126* (31), 9724–9734.

(70) Molina de la Torre, J. A.; Espinet, P.; Albéniz, A. C. Solvent-Induced Reduction of Palladium-Aryls, a Potential Interference in Pd Catalysis. *Organometallics* **2013**, *32* (19), 5428–5434.
(71) Stephenson, T. A.; Morehouse, S. M.; Powell, A. R.; Heffer, J. P.; Wilkinson, G. 667. Carboxylates of Palladium, Platinum, and Rhodium, and Their Adducts. *J. Chem. Soc. Resumed* **1965**, 3632.
(72) Stolyarov, I. P.; Demina, L. I.; Cherkashina, N. V. Preparative Synthesis of Palladium(II) Acetate: Reactions, Intermediates, and by-Products. *Russ. J. Inorg. Chem.* **2011**, *56* (10), 1532–1537.
(73) Carole, W. A.; Colacot, T. J. Can Palladium Acetate Lose Its "Saltiness"? Catalytic Activities of the Impurities in Palladium Acetate. *Org. Lett.* **2015**, *17* (21), 5472–5475.
(74) Lash, T. D. Metal Complexes of Carbaporphyrinoid Systems. *Chem. – Asian J.* **2014**, *9* (3), 682–705.
(75) Patnaik, P. *Handbook of Inorganic Chemicals*; McGraw-Hill handbooks; McGraw-Hill: New York, **2003**.
(76) Lawrance, G. A. Introduction to Coordination Chemistry. A Wiley Series of Advanced Textbooks ISSN: 1939-5175
(77) Griffith, J. S.; Orgel, L. E. Ligand-Field Theory. *Q. Rev. Chem. Soc.* **1957**, *11* (4), 381–393.
(78) Anderson, G. K.; Lin, M.; Sen, A.; Gretz, E. Bis(Benzonitrile)Dichloro Complexes of Palladium and Platinum. *Inorganic Syntheses*, **1990**; pp 60–63.

3. Photophysical characterization of the TTA-UC system and its components

This section aims to present the photophysical data acquired on the properties and characteristics of each individual TTA-UC system component as well as for the system as a whole. Starting the discussion with a topic describing the behavior of light and matter, following with an insight in the behavior of the sensitizers and annihilators under study and their characteristics, then the chapter concludes with the spectroscopic characterization of the systems as a whole.

3.1. Light and matter

Electromagnetic radiation consists of waves that exhibit two oscillating fields, one magnetic and one electric perpendicular to each other, and with the same direction of propagation. The electromagnetic spectrum is made up of different forms of electromagnetic radiation. Depending on the type of electromagnetic radiation, the spectrum may be split into many areas, each with a unique oscillatory field. This difference can be observed by changes of wavelength or frequency. Wavelength, denoted λ, is considered the distance between two peak maximum (or two minimum) of the corresponding electromagnetic wave. Frequency, denoted ν, is described as the number of complete oscillations produced by an electromagnetic wave per unit of time. So, light is electromagnetic radiation, from a specific region of the electromagnetic spectrum that extends from just a few nanometers to several micrometers in wavelength. Light with a wavelength inferior to 400nm is considered Ultra-Violet light or UV and light with wavelength higher than 700nm is considered Near Infrared light, in between the two region the visible light region is found, and it's this region that is perceived by the human eye. Light, as seen before, can be described as an electromagnetic wave but it can also be described as being comprised of discrete packets of energies without mass known as photons. Photons are described by Planck as having specific energies, E, which are dependent on the relation between the frequency, ν, of their electromagnetic wave through the Planck's constant, h, (h = 6.626 x 10^{-34} J s) as described by Equation 3.1.

$$E = h\nu = \frac{hc}{\lambda} \qquad \text{Equation 3.1}$$

The photon energy is also related to the Planck's constant through the speed of light (c, 2.998×10^8 m s^{-1}) and inversely related to the wavelength of its electromagnetic wave, also seen in Equation 3.1. This promotes an energetic gradient in light directly proportional to the changes in frequency of the electromagnetic wave, resulting in light decreasing in energy from UV light to visible light and then to IR light that is the less energetic of the three.

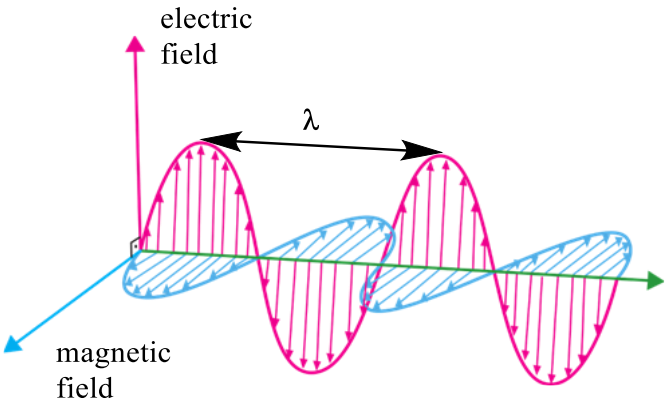

Scheme 3.1 – Electro-magnetic wave consisting of an oscillating magnetic field (in blue) perpendicular to the oscillating electronic field (in pink), both propagating in the same direction of the green axis.

Matter on the other hand, is a substance that has a specific mass and volume, and has for its component's protons, neutrons, and electrons. These particles that are the building blocks of matter have a different behavior than larger objects that are described by classic mechanics requiring a specific method, quantum mechanics, for their description.

These particles when combined together can produce atoms, different atoms have in their center nucleus comprised off different numbers of proton and neutrons, the former are positive and with the latter being neutral in charge, meaning that the nucleus has positive charge. For an atom to be neutral it requires that around the nucleus the electronic cloud be comprised of an equal number of electrons that have a negative electronic charge counterbalancing the positive charge of the nucleus. Similar to photons, electrons have a dual nature, which means that it is possible to describe their behavior as having characteristics of both

wave and particle. As mentioned earlier, these particles have a reduced size and mass, requiring the application of quantum mechanics for their description, were concepts such as particle-wave duality, the Heisenberg uncertainty principle, the quantization of energy, wavefunction and probability density appear and are used for the description of systems of a single or multiple particles. The wavefunction, ψ, is a fundamental solution of the Schrödinger equation used in the description of a quantum state of a particle or system of particles and how it evolves in time. Probability density, $|\psi|^2$, is the square of the absolute value of the wavefunction yielding the probability density of finding in a particular state of the system under study. The information provided from the probability density is the likelihood of observing a particle in a state with a specific value for the position, momentum, or energy.

Also, the Schrödinger equation can be applied for a specific atom like hydrogen that only has a single electron, we obtain a series of quantum numbers that describe the energy, shape, orientation in three-dimensional space of atomic orbitals (AOs) of the hydrogen atom. There are four quantum numbers and each of them describes a different property (energy, atomic orbital, orientation, and spin of the electron) and by combination of these different quantum numbers can be used to describe the quantum state where the electron exists. The first quantum number or principal quantum number, n, is described as a positive integer value (meaning that n=1, 2, 3, …) and arises from the solution of the radial partial differential equation of the Schrödinger equation and this value relates to the energy of each state. Next is the second quantum number or the azimuthal quantum number, l, described by the colatitude partial differential equation which collects all the angular dependent factors of the Schrödinger equation, the resulting values are related to the principal quantum number and can take *n-1* values, starting at 0 ($l = 0, 1,2,3, n-1$) and depending on the values of this quantum number the shape of the state (orbital) can be determined. The third quantum number or magnetic quantum number, m_l, relates to the former quantum numbers and takes the value of ($m_l = 0, \pm1, \pm2, \pm3, \pm l$) and describes the orientation of the orbitals described by n and l. The fourth quantum number or spin magnetic quantum number, m_s, is an intrinsic property of a particle that describes the orientation in which the electrons

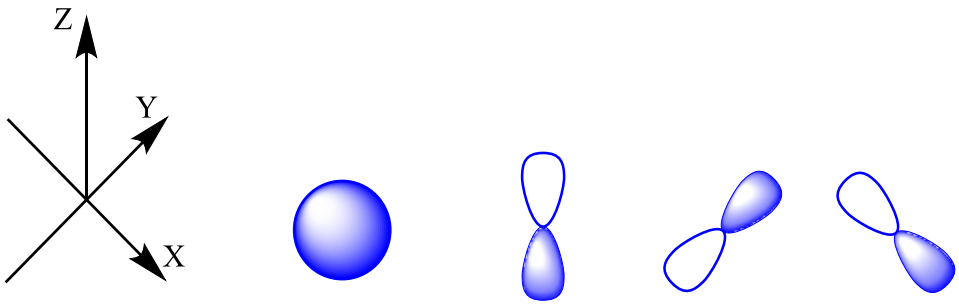

Quantum numbers	s	p_z	p_y	p_x
n	1, 2, ...	2, 3, ...	2, 3, ...	2, 3, ...
l	0	1	1	1
m_l	0	+1	0	-1

Scheme 3.2 – Schematic representation of s and p orbitals and the possible quantum numbers associated with each orbital. It's noteworthy the representation of orientation defined by the m_l resulting in the p orbitals being oriented along the X, Y, and Z axis.

angular momentum vector is oriented regarding an imaginary axis (this imaginary axis, will call it z-axis, can be produced using an external magnetic field resulting in the electrons adopting a parallel or antiparallel configuration). The spin quantum number is related to the spin magnetic quantum number by multiplying the spin magnetic quantum number value with the reduced plank constant, $\hbar$, resulting in equation 3.2.

$$s = m_s \times \hbar \qquad \text{Equation 3.2}$$

The spin quantum number, s, of a particle is a non-negative value (for the electron this value is s=1/2). When the value of spin is described as vectorial quantity along the z-axis, m_s will adopt values ranging from +s to -s, varying in integer increments. Each value of m_s will depict a different orientation that the vector describing the projection of the angular momentum that an electron can adopt with regard to the z-axis.

The magnitude of the spin is described as $\{s(s+1)\}^{1/2}\hbar$, so for electrons and when s=1/2 we observe that the vector obtained will have a magnitude of $\frac{\sqrt{3}}{2}\hbar$, and accounting for the orientation factor in regard to the z-axis, from Equation 3.2, will result in $s = \pm\frac{1}{2}\hbar$. Spin up (α *or* ↑) and spin down (β *or* ↓) are often used as terms denoting such spin orientation with the spin up referring to m_s =+1/2 and spin down to m_s =-1/2, respectively. In a system of multiple electrons, e.g., a system with two coupled electrons, there will be a combination of spin values of the electrons in a total spin value for the system, being a combination of orientation that the various particles can adopt yielding the total spin quantum number, S, that can be obtained using the Equation 3.3:

$$S = s_1 + s_2, s_1 + s_2 - 1, \ldots, |s_1 - s_2| \qquad \text{Equation 3.3}$$

where s_1 *and* s_2 are the spin quantum number of each individual electron. So, in the given example, for two electrons there are two possible values for the total quantum spin, S=0 (singlet state, with one electron in +1/2 orientation and another in -1/2) and S=1 (triplet state, with both electrons with the same m_s). Spin multiplicity, M, describes the number of possible configurations in a system of multiple particles and is described by Equation 3.4,

$$M=2S+1 \qquad \text{Equation 3.4}$$

with S the total spin multiplicity. When S=0 there is only one possible configuration (M=1) of the spins, however if S=1 then there will be three possible configurations (M=3) for the two particles spins. The total magnetic quantum number, M_S, will have values comprised between S and $-S$ and will describe the different possible orientations obtained for each configuration of the spin multiplicity of the total spin. So, when S=0 with M=1 there is only one configuration possible (M_S=0) and when S=1 with M=3 then there will be three possible orientations (M_S=-1, 0, +1). In some cases, higher values of S are possible (e.g.: S=2) when the system under study possesses multiple electrons resulting in an even bigger set of orientation being possible.

In a quantum system these four quantum numbers can describe the possible state (or orbital) with a specific energy, shape and orientation in space where an electron can exist in an atom and the spin that this atom possesses. Two electrons in the same atom can't be described by the same four quantum numbers. The Aufbau principle dictates how the electrons populate the atoms orbitals, starting from the lowest energy to the highest energy orbital. As each orbital can only contain two electrons as per the Pauli exclusion principle (that states that no two particles that are described by a half-integer spin cannot occupy the same quantum state) resulting a need for the two electrons to have different spin values to be paired in the same atomic orbital (these two particles will only differ in their spin magnetic quantum number). When an atom has an open shell configuration the last orbitals will have a degenerate nature. In this case, and in accordance with the Hund's rule, the electrons will populate each individual orbital with one electron each before pairing them in the same orbital. This reduces the overall energy of the system by reducing the repulsion between the electrons in the same orbital.

Linear combinations of AOs produce molecular orbitals (MOs), and they describe molecular electronic structure. MOs are ruled over by the same principles as the AOs. When considering the reactivity of molecules and the capability of the molecule to interact with light, two orbitals have especial importance, first the HOMO that stands for highest occupied MO and LUMO that stands for lowest unoccupied molecular orbital.

To better understand electronic transitions, one must understand the influence that light, as an electromagnetic wave, has on electrons, as negatively charged particles that are susceptible to perturbations produced by said wave resulting in changes at the atomic and molecular level. If the result of the irradiation of an atom or molecule by light produces a significant perturbation on the wavefunction (ψ_1) of an electron in the ground state resulting in ψ_1 having a high constructive overlap with wavefunction (ψ_2) of a higher state, then the transition is probable. Then again, for the transition to occur the photon absorbed by the electrons must have sufficient energy as to surmount the energy gap necessary to populate the excited state. Then the molecule, if the transition in fact occurs, will leave the ground-state to populate an excited-state, leaving the ground state orbital

with one electron and the excited state orbital with another resulting in a state with two unpaired electrons. This probabilistic effect is explained by the Fermi Golden rule, Equation 3.5,

$$k \propto \rho = \langle \psi_1 | P | \psi_2 \rangle^2 \qquad \text{Equation 3.5}$$

where the k is the rate of the transition from state 1 to state 2 of different energies respectively described by ψ_1 and ψ_2, ρ is the density of states that represent favorable (or constructive) overlap of ψ_1 and ψ_2; P describes the perturbation applied on the system that induces the described transition. From the absorption of a photon, the electron density in a molecule or atom will produce a transition dipole moment that results from the electrons interaction with the electric field of the absorbed photon promoting a fluctuation in the electronic cloud. It's through coupling that such perturbation occurs altering the dipole momentum of the particle, but the transition is only possible if this transition dipole momentum orientation is aligned with the electric field of the photon. Large fluctuation in the electronic cloud result in large transition dipoles, that consequently result in a higher probability of the transition of occurring.

This transitions from the ground state to higher excited states tend to occur, in organic molecules, from the HOMO to the LUMO as referred earlier. The energy associated to such transitions is commonly observed in photons ranging, in the electromagnetic spectrum, from the near infrared region throughout the visible region and sometimes close to the ultraviolet region. This results in the general notion that for electronic transitions of organic molecules the visible spectrum is of outmost importance as it will be in this region that most of the process will be assessed and studied. In the following section the behaviour of molecules, as well as the processes that molecules undergo in the excited state, will be discussed.

3.2. Photoinduced processes

A Jablonski diagram, Scheme 3.3, can be used to schematically depict the various photoinduced processes that molecules might undergo. In general, most

molecules are found in the ground state (in S_0 configuration), but when exposed to light, the photons impacting and exchanging energy with the molecule's electrons may have sufficient energy to promote an electronic transition, causing the electron to populate a higher energy state (excited state, S_n with $n \geq 1$) this process is called absorption. Each electronic state can also be divided into a set of vibrational states as these states describe atomic motion in the molecule. When an electron undergoes electronic transitions, such as absorption or emission, frequently, these transitions occur from the lowest vibrational level of the starting electronic state and transit to a higher vibrational level of the final electronic state. Known as the Frank-Condon principle it depicts that during an electronic transition, that occurs in a relatively instantaneous manner when compared to the nuclear motion of the atom, is more likely to occur when the nuclear position has little to no change for the starting and the final vibrational energy levels, meaning that the two vibrational wavefunction describing each of these vibronic energy levels have a significant constructive overlap. In some cases, molecules are also excited beyond the first excited energy state (S_n or T_n, with $n>1$, e.g., S_2) but from these states the molecules in general tend to return, in a rather quick manner, to the lowest energy electronic excited-state S_1 or T_1. This relaxation may occur through internal conversion (IC), which is the dissipation of electronic energy by converting it to vibrational and rotational energy, as well as vibrational relaxation (VR), in which the excited vibrational state decay to the ground vibrational state of said excited electronic state by interacting with the environment or by converting their energy to other degrees of freedom in the molecule. These two relaxation mechanisms promote the dissipation of excess energy, allowing the molecule to return to its lowest energy vibronic and electronic state. They are non-radiative relaxation processes (processes that do not convert energy in photons). According to Kasha's rule, the radiative relaxation process in molecules, where the energy is dissipated by the emission of photons, generally occurs in an appreciable yield from the S_1 and T_1 states.

When the relaxation occurs from S_1 to S_0 it can take both the radiative and nonradiative pathway. The nonradiative decay pathway to S_0 occurs in a similar manner to the relaxation of S_n (with $n>1$) to the S_1 state, through IC and VR as referred earlier. The radiative decay pathway from a singlet state is called

fluorescence and results in the emission of a photon. In some cases, the first singlet excited state can undergo a process called intersystem crossing (ISC), through spin-orbit coupling interaction, a change in the spin value (spin-flip) on the excited electron resulting in the transformation of the S_1 state to a T_1 state. ISC is a nonradiative process that occurs between two states of different multiplicity which makes it spin-forbidden. As spin angular momentum changes, the orbital angular momentum needs to compensate for this transition through coupling. This process of spin-orbit coupling is dependent on the total angular momentum (the sum of orbital and spin angular momentums) of the molecule and its magnitude is proportional to the Z^4 (Z is the atomic number and corresponds to the number of protons in the atom). This proportionality describes an increase in the spin-orbit coupling induced by the presence of heavy atoms (i.e., whose atomic number is large, for example Br, Pb) in the system. This effect can be internal, when the molecule under study includes heavy atoms in their molecular structure or external, when the molecules are influenced by the presence of heavy atoms in the surroundings, such as heavy atoms bearing solvent. In both cases the presence of a heavy atoms carrying large orbital angular momentums will strengthen the spin-orbit coupling in the chromophore increasing the likelihood of spin forbidden process such as ISC of occurring.[1–4]

From the triplet state, molecules can also undergo radiative and nonradiative relaxation to the ground state. However, this transition is spin-forbidden and as there is a need for a spin-flip to occur, the resulting relaxation process to the ground state will take longer to be achieved. In a nonradiative relaxation from T_1 occurs first through ISC and then followed by VR.

The radiative relaxation from the T_1 is known as phosphorescence, and then again, according to Kasha's rule, occurs from the lowest vibrational state of T_1. Even if this transition is a spin-forbidden the molecule can still emit photons from this state as the spin-orbit coupling that ensured the population of T_1 once again increases the probability of such forbidden transitions.

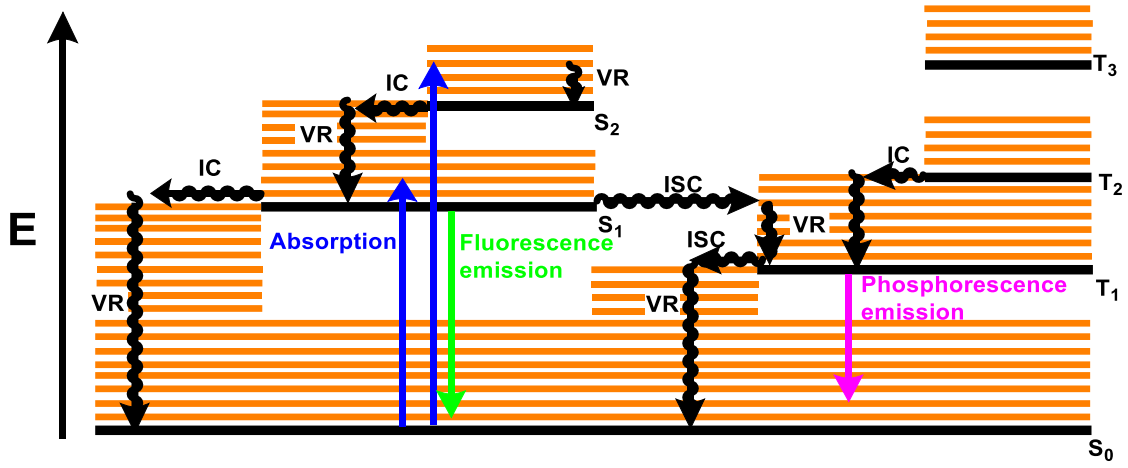

Scheme 3.3 - Photophysical processes such as absorption, fluorescence, phosphorescence, internal conversion (IC), vibrational relaxation (VR), and intersystem crossover (ISC) are all depicted in the Jablonski diagram. Black lines represent electronic energy levels, whereas orange lines represent vibrational energy levels. S_n and T_n represent the singlet and triplet states, respectively. Straight and undulated arrows show radiative and non-radiative transitions, respectively.

In terms of rate constants, fluorescence is faster than phosphorescence as it normally occurs in a few nanoseconds ($10^{-9}s$) compared to a few microseconds ($10^{-6}s$) to seconds for the later process. By determining the rates of all relaxation processes that a molecule can undergo one can understand the behavior of a molecule in its excited-state and the predominant mechanism of deactivation of the excited state. A molecule that transitions from its ground state to higher electronic state tends to return to it by dispersing the excess energy from the excited state. In accordance with the principle of conservation of energy, the energy difference between the excited and ground state will be equal to the sum of the energies lost during each relaxation process. The sum of the yields for all the decay processes possible will be equal to 1 meaning that there is always a probability of describing the systems decay through one of said relaxation processes ($\phi_F + \phi_{ISC} + \phi_{IC} = 1$). The probability of a molecule of emitting fluorescence is described by the fluorescence quantum yield, ϕ_F, and this value is described by equation 3.6, were the k_F is the rate of radiative decay representing the number of photons emitted by

fluorescence, the k_{nr} is the rate of nonradiative relaxation corresponding to the sum of all nonradiative decays (ISC and IC).

$$\phi_F = \frac{rate\ or\ Nº\ of\ emited\ photons}{rate\ or\ Nº\ of\ photon\ absorption} = \frac{k_F}{\sum k_{nr} + k_F} \qquad \text{Equation 3.6}$$

Fluorescence quantum yield, ϕ_F, is a process that determines how many photons are emitted from S_1 state and is written as the ratio of the number of photons absorbed to the number of photons emitted by the molecule or chromophore. The ϕ_F has values in between 0 and 1 but since there are always nonradiative processes undergoing this value is never reaches unity. In the simplest of cases, the emission of fluorescence decays in a mono exponential manner and the time it takes for the depopulation of the first excited state to occur is given by the fluorescence lifetime or the lifetime of the first excited singlet state, τ_{S_1}. The τ_{S_1} is inversely proportional to the rates of deactivation of that state (Equation 3.7), meaning that the energy of the excited state can decay in a nonradiative manner (ISC and IC) or through fluorescence emission. The relation between the ϕ_F and τ_{S_1} can also be established as seen bellow:

$$\tau_{S_1} = \frac{1}{\sum(k_{nr}) + k_F} = \frac{\phi_F}{k_F} \qquad \text{Equation 3.7}$$

This expression gives us the mean time that the molecule under study will occupy this excited state before decaying. The ϕ_F and τ_{S_1} are two important parameters used to describe the S_1 state and its deactivation behavior and can be obtained experimentally. The τ_{S_1} can be obtained by fitting an exponential decay function to the observed fluorescence decay, while the ϕ_F can be quantified using two distinct methods, the absolute and the relative methods.

The absolute method consists in the direct quantification of the fluorescence quantum yield by the variation of the number of absorbed/emitted photons requiring the use of an integration sphere to quantify the intensity of the fluorescence emission. While the relative method uses a reference compound with

a well established ϕ_F value to which the sample will be compared. Equation 3.8 shows the fluorescence quantum yield equation for the relative method used during this work.

$$\phi_{F,Sample} = \phi_{F,ref}\left(\frac{Abs_{ref}}{Abs_{sample}}\right)\left(\frac{I_{sample}}{I_{ref}}\right)\left(\frac{n_{sample}}{n_{reference}}\right)^2 \qquad \text{Equation 3.8}$$

where the $\phi_{F,ref}$ is the fluorescence quantum yield of the known reference. The Abs_{ref} and Abs_{sample} are the absorption at the excitation wavelength of the reference and of the sample, the I_{ref} and I_{sample} are the integrated values for the fluorescence emission obtained for the reference and the sample, and the n_{ref} and n_{sample} are the refractive indexes of the solvent used in the reference and sample, respectively. In general, the samples are degassed, and the Abs_{ref} and Abs_{sample} are measured then the sample can be excited at the set wavelength obtaining the I_{ref} and I_{sample}.

3.2.1. Absorption features of porphyrins

Porphyrins are a spectacular chromophores and their structure consists of four pyrrole rings linked to one another through methine groups producing a cyclic aromatic macrocycle. From their aromaticity, the porphyrin has 18-π electrons in its conjugated system delocalized throughout its structure. This characteristic ensures that the porphyrin has a strong absorption across a broad range of wavelengths, generally absorbing from 400 to 750nm. This absorption is very characteristic to this kind of macrocycle and was described by many but most noteworthy was the work done by *Gouterman*.[5–8] He proposed that in the case of free-base porphyrins their absorption profile came from their conjugated electronic system, more precisely from their π-π transitions, that would be produce from the four molecular orbitals, that *Gouterman* labeled as b_1, b_2, c_1, and c_2. The b orbitals correspond to the highest occupied molecular orbitals (HOMO and HOMO-1) and have two types of symmetry a_{1u} and a_{2u} while the c orbitals correspond to the lowest

unoccupied molecular orbital (LUMO and LUMO+1) and have e_g symmetry, their representation can be seen in Scheme 3.4.

The absorption spectrum profile is characterized by having several absorption bands, *Platt* characterized them as Q-bands for the lower energy ones and B-band (or Soret band) for the higher energy one.[9,10] *Gouterman* also says that the B band of higher intensity near the ultra-violet region (around 400nm range) originates from $b_2 \rightarrow (c_1,c_2)$ allowed transitions and can have two transition split states, B_X and B_Y, taking into account the direction from which the transition occurs to the excited state. This directional factor is obtained by dividing the porphyrin plane in a x and y axis (with a slightly distorted perpendicular overlap of the axis that is produced by a small distortion along the porphyrin plane) over which each corresponding transition will proceed. The four Q bands with lower intensity (around 500-750 nm) originate from $b_1 \rightarrow (c_1,c_2)$ forbidden transitions, and in a similar manner to the previous bands, will also have split transition states, namely Q_X and Q_Y. Deriving from this notion, and from the fact that when the porphyrin is excited from its fundamental state (and consequently from its lowest vibrational level) to the lowest vibrational level of its excited state we can represent the bands as $B_X(0,0)$, $B_Y(0,0)$, $Q_X(0,0)$ and $Q_Y(0,0)$. Sometimes the transition occurs with a consistent vibronic energy separation from the fundamental vibronic state, (0,0), producing a vibronic overtone which in consequence produces splitting in the Q bands that can be characterized as $Q_X(1,0)$ and $Q_Y(1,0)$.

In general, the absorption spectrum profile of the free-base porphyrin only presents a single B-band resulting from the overlap of the B_X and B_Y transition. Also in recent accounts, the complex nature of the electronic transition has seen a lot of attention, especially for the B band, for the possibility of mixing transitions produced by vibronic coupling that may complicate its understanding.[11,12]

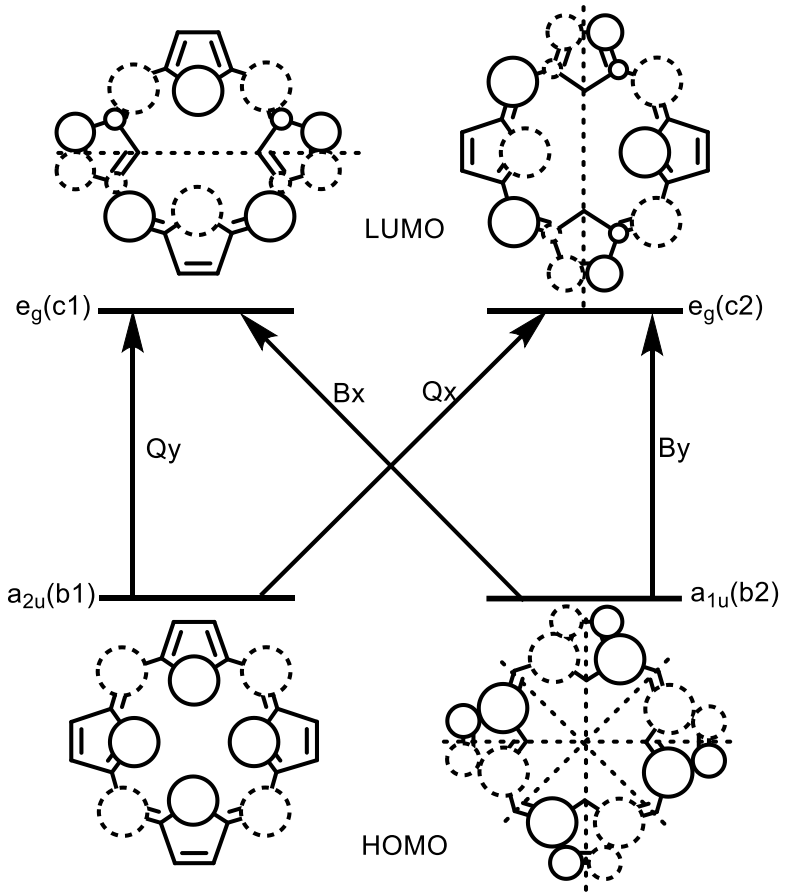

Scheme 3.4 – A) Adapted representation of *Gouterman's* proposed porphyrin Molecular Orbitals (HOMO and LUMO) for D_{4h} symmetry with the nodes being represented by dashed lines.[5]

Metalloporphyrins arise from the insertion of transition metals in the porphyrins core, this insertion produces a change in the symmetry of the macrocycle from a D_{2h} to a D_{4h} symmetry, as seen in Scheme 3.5. In agreement with the change in the symmetry, the d-orbitals of the metal will interact through coupling with the π-electronic system of the macrocycle, promoting: (i) a planar structure; (ii) and change in the energy of the orbitals producing degenerate orbitals, meaning that the x and y polarized transitions will be equal, resulting in a single B band and two Q bands (Q(0,0) and Q(1,0)).

The type of metal that would be inserted would be characterized by *Gouterman* as "open shell" or "closed shell" metal depending on its valence electrons. A "closed shell" metal has the last orbital completely empty (in the case of d^0 e.g., Ba^{+2}) or completely full (in the case of d^{10} e.g., Cd^{+2}) while an "open shell" metal has

incomplete valence with paired (diamagnetic d^8 e.g., Pd^{+2}) or unpaired electrons (paramagnetic d^9 e.g., Cu^{+2}). The "closed shell" metal will exhibit spin-orbit coupling but to a smaller degree when compared to the "open shell" metals that have incomplete orbitals. The "closed shell" metals spin-orbit coupling will depend mainly on the atomic number of the metal, as referred to earlier. Metal such as Mg have small spin-orbit coupling resulting in a strong fluorescence and weak phosphorescence, on the other hand the Ba has a high atomic number leading to a strong spin-orbit coupling resulting in weak fluorescence and strong phosphorescence emission. The "open shell" (d^n with $1 \leq n \leq 9$) metals can have an incomplete valence with paired electrons, such as palladium, where the phosphorescence emission is enhanced by spin-orbit coupling on the $\pi-\pi$ transitions populating the lower laying triplet state. In the case of "open shell" metals with unpaired electrons a charge transfer state can occur, since these metals are good electron acceptors and by interacting through coulombic exchange with it the porphyrins fluorescence is quenched by enhancing nonradiative transitions. "Open shell" metal atoms can also promote two different effects in the spectral profile of the porphyrins, a bathochromic shift or an hypsochromic shift. The word bathochromic is derived from the prefix "Batho-" which derives from the Greek *"bathys"* meaning "deep" and the suffix "-chromic" derived from the word *"chroma"* meaning color, the phenomenon is described as color change and a shift in the molecule's spectral bands to a higher wavelength. One such shift is also known as a red-shift and can be observed by introducing in the porphyrin atoms, such as, manganese(III) and tin(II). On the other hand, hypsochromic derives from the prefix "hypso-" from the Greek word *"upsos"* which translated means "height", and contrary to the bathochromic shift, will produce a band shift to lower wavelengths, resulting ultimately in the change of the color of the molecule and its spectroscopic properties. This shift is also commonly known as a blue-shift and can be obtained by incorporation of atoms like palladium(II) and platinum(II) in the porphyrin core.

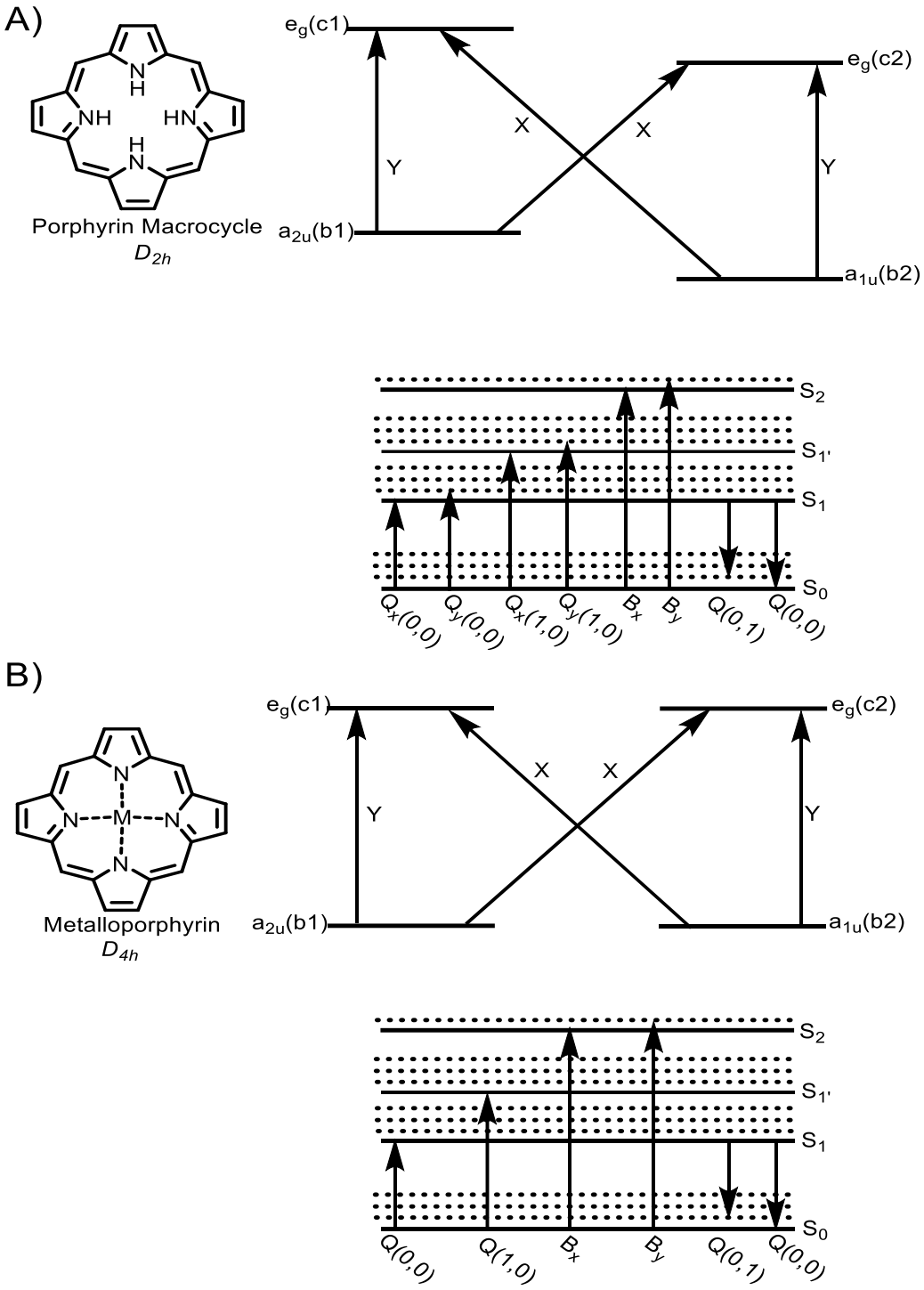

Scheme 3.5 – Adapted representation of *Gouterman*'s proposed four orbital model and proposed diagram for the excited energy states that occur from the transition between the porphyrins orbitals for (A) free-base porphyrin and (B) metalloporphyrin.[5]

3.2.2. Spectroscopic and photophysical measurements

After the synthesis of the free-base porphyrins and respective metalloporphyrins the work continued by performing a spectroscopic analysis of the compounds. The metalloporphyrins are to be used as photosensitizer in a formulation of a TTA-UC system, thus, the purity of the compounds must be guaranteed to reduce the probability of any unwanted chromophores the system that could influence the desired photophysical effect. After the synthesis and purification of the compounds the fluorescence emission and excitation spectra were collected to ascertain the presence of the desired metalloporphyrin. It's worth mentioning that two distinct methods were used in the synthesis of the metalloporphyrins, as referred in Chapter 2, the DMF and the acetonitrile method. The latter method was employed as the main synthetic procedure since it produced the desired compound without free-base porphyrin impurity. The purity of the metalloporphyrins was proven spectroscopically, see Chapter 6.2.

The characterization of the TTA-UC system's sensitizers starts by considering the absorption spectrums of the free-base porphyrins and their metalated equivalents as seen in Figure 3.1, and determining the correlation between its concentration and absorption through the Beer-Lambert law:

$$A(\lambda) = l * C * \varepsilon(\lambda) \qquad \text{Equation 3.9}$$

with $\varepsilon(\lambda)$ the molar extinction coefficient (mol cm-1 L^{-1}) at a wavelength λ (nm), C the concentration in solution (mol/L), l the optical path and $A(\lambda)$ is the absorption. From this equation (3.9) a fundamental relation between the concentration of a chromophore molecule in solution and the quantity of light absorbed is established. Also, from this equation the molar extinction coefficient is determined specific chromophore under study.

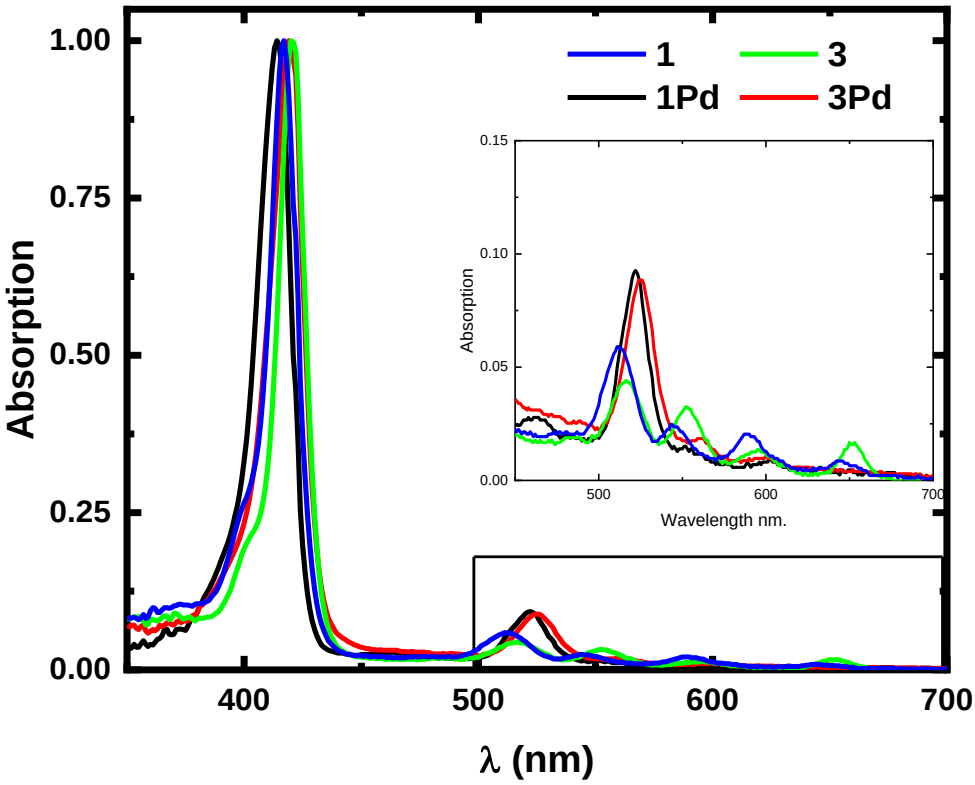

Figure 3.1 – Room temperature absorption spectra for the investigated porphyrins in 2-methyltetrahydrofuran (in inset a zoomed area where the Q-bands are easily distinguishable).

To obtain the molar extinction coefficient for the various porphyrins, individual solutions were prepared with known concentrations of chromophore. For each solution several spectra with different concentration but with the same volume were taken. The plot of the absorbance (λ) vs. chromophore concentration were fitted with a first order for the equation, with the slope yielding the molar extinction coefficient (see annex 6.1). The results for the free-base porphyrins synthesized in this work are presented in Table 3.1 and the results for the metal bearing corresponding porphyrins can be seen in Table 3.2.

This constant determines the quantity of light that a chromophore under study can absorb at a set wavelength. This constant is not only dependent on the compound under study it also depends on the condition applied to the system such as the solvent used, the pH of the solution, the temperature and the concentration.[13–15]

Table 3.1 – Molar Extinction Coefficient (ε) of free-base porphyrins, obtained in the wavelengths of the corresponding band peaks in 2-MeTHF solution.

	λ_{max} (nm), ε(L.mol^{-1}cm^{-1})				
Compound	**B(0,0)**	**Q_y(1,0)**	**Q_y(0,0)**	**Q_x(1,0)**	**Q_x(0,0)**
1	(416nm)	(512nm)	(545nm)	(588nm)	(644nm)
	2.1×10^5	**1.7×10^4**	**8.0×10^3**	**7.2×10^3**	**3.7×10^3**
3	(420nm)	(517nm)	(553nm)	(596nm)	(650nm)
	3.7×10^5	**1.1×10^4**	**9.8×10^3**	**4.4×10^3**	**4.8×10^3**

Table 3.2 - Molar Extinction Coefficient (ε) of palladium(II)porphyrins, obtained in the wavelengths of the corresponding band peaks in 2-MeTHF solution.

	λ_{max} (nm), ε(L.mol^{-1}cm^{-1})		
Compound	**B(0,0)**	**Q(1,0)**	**Q(0,0)**
1Pd	(414nm)	(522nm)	(552nm)
	5.8×10^5	**2.2×10^4**	**1.8×10^3**
3Pd	(419nm)	(525nm)	(561nm)
	6.1×10^5	**2.1×10^4**	**2.0×10^3**

From the analysis of the absorption spectra, in Figure 3.1, of the free-base porphyrins it is noted that the TPP and Tri-Alkyl have a similar spectrum with the Soret band (corresponding to $S_0 \rightarrow S_2$ transitions) being found at 416 and 420 nm, respectively.

The introduction of the electron donating groups (alkoxy- and hydroxyl-groups) in the para-positions of the porphyrin core is responsible for the bathochromic shift and increase in the molar extinction coefficient of the Soret band, going from the **1** to the **3** derivative.[16,17] This effect result from the lowering of the energy barriers between the ground and excited states by lowering the energy gap between the HOMO and LUMO orbitals.[16–18] This effect seems to originate from the oxygen groups, these electron donating groups have nonligand electrons that can be delocalized to the macrocycle of the porphyrins promoting the observed band shift. From the literature[16,19] it can be seen that alkyl chains don´t seem to meaningfully impact the absorption spectrum of porphyrins proving that most likely the effect on

the absorption of the porphyrin comes from the oxygen atom alone. With the insertion of palladium in the porphyrin a small blue-shift for the Soret-band, of about 1 to 2 nm, is observed when compared to the free-base porphyrins absorption spectra (Figure 3.1). Moreover, the Q band after metalation, as described earlier, will degenerate from four bands to only two Q(1,0) and Q(0,0), see Table 3.2. Palladium(II) with an electronic configuration of [Kr] $5s^0$ $4d^8$ and a diamagnetic nature (as $(d_{xz}\ and\ d_{yz})^4$ $(d_{xy})^2$ and $(d_{z^2})^2$ orbitals are fully filled leaving the $(d_{x^2-y^2})^0$ orbital unfilled) form a closely packed coordination complex with the porphyrin ring resulting in a square planar configuration, as the porphyrins acts as a tetradentate ligand with the metal in its center. The blue-shift in the absorption spectra after complexation has its origin in the strong interaction between the electrons in the d-orbitals of the metal (d_{xz} and d_{yz} orbitals), which are perpendicular to the porphyrin ring, and the $e_g(\pi^*)$ orbital of the porphyrin. This results in the increase of the energy gap between the HOMO and LUMO orbitals promoting the observed spectral shift to higher energies.[6,20,21] One more aspect observed from the absorption spectra is the low ratio of the Q bands (Q(0,0)/Q(1,0)) that results in the Q(1,0) band being much more pronounced than its Q(0,0) counterpart. This effect originates from the energy difference from the S_0 ground state to the S_1 excited state, as by having a very similar energy or being almost degenerated, resulting in their transition dipoles nearly canceling out and the near disappearance of the Q(0,0).[20]

Following the analysis of the sensitizer absorption characteristics the focus shifted to the characterization of the fluorescence emission spectra under atmospheric air and degassed conditions for the solutions of **1Pd** and **3Pd** in 2-MeTHF which were in agreement with the reported literature, and are presented in the Figure 3.2.[22–24] In Figure 3.2 A), the luminescence spectrum at atmospheric oxygen conditions has a similar profile for both porphyrins whit one emission band with two peak maxima. **1Pd** has its peak maxima at 560 and 608 nm while the **3Pd** has its maxima at 569 and 613 nm, with a short red shift when compared to the latter which were associated to the palladium porphyrin small residual fluorescence emission corroborated from the literature.[24–26] On closer inspection of the luminescent spectrum a very small emission band appears in both

metalloporphyrins at higher wavelengths (higher than 675nm), this band was assigned to room temperature phosphorescence that wasn´t fully quenched by the molecular oxygen in solution. Further in this work, studies of oxygen singlet generation by 2-MeTHF solution of the metalloporphyrins under atmospheric oxygen conditions were conducted that validate this claim.

Although small the fluorescence quantum yields for both metalloporphyrins were quantified using the comparative method, with TPP in toluene as the reference (ϕ_F=0.11) resulting in values of 1.83×10^{-4} and 2.17×10^{-4} for **1Pd** and **3Pd**, respectively.[22,25,27,28] The fluorescence lifetimes were not quantified since the small intensity of the signal was not picked-up by the experimental apparatus detector.

Following the investigation of the triplet-state dynamic, taking a closer look at the phosphorescence, its lifetimes, the singlet oxygen generation, and the transient absorption spectra of the synthesized metalloporphyrins. In figure 3.2 B), the spectra of the metalloporphyrins solution purged of molecular oxygen can be seen, were the room-temperature phosphorescence is revealed. The profiles for the phosphorescence emission of both porphyrins are relatively similar to what is found in the literature resulting from $T_1 \rightarrow S_0$ transition (resulting from the low-lying state ($\pi\pi^*$)).[26,29] Both **1Pd** and **3Pd** had very intense phosphorescence emission with peak maxima at 696 and 771nm and at 715 and 783 nm, respectively. The observed red-shift in the phosphorescence emission of **3Pd** when compared to **1Pd** is assigned to the electron donating nature of the oxygen groups found in the *para*-position of the **3Pd** derivative, since these substituent groups tend to reduce the energy gap between the HOMO and LUMO states by increasing the electronic density and energy of the HOMO orbital, while the energy of the LUMO orbitals remains unchanged.[17,18]

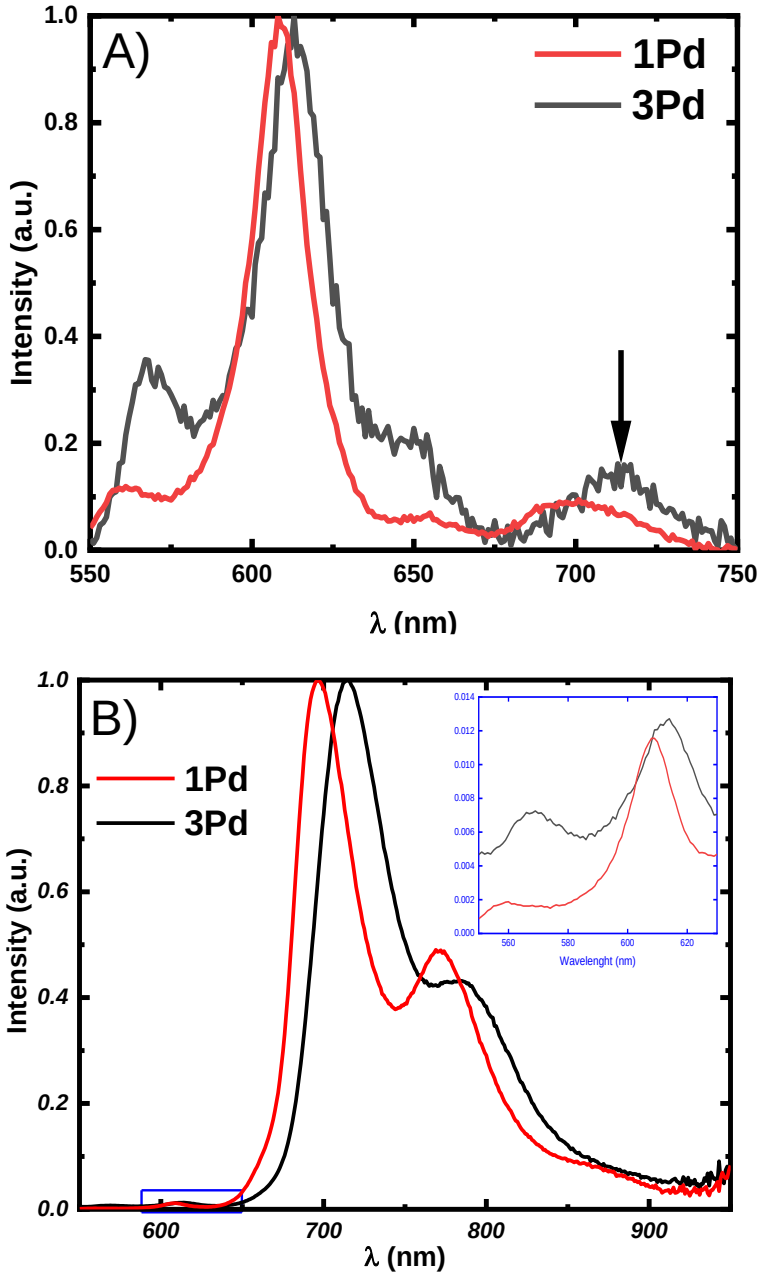

Figure 3.2 – Room temperature photoluminescence spectra for the investigated porphyrins in 2-MeTHF solution (A) under atmospheric air (arrow signals a small room temperature phosphorescence emission peak not being fully quenched by atmospheric oxygen); (B) under nitrogen degassed conditions (in inset the residual fluorescence emission).

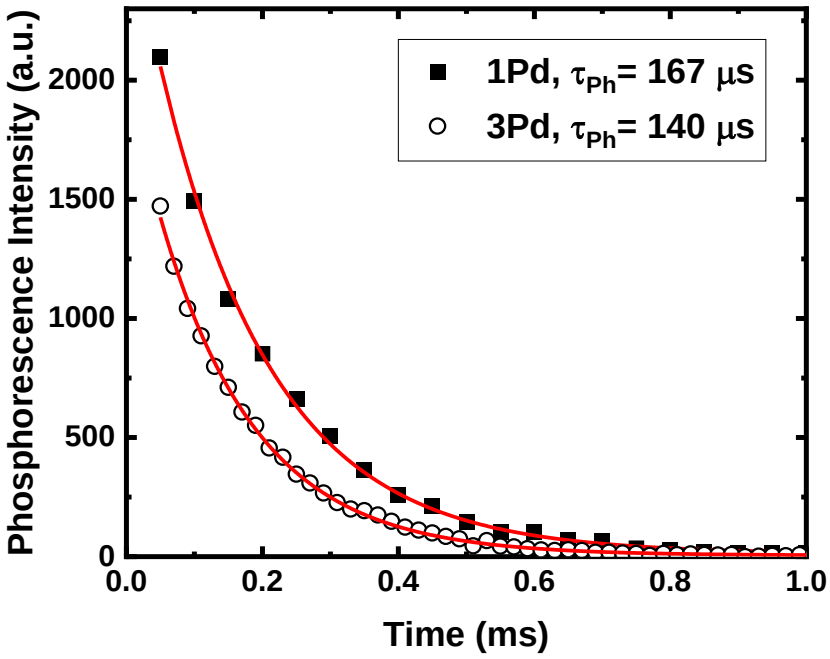

Figure 3.3 – Room temperature phosphorescence decays for the investigated porphyrins in N_2 degassed 2-MeTHF solutions collected at the corresponding phosphorescence emission maximum.

The **1Pd** has a phosphorescence lifetime of 167 μs and **3Pd** has a phosphorescence decay of 140 μs and can be seen in Figure 3.3. The phosphorescence lifetimes obtained for the investigated porphyrins samples remain approximately constant. Nonetheless, the small observed difference can fall in the experimental error, the smaller phosphorescence lifetime of the **3Pd** could be attributed to non-radiative relaxation interaction that the bulkier porphyrin has with the solvent. Indeed as previously reported the solvent also decreases the luminescence quantum yields apart from the lifetimes since it promotes the non-radiative relaxation of the chromophore, and this effect increases with the polarity of the solvent.[30] The room temperature phosphorescence lifetimes for **1Pd** were reported to be 208.5 μs[31] and 401 μs[32] in degassed 2-MeTHF and toluene solutions, respectively. Thus, in good agreement with the values obtained in the present study.

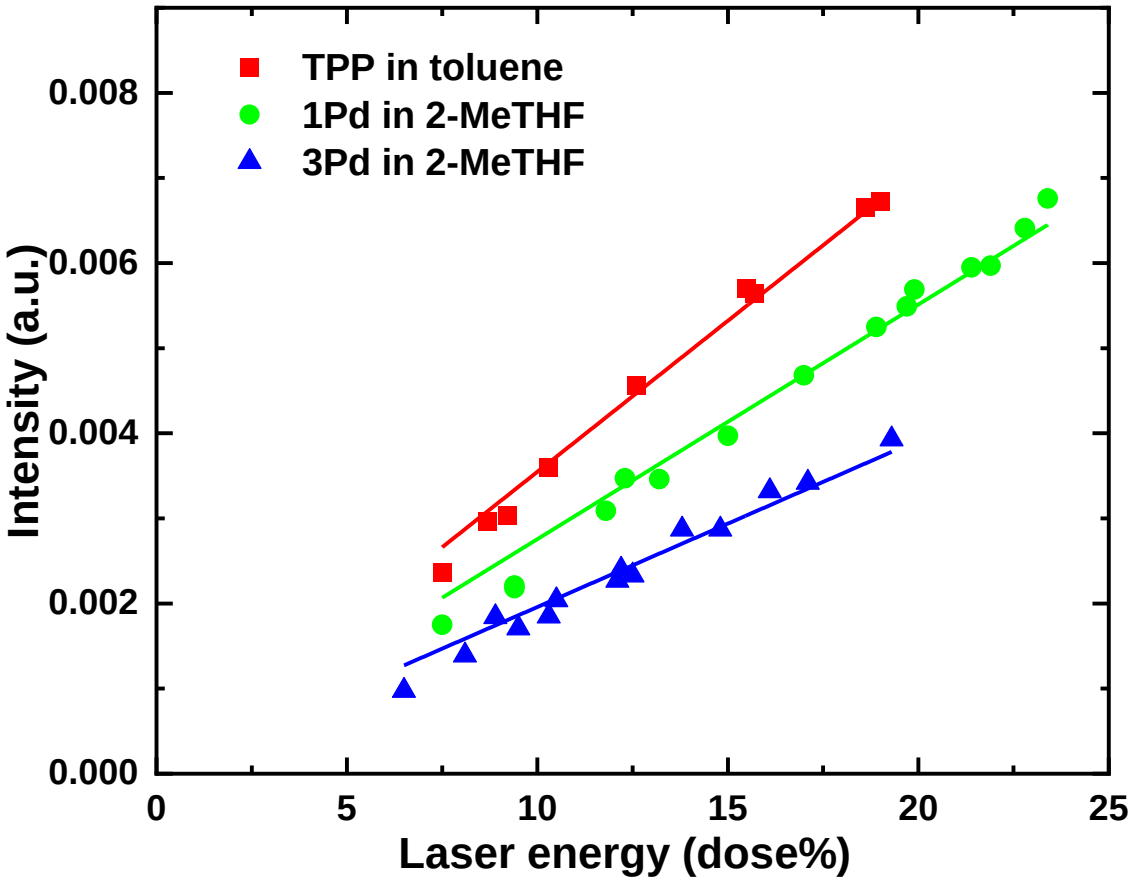

Figure 3.4 – Singlet oxygen phosphorescence measurements collect with excitation at 355 nm and emission at 1270 nm for the palladium porphyrins under study and the reference compound TPP in aerated 2-MeTHF and toluene solutions, respectively.

Singlet oxygen photosensitization quantum yields for the metalloporphyrins were obtained following laser irradiation at 355 nm of aerated 2-MeTHF solutions of the compounds and comparing the singlet oxygen phosphorescence signal with that generated by photosensitization of a reference compound (TPP in toluene, $\phi_\Delta = 0.66$)[33] see Figure 3.4. The obtained values for **1Pd** and **3Pd** are $\phi_\Delta = 0.46$ and $\phi_\Delta = 0.30$, respectively. These values are far lower than the values reported in the literature for similar palladium porphyrins ($\phi_\Delta = 0.90$)[34] in CH_2Cl_2 demonstrating that the singlet oxygen photosensitization efficiency ($S_\Delta = \frac{\phi_\Delta}{\phi_T}$) is not unitary. These findings support the observation of room temperature phosphorescence emission in the aerated solutions of the metalloporphyrins, Figure 3.2 A).

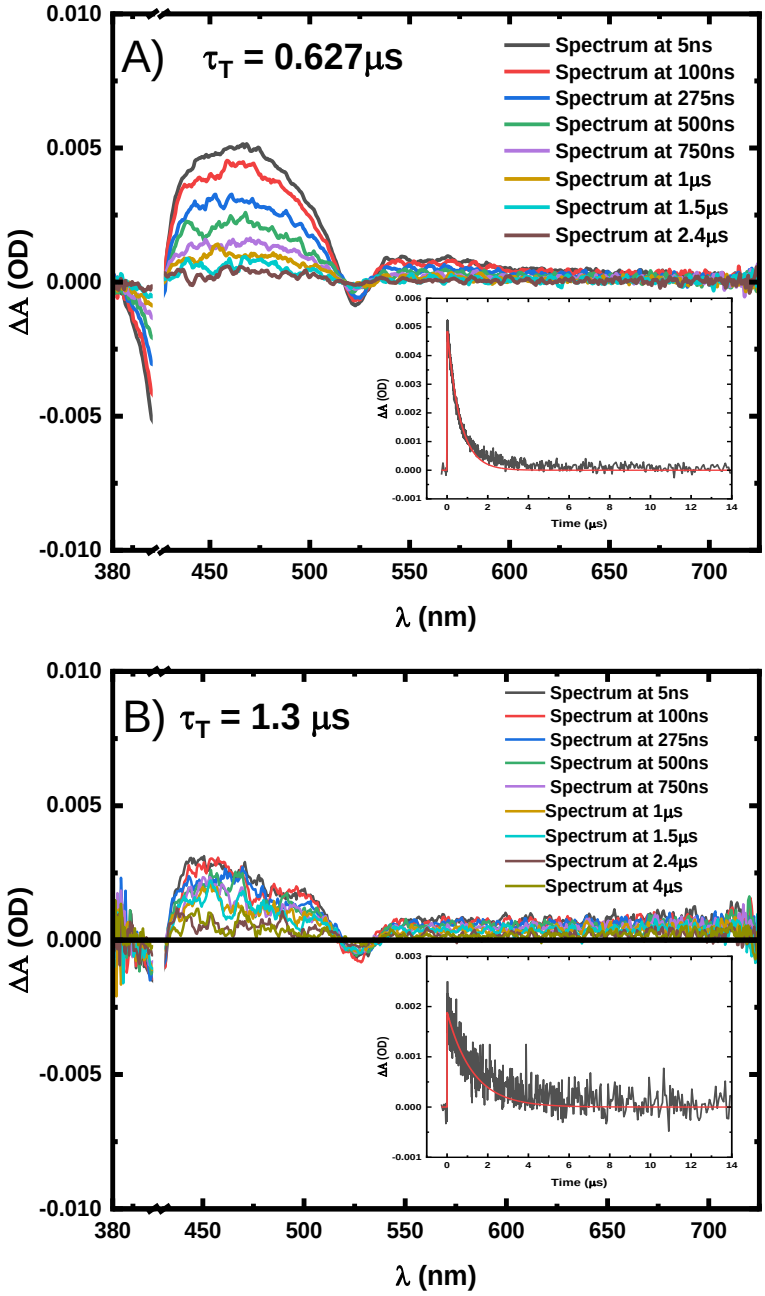

Figure 3.5 – Nanosecond time-resolved transient absorption data for a) **1Pd** and b) **3Pd** collected with excitation at 420nm (the gap between 400 and 431nm was made to limit the instrumental influence on the data). In inset presents the transient absorption decay collected at 461 nm.

To better understand the excited state dynamics of the sensitizers, the molecules were studied by nanosecond-transient absorption spectroscopy. The data obtained for the studied porphyrins in 2-MeTHF degassed solutions can be seen in Figure 3.5. The transient absorption experiment for a pure sample of **1Pd**

revealed a triplet-triplet absorption bands in the range 428-516 nm and 532-700nm, together by a negative signal in the 516 – 532 nm range, attributed to the ground-state absorption of the Q-band of these derivatives. The signal intensity variation over a period of time can also be observed at a specific set wavelength, we choose the triplet-triplet maximum at 465nm and at 457nm for **1Pd** and **3Pd**, respectively. The triplet lifetimes of the referred triplet-triplet maximum were 627 ns and 1.3 μs for the **1Pd** and **3Pd**, respectively (Table 3.3). In the literature[22,25] the **1Pd** triplet state has a lifetime vales of 110 μs[22] in degassed 2-MeTHF solution and 225 μs[25] in degassed toluene while having values two and three orders of magnitude longer than the values obtained experimentally for the **3Pd** and **1Pd**, respectively. On the other hand the value of 0.336 μs[25] in air saturated toluene solution comes closer to the values obtained experimentally. The observed difference in values of triplet lifetimes of the studied porphyrins compared to the literature values was attributed to the degassing method. The freeze-pump-thaw procedure used by Hooi Ling Kee et al.[22] allows a full removal of molecular oxygen from the porphyrin's solution, in contrast to the degassing of the solution utilizing a N_2 gas stream, which appears to be incapable of degassing the sample in the same thorough manner.

All the spectroscopic data obtained in chapter 3.2.1, of the investigated metalloporphyrins (**1Pd** and **3Pd)** in solution with the data obtained of solid-state films of pure sensitizers, can be seen in table 3.3.

Table 3.3 – Spectroscopic (absorption, $\lambda_{máx}^{Abs}$, fluorescence, $\lambda_{máx}^{Fluo}$, and phosphorescence emission maxima, $\lambda_{máx}^{Phosph}$) and photophysical data (fluorescence quantum yields;, ϕ_F, phosphorescence, τ_{Ph}, and triplet state lifetimes, τ_T, together with singlet oxygen sensitization quantum yields, ϕ_Δ) for the metalloporphyrins in 2-methyltetrahydrofuran solution and in solid state (cellulose acetate films) at 293 K.

Compound	$\lambda_{máx}^{Abs}$ (nm)	$\lambda_{máx}^{Fluo}$ (nm)	ϕ_F $\times 10^{-4}$	$\lambda_{máx}^{Phosph}$ (nm)	τ_{Ph} (μs)	ϕ_Δ	τ_T (ns)
1Pd	414; 522; 552	560; 608	1,83	696; 771	167	0,46	627
1Pd Film (0.5mg 1Pd)	415; 522; 556	-	-	699; 777	62	-	-
3Pd	419; 525; 561	569; 613	2,17	715; 783	140	0,30	1272
3Pd Film (0.5mg 3Pd)	423; 527; 562	615	-	718; 788	66	-	-

3.3. Immobilization in Solid matrix and Spectroscopic characterization of the TTA-UC system

The assembly of the TTA-UC system was made using as building blocks the sensitizers (palladium porphyrins) mixed with the annihilator (TPE) and as the immobilization matrix cellulose acetate was used, producing cellulose acetate films with TTA-UC capabilities. When working in the solid state, common organic fluorophores tend to become weakly emissive or lose their emission in its entirety due to aggregation-caused quenching (ACQ). ACQ causes the quenching of luminescence molecules due to strong interaction with adjacent molecules through π-π stacking, in the aggregate or solid phases, leading to deactivation through non-radiative pathways.[35–37] Some molecules can experience the opposite effect, resulting in these chromophores having little to no emission in solution, but when aggregation is promoted or they are found in the solid state, they develop an emission; this process is also known as AIE (aggregation induced emission). TPE is one such molecule, and when in solution, the intramolecular rotation of its four

phenyl groups leads to the excited-state being predominantly deactivated through radiationless transitions. Constraints in the molecular rotation of the phenyl groups, as in the solid or aggregated states, lead to the restriction of the non-radiative decay pathways leading to the emission of the compound. The characteristics of AIE luminogens make them an very attractive group of molecules for application in the construction of solid state system compared to conventional fluorophores.[38]

As for choice of polymeric matrix we decided to use cellulose acetate. Cellulose acetate (CA) is produced from the acetylation of cellulose, one of the most abundant biomaterials on earth. This polymer matrix has been used in several optical systems for its good optical transparency, mechanical strength, and the fact that it is a biogenic material makes it ideal to be used as the matrix of the TTA-UC system.[39–42]

Preliminary CA films were produced containing only annihilator or sensitizer. The absorption and emission spectra of the films were taken, as seen in Figure 3.6 and the values of the maximum peaks for each band are presented in Table 3.3. The films containing pure TPE display three absorption maximum at 211 nm, 241 nm, and 304 nm. When excited at 310 nm, a strong emission between 400 and 600 nm with a maximum at 465 nm is observed related to the prompt fluorescence of TPE in the solid state. The films bearing only porphyrins also had their emission data accessed after excitation at the Soret band maximum. The resulting fluorescence emission was very low just as in solution leading to only the phosphorescence being characterized. The phosphorescence emission of the studied porphyrin in solid state presents a similar profile to the room temperature phosphorescence spectra in 2-MeTHF solution (with a small red-shift). The phosphorescence emission for the **1Pd** exhibits two bands with maximum the first at 699 nm and the second at 777 nm, while for the **3Pd** the phosphorescence emission also displays two maximum centered at 718 and 788 nm. The phosphorescence decays collected from the polymeric blends containing only **1Pd** and **3Pd**, were found to be well fitted with a monoexponentially decay law, with phosphorescence lifetimes, τ_{Ph}, of 62 μs and of 66 μs, respectively (Table 3.3).

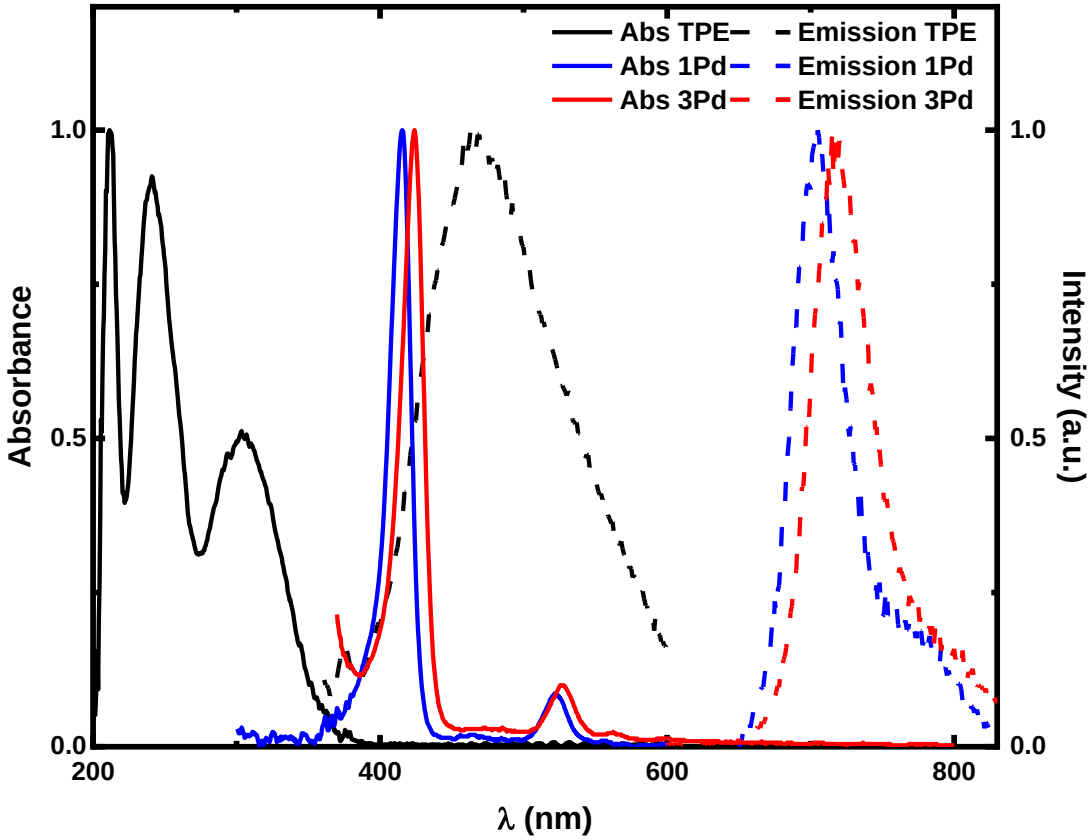

Figure 3.6 – Normalized absorption/emission spectra for the investigated sensitizer (blue and red spectra) and annihilator (black spectra) molecules in cellulose acetate films.

Giorgio Macchi et al[43] obtained similar results when preparing polymeric blends of cellulose acetate with palladium octaethylporphyrin under atmospheric air conditions (60 μs). However, they demonstrated that preparing the same polymeric films in a glove box and with deoxygenated solvent results in an increase of the τ_{Ph} (1.2 ms). This shows that under atmospheric conditions the presence of oxygen in the sample is inevitable leading to a decrease in the phosphorescence lifetime of the films. When comparing the values obtained in solution and in the polymer films, as expected a reduction of the phosphorescence lifetime is observed, since the solution samples analyzed were deoxygenated with N_2, reducing the presence of oxygen in the sample. *Monguzzi et. al* prepared CA films with a similar loading of sensitizer and when combining the annihilator in the polymeric films they observed a substantial decrease of the phosphorescence decay (<3 μs), which gave support for their observation of efficient TTA-UC in a very efficient manner.[40]

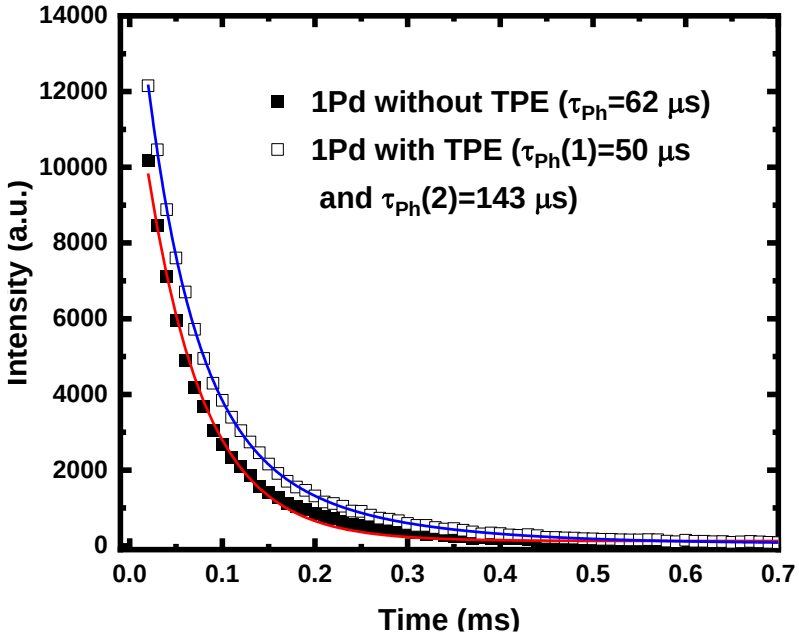

Figure 3.7 – Phosphorescence decays comparison of cellulose acetate polymer film with loadings of only **1Pd** (1.39×10^{-4} M) with films with TPE (0.015 M) and the same loading of **1Pd**.

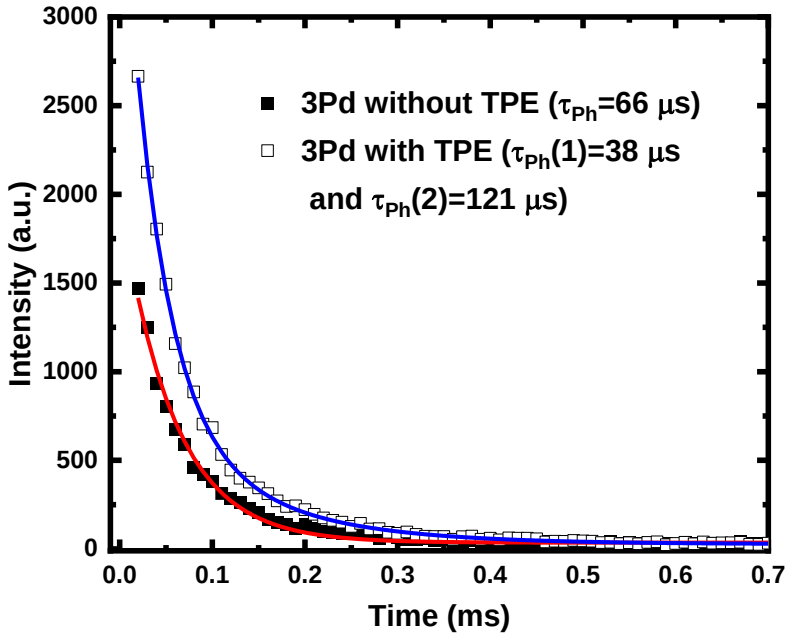

Figure 3.8 – Phosphorescence decays comparison of cellulose acetate polymer film with loadings of only **3Pd** (9.84×10^{-5} M) with films with TPE (0.015 M) and the same loading of **3Pd**.

The effect of the annihilator presence in the system was studied by collecting the phosphorescence emission at the peak maximum of the investigated sensitizer,

the results are shown in Figures 3.7 and 3.8. Polymer films containing solely sensitizer were fitted with a mono-exponential decay law while the films containing both sensitizer and annihilator were better fitted with a bi-exponential decay law. This observation suggests that the films compositions have two distinct populations of sensitizer, those that have access to the annihilator and those that have not. In films containing **1Pd** and annihilator the phosphorescence lifetimes are 50 μs and 143 μs, while for films containing **3Pd** and annihilator the phosphorescence lifetimes are 38 μs and 121 μs. This bi-exponential behavior was attributed to: (i) the sensitizer molecules with TPE in their proximity have short decay lifetimes, stemming from the emergence of a new decay route for the deactivation of the sensitizer's T_1 excited state (energy transfer to the TPE); (ii) additionally, the films will also have a population of sensitizer molecules that do not have TPE molecules nearby, causing the sensitizer to decay in a monoexponential manner having longer decay lifetimes. The transfer of energy occurs through the Dexter mechanism, as referred earlier (Chapter 1.4), requiring the close proximity between the species as to promote the overlap of their orbitals, since the components positions are static the collisions are negligible, leading to limitations on the number of overlapped components leading to reduced energy transfer. This incomplete deactivation of the sensitizer triplet state by energy transfer to the surrounding annihilator molecules leads to two conclusions, first the components concentration may not be the most adequate to ensure complete energy transfer and second the distribution of the components in the matrix may not be the most efficient, therefore leading to less favorable energy transfer, as the formation of trap states is still a factor to be controlled.

The intensity of the TPE delayed upconversion emission (obtained by TTA-UC) in the films was accessed using a Horiba-Jobin-Yvon FL3.2.2. spectrofluorometer (equipped with a 450 W Xenon lamp as excitation source) while the irradiation was performed at 560 and 600 nm.

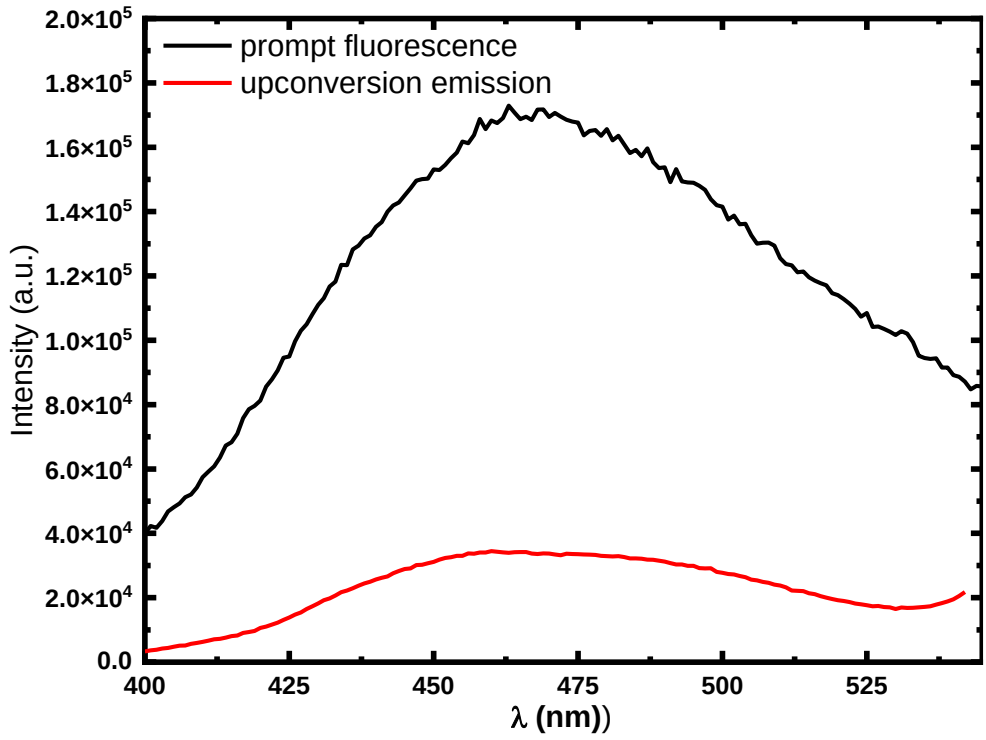

Figure 3.9 – Comparison between prompt fluorescence (black line) of the TPE when excited at 310 nm and upconversion emission (red line) of TPE in the polymer blend film of **1Pd** ($1.39 \times 10^{-4}\ M$) when irradiated at 650 nm.

In Figure 3.9, a luminescent emission spectra of a cellulose acetate film loaded with TPE (15 mM) and metalloporphyrin ($1.39 \times 10^{-4}\ M$) is shown. In the spectrum the comparison of two emission were made at the same wavelength, depicting the radiative decay of TPE, when the films were excited at 310 nm (in black), a region where the TPE absorbs, and at 560 nm (in red) a region that only the porphyrins emit. The observation of emission even when the film was excited at a wavelength far from the TPE absorption region leads to the conclusion that the resulting emission, seen in red, being assigned to the delayed fluorescence by the TTA-UC process. To optimize the polymeric films, several samples of polymeric blends were prepared with different loadings (concentrations) of porphyrin while maintaining the same concentrations of annihilator (15 mM) to ascertain at which sensitizer concentrations the upconversion has higher intensity.[40,44] In Figure 3.10A) the obtained upconverted emissions for the various films with different loading of **1Pd** when irradiated at 560 nm while the point B) represents the relation between the concentration of each polymeric film and the maximum intensity of the

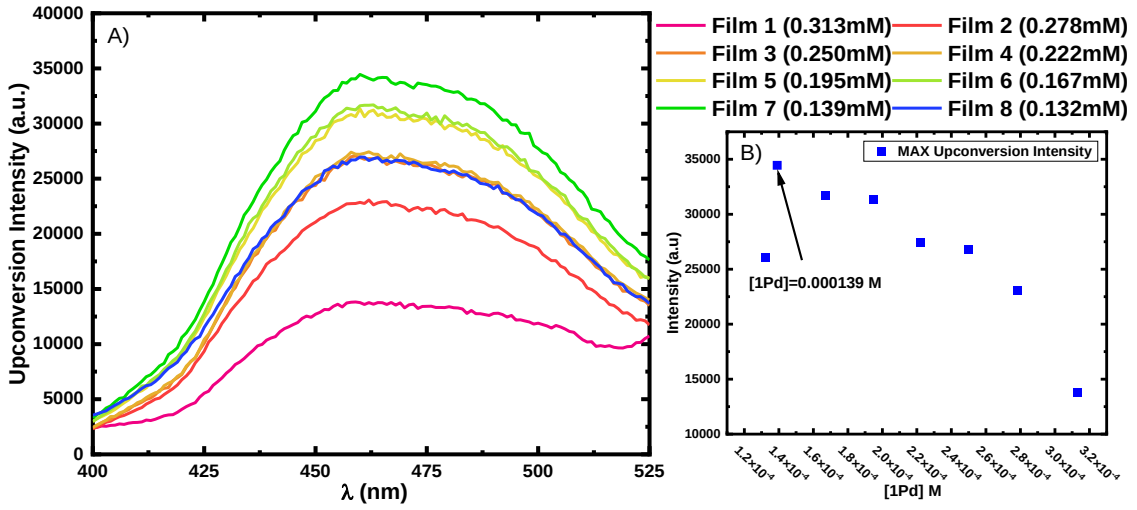

Figure 3.10 – A) upconverted emission of various cellulose acetate polymer blends with different loading of **1Pd** while maintaining the concentration of TPE (0.015 M), when irradiated at 560 nm; B) maximum intensity concentration relation plot showing the concentrations with the highest upconversion intensity.

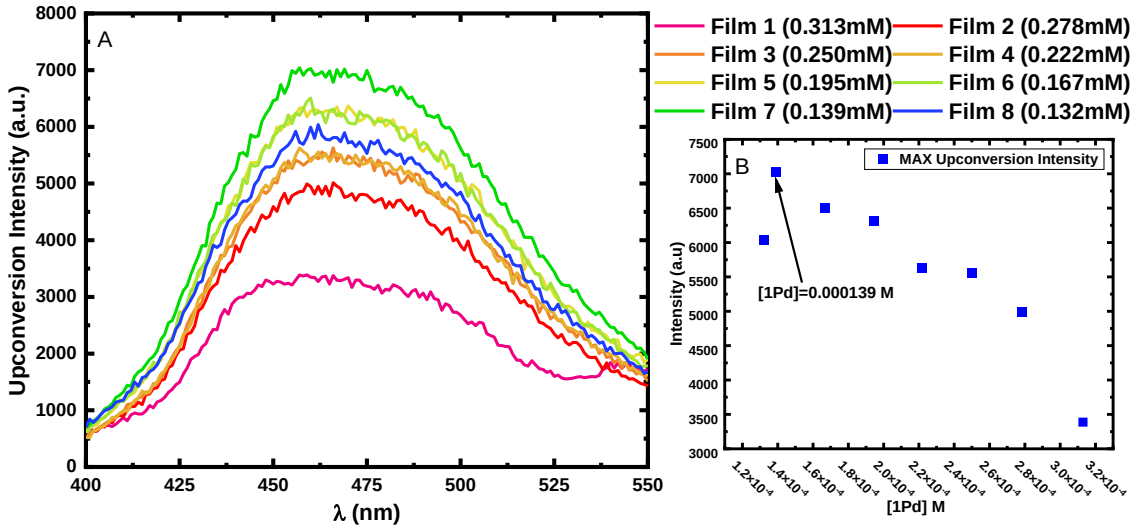

Figure 3.11 – A) upconverted emission of various cellulose acetate polymer blends with different loading of **1Pd** while maintaining the concentration of TPE (0.015 M), when irradiated at 600 nm; B) maximum intensity concentration relation plot showing the concentrations with the highest upconversion intensity.

emission. Higher concentration of sensitizer may not always provide a high emission of upconversion. This fact can be proven with the data in Figure 3.11 where the films with the highest concentration are those with the lowest intensity of

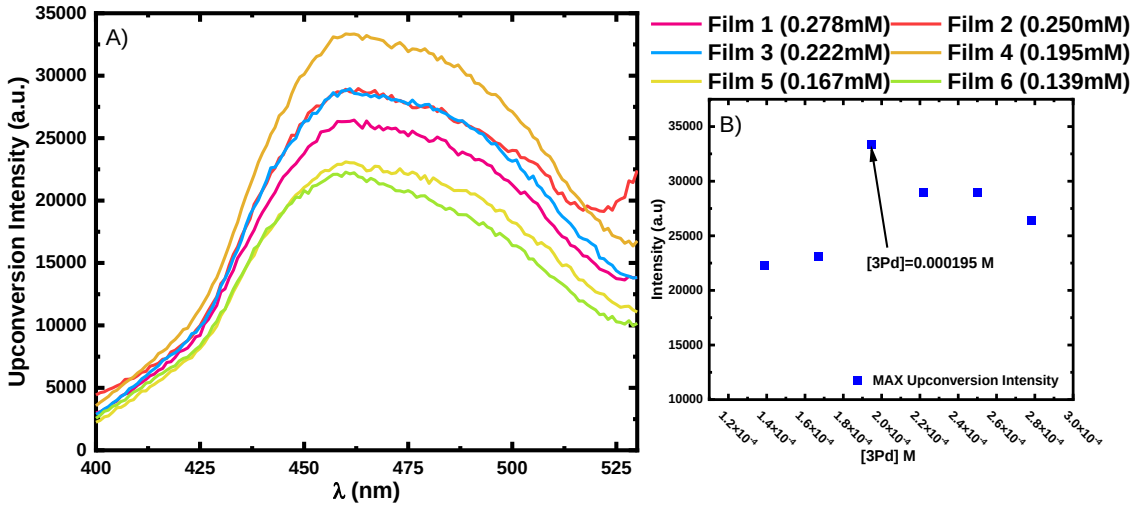

Figure 3.12 - A) upconverted emission of various cellulose acetate polymer blends with different loading of **3Pd** while maintaining the concentration of TPE (0.015 M), when irradiated at 560 nm; B) maximum intensity concentration relation plot showing the concentrations with the highest upconversion intensity.

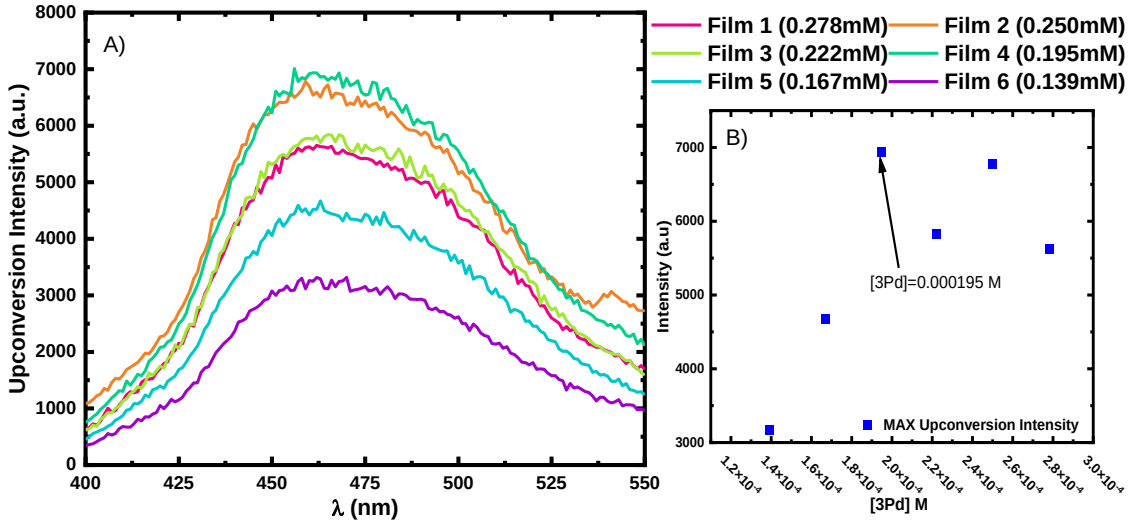

Figure 3.13 - A) upconverted emission of various cellulose acetate polymer blends with different loading of **3Pd** while maintaining the concentration of TPE (0.015 M), when irradiated at 600 nm; B) maximum intensity concentration relation plot showing the concentrations with the highest upconversion intensity.

upconversion. The concentration of sensitizer was lowered gradually resulting in a concomitant increase in upconversion intensity. When a film with the concentration of 1.32×10^{-4} M was measured the resulting upconversion intensity was smaller

than for case the previous concentration of 1.39×10^{-4} M which was identified as the best sensitizer concentration for this system.

The same concentration studies were performed for the **3Pd** obtaining similar results as shown in Figure 3.11 and 3.13. The film with the best upconversion emission has a concentration of 1.95×10^{-4} M a slightly higher concentration that for **1Pd** (1.39×10^{-4} M). As seen with **1Pd** high concentrations of sensitizer doesn´t favor the increase in upconversion intensity but even so **3Pd** film with the best upconversion emission had a higher concentration than for the previous porphyrin. This effect is, most likely, related to the increased solubility in THF that the alkyl chains provide in the porphyrin leading to a better distribution of the sensitizer within the polymer matrix. Whit the analysis of the same polymer films but with excitation set at 600 nm lead to upconversion similar to the one observed in **1Pd** with the highest upconversion being again in the film with 1.95×10^{-4} M sensitizer concentration. Nonetheless, the polymer film of **3Pd** with 2.5×10^{-4} M concentration had an unexpected high upconversion emission, when excited at this wavelength, closing in intensity to the film with the best concentration conditions. Additional testing is required to solidify the observed effect as there are still a lot of variables to consider such as the random distribution of the components in the matrix as well as the production of aggregated state, or even the production of crystalline structures within the material.[45,46]

In addition, while in solution the palladium porphyrins don´t absorb at 600 nm in the polymer blend films a small absorption band (aggregates) can be found centered at this wavelength. The irradiation of the polymer films in this region lead to an upconversion emission, although smaller than when irradiated at 560nm the upconversion was still detected. The results of this study are shown in Figures 3.11 and 3.13 and a plausible explanation for the observed effect may come from the formation of a small quantity of "J-aggregates" dispersed in the film, that although small had the capacity to promote upconversion with TPE molecules adjacent to the aggregate. This results show promise in the formulation of materials, such as the films produced in this work, that have in their composition aggregates capable of emitting delayed fluorescence (by TTA-UC) while being excited further in the electromagnetic spectrum (at higher wavelengths).

The prompt fluorescence observed has five-times the intensity of the strongest upconversion emission, this result could be expected since not all the TPE molecules are in contact with the sensitizer (as seen previously) and/or form adequate collisional pockets that lead to upconversion. The upconversion could achieve higher values of intensity at the same concentration of sensitizer by changing the concentration of annihilator leading to better concentration condition. The same could be said about the distribution of the components in the polymeric matrix, since the type of casting employed in this work resulted from the diffusion of both the sensitizer and annihilator in the polymer matrix leading to, most likely, production of inhomogeneous polymer films that could be plagued by formation of trap states.

Overall, the observed upconversion emission is quite strong when exciting at the last Q-band (650 nm) of the porphyrin while the excitation at 600 nm was small it ascertained the presence of a small number of J-aggregates as well as the possibility for them to promote TTA-UC. This demonstrates the viability of this system to be used in the construction of a solid TTA-UC material with application in bioimaging based on upconverting aggregates showing that show promising results in the upconversion of radiation closer to the therapeutic window.[47,48]

2.4. References

(1) Cheng, T. H.; Hirota, N.; Mao, S. W. PMDR Studies in Heavy Atom Containing Hosts; Naphthalene and Quinoxaline in 1,4-Dibromobenzene. *Chem. Phys. Lett.* **1972**, *15* (2), 274–278.

(2) Romanova, Z. S.; Deshayes, K.; Piotrowiak, P. Remote Intermolecular "Heavy-Atom Effect": Spin−Orbit Coupling Across the Wall of a Hemicarcerand. *J. Am. Chem. Soc.* **2001**, *123* (10), 2444–2445.

(3) Veedu, S.; Popovic, Z.; Satpathy, s. Theoretical Model for Rashba Spin-Orbit Interaction in d Electrons. *Phys. Rev. B* **2014**, *90*.

(4) Koziar, J. C.; Cowan, D. O. *Photochemical heavy-atom effects*. *ACS Publications.* **1978**, 11, 334-341

(5) Gouterman, M. Spectra of Porphyrins. *J. Mol. Spectrosc.* **1961**, *6*, 138–163.

(6) Gouterman, M. Spectra of Porphyrins: Part II. Four Orbital Model. *J. Mol. Spectrosc.* **1963**, *11* (1), 108–127.

(7) Weiss, C.; Gouterman, M. Spectra of Porphyrins: Part III. Self-Consistent Molecular Orbital Calculations of Porphyrin and Related Ring Systems. *J. Mol. Spectrosc.* **1965**, *16* (2), 415–450.

(8) Gouterman, M. A Theory for the Triplet-Triplet Absorption Spectra of Porphyrins. *J. Chem. Phys.* **2004**, *33* (5), 1523–1529.
(9) Platt, J. R. Molecular Orbital Predictions of Organic Spectra. *J. Chem. Phys.* **2004**, *18* (9), 1168–1173.
(10) Longuet-Higgins, H. C.; Rector, C. W.; Platt, J. R. Molecular Orbital Calculations on Porphine and Tetrahydroporphine. *J. Chem. Phys.* **2004**, *18* (9), 1174–1181.
(11) Petropoulos, V.; Russo, M.; Rukin, P.; Quintela, F.; Moretti, L.; Moore, A.; Moore, T.; Gust, D.; Prezzi, D.; Scholes, G.; Molinari, E.; Troiani, F.; Cerullo, G.; Rozzi, C.; Maiuri, M. Unveiling Vibronic Coupling within the Q-Bands of a Free-Base Porphyrin. *Optica Publishing Group*, **2022**; p M1A.3.
(12) Gladkov, L. L.; Starukhin, A. S.; Shulga, A. M. Vibronic Coupling in Quasidegenerate Electronic States of Metal Porphyrin Molecules. *J. Struct. Chem.* **1995**, *36* (2), 328–332.
(13) Eyer, P.; Worek, F.; Kiderlen, D.; Sinko, G.; Stuglin, A.; Simeon-Rudolf, V.; Reiner, E. Molar Absorption Coefficients for the Reduced Ellman Reagent: Reassessment. *Anal. Biochem.* **2003**, *312* (2), 224–227.
(14) Giusti M. M. *Molar Absorptivity and Color Characteristics of Acylated and Non-Acylated Pelargonidin-Based Anthocyanins J. Agric. Food Chem.* **1999***, 47, 11, 4631–4637*
(15) Ksenofontov, A. A.; Lukanov, M. M.; Bocharov, P. S. Can Machine Learning Methods Accurately Predict the Molar Absorption Coefficient of Different Classes of Dyes? *Spectrochim. Acta. A. Mol. Biomol. Spectrosc.* **2022**, *279*, 121442.
(16) Charisiadis, A.; Costa, R. D. Peripheral Substitution of Tetraphenyl Porphyrins: Fine-Tuning Self-Assembly for Enhanced Electroluminescence. *ChemPlusChem* **2018**, *83* (4), 254–265.
(17) Ha, J.-H.; Kim, Y.-R. Substitution Effect of Hydroxyl Group on Photophysical Properties of Tetraphenylporphyrin (H2TPP) and Germanium(IV) Tetraphenylporphyrin Dichloride (Ge(IV)TPPCl2). *J. Mol. Struct.* **2002**, *606* (1), 189–195.
(18) Hanna, L.; Teprovich Jr., J. A.; Ward, P. A. Spectroscopic Investigation of the Electronic and Excited State Properties of Para-Substituted Tetraphenyl Porphyrins and Their Electrochemically Generated Ions. *Spectrochim. Acta. A. Mol. Biomol. Spectrosc.* **2022**, *278*, 121300.
(19) Chen, C.-H.; Liu, B. The Effect of Alkoxyl Groups on the Photoproperties of Meta-Octasubstituted Tetraphenyl Porphyrins. *Inorg. Chem. Commun.* **2022**, *146*, 110139.
(20) Spellane, P. J.; Gouterman, M. *Porphyrins. 40. Electronic spectra and four-orbital energies of free-base, zinc, copper, and palladium tetrakis(perfluorophenyl)porphyrins*. *Inorg. Chem.* **1980**, 19, 386-391
(21) Arnaut, L. Design of Porphyrin-Based Photosensitizers for Photodynamic Therapy. *Adv. Inorg. Chem. - ADVAN INORG CHEM* **2011**, *63*, 187–233.
(22) Kee, H. L.; Holten, D. Photophysical Characterization of Imidazolium-Substituted Pd(II), In(III), and Zn(II) Porphyrins as Photosensitizers for Photodynamic Therapy. *J. Photochem. Photobiol. Chem.* **2008**, *200* (2), 346–355.
(23) Lamoen, D.; Parrinello, M. Geometry and Electronic Structure of Porphyrins and Porphyrazines. *Chem. Phys. Lett.* **1996**, *248* (5), 309–315.

(24) To, W.-P.; Liu, Y.; Lau, T.-C.; Che, C.-M. A Robust Palladium(II)–Porphyrin Complex as Catalyst for Visible Light Induced Oxidative C-H Functionalization. *Chem. – Eur. J.* **2013**, *19* (18), 5654–5664.
(25) Wiehe, A.; Stollberg, H.; Runge, S.; Paul, A.; Senge, M.; Röder, B. PDT-related Photophysical Properties of Conformationally Distorted Palladium(II) Porphyrins. *J. Porphyr. Phthalocyanines* **2001**, *5*, 853–860.
(26) Harriman, A. Luminescence of Porphyrins and Metalloporphyrins. Part 3.—Heavy-Atom Effects. *J. Chem. Soc. Faraday Trans. 2 Mol. Chem. Phys.* **1981**, *77* (7), 1281–1291.
(27) Volostnykh, M. V.; Borisov, S. M.; Konovalov, M. A.; Sinelshchikova, A. A.; Gorbunova, Y. G.; Tsivadze, A. Yu.; Meyer, M.; Stern, C.; Bessmertnykh-Lemeune, A. Platinum(II) and Palladium(II) Complexes with Electron-Deficient *Meso* -Diethoxyphosphorylporphyrins: Synthesis, Structure and Tuning of Photophysical Properties by Varying Peripheral Substituents. *Dalton Trans.* **2019**, *48* (24), 8882–8898.
(28) Montalti M. Handbook of Photochemistry*. Taylor & Francis Group* **2006**
(29) Kubát, P.; Mosinger, J. Photophysical Properties of Metal Complexes of Meso-Tetrakis(4-Sulphonatophenyl)Porphyrin. *J. Photochem. Photobiol. Chem.* **1996**, *96* (1), 93–97.
(30) Helsenbeck, S. J.; Haustein, C. Helsenbeck, S. J.; Haustein, C. Solvent Effects in Room Temperature Phosphorescence. **1988**, 4, 95.
(31) Gorski, A.; Knyukshto, V.; Zenkevich, E.; Starukhin, A.; Kijak, M.; Solarski, J.; Semeikin, A.; Lyubimova, T. Temperature Dependent Steric Hindrance Effects in Triplet State Relaxation of Meso-Phenyl-Substituted Pd-Octaethylporphyrins. *J. Photochem. Photobiol. Chem.* **2018**, *354*, 101–111.
(32) Önal, E.; Saß, S.; Hurpin, J.; Ertekin, K.; Topal, S. Z.; Kumke, M. U.; Hirel, C. Lifetime-Based Oxygen Sensing Properties of Palladium(II) and Platinum(II) Meso-Tetrakis(4-Phenylethynyl)Phenylporphyrin. *J. Fluoresc.* **2017**, *27* (3), 861–868.
(33) Pineiro, M.; Carvalho, A. L.; Pereira, M. M.; Gonsalves, A. M. d'A. R.; Arnaut, L. G.; Formosinho, S. J. Photoacoustic Measurements of Porphyrin Triplet-State Quantum Yields and Singlet-Oxygen Efficiencies. *Chem. - Eur. J.* **1998**, *4* (11), 2299–2307.
(34) Şen, P.; Hirel, C.; Gürek, A.-G.; Andraud, C.; Bretonnière, Y.; Lindgren, M. Photophysical Properties and Study of the Singlet Oxygen Generation of Tetraphenylporphyrinato Palladium(II) Complexes. *J. Porphyr. Phthalocyanines* **2013**, *17* (10), 964–971.
(35) Birks, J. B. *Photophysics of Aromatic Molecules*; Wiley-Interscience: London, New York, **1970**.
(36) Qi, J.; Hu, X.; Dong, X.; Lu, Y.; Lu, H.; Zhao, W.; Wu, W. Towards More Accurate Bioimaging of Drug Nanocarriers: Turning Aggregation-Caused Quenching into a Useful Tool. *Adv. Drug Deliv. Rev.* **2019**, *143*, 206–225.
(37) Turro, N. J. *Modern Molecular Photochemistry*; University Science Books, **1991**.
(38) Anslyn, E. V. and D. *Modern Physical Organic Chemistry*; University Science Books: Sausalito, California, **2006**.
(39) Kim, J.-H.; Deng, F.; Castellano, F. N.; Kim, J.-H. High Efficiency Low-Power Upconverting Soft Materials. *Chem. Mater.* **2012**, *24* (12), 2250–2252.

(40) Monguzzi, A.; Tubino, R.; Meinardi, F. Multicomponent Polymeric Film for Red to Green Low Power Sensitized Up-Conversion. *J. Phys. Chem. A* **2009**, *113* (7), 1171–1174.
(41) Vatanpour, V.; Pasaoglu, M. E.; Barzegar, H.; Teber, O. O.; Kaya, R.; Bastug, M.; Khataee, A.; Koyuncu, I. Cellulose Acetate in Fabrication of Polymeric Membranes: A Review. *Chemosphere* **2022**, *295*, 133914.
(42) Arthanareeswaran, G.; Thanikaivelan, P.; Srinivasn, K.; Mohan, D.; Rajendran, M. Synthesis, Characterization and Thermal Studies on Cellulose Acetate Membranes with Additive. *Eur. Polym. J.* **2004**, *40* (9), 2153–2159.
(43) Macchi, G.; Meinardi, F.; Tubino, R. Light-Scribing Emissive Patterns on Polymer Films Through a Light-Induced Depletion of Phosphorescence Quenching. *Adv. Mater.* **2010**, *22* (32), 3553–3557.
(44) Edhborg, F.; Olesund, A.; Albinsson, B. Best Practice in Determining Key Photophysical Parameters in Triplet–Triplet Annihilation Photon Upconversion. *Photochem. Photobiol. Sci.* **2022**, *21* (7), 1143–1158.
(45) Zavadskii, A. E.; Golubev, A. E.; Kuvshinova, S. A.; Burmistrov, V. A.; Koifman, O. I. Effect of Tetraphenylporphine on the Supramolecular Structure of Cellulose Acetates. *Russ. J. Gen. Chem.* **2016**, *86* (6), 1453–1458.
(46) Zavadskii, A. E.; Kuvshinova, S. A.; Burmistrov, V. A. Effect of Tetraphenylporphine on the Supramolecular Structure of Cellulose Triacetate. *Fibre Chem.* **2009**, *41* (5), 298–301.
(47) Li, X.; Zheng, Z.; Han, M.; Chen, Z.; Zou, G. Tuning J-Aggregates of Tetra(p-Hydroxyphenyl)Porphyrin by the Headgroups of Ionic Surfactants in Acidic Nonionic Micellar Solution. *J. Phys. Chem. B* **2007**, *111* (17), 4342–4348.
(48) Guillén, M. G.; Gámez, F.; Roales, J.; Lopes-Costa, T.; Pinto, S. M. A.; Calvete, M. J. F.; Pereira, M. M.; Pedrosa, J. M. Molecular-Based Selection of Porphyrins towards the Sensing of Explosives in the Gas Phase. *Sens. Actuators B Chem.* **2018**, *260*, 116–124.

4. Conclusion and Future Research Prospects

In this work, solid-state polymeric films with delayed fluorescence emitting capabilities, employing the TTA-UC mechanism, were conceived. For this end, palladium porphyrin, **1Pd** and **3Pd**, were successfully synthesized and purified allowing for its use as the systems sensitizer or acceptor molecule. The metalloporphyrins were characterized with various distinct methods, allowing for the quantification of the fluorescence and to determine the regions of absorption and emission of the components in the system. The palladium bearing porphyrins in this study exhibited strong phosphorescence accompanied with a very weak emission of fluorescence (ϕ_F values in the 1.8 to 2.2 $\times 10^{-4}$ range), an expected behavior of porphyrins containing heavy atoms that facilitate the ISC process through a strong spin-orbit coupling. The phosphorescence lifetimes and the triplet state lifetimes although quenched by the presence of oxygen in both solution and solid state showed promising results since by thorough elimination of the molecular oxygen these values are expected to increase to values described in the literature. The sensitizers: annihilator pairs were successfully encapsulated in cellulose acetate polymer matrix, while accessing the best concentration of sensitizer to achieve the best TTA-UC emission. More so, the observation of delayed fluorescence of TPE with a standard spectrofluorometer demonstrated the viability of the developed TTA-UC pairs to be used with low excitation power, which could be interesting for application in the bioimaging domain (thus avoiding tissues damage through the use of lasers of higher energy).

All things considered, the current research resulted in the development of a solid-state TTA-UC emitter system with an upconversion emission (excited at 560nm) of 1/5 the intensity of the prompt fluorescence (excited at 310nm), which is a particularly good result. Nonetheless additional tests are needed, to ensure that the polymeric blend films achieve stronger upconversion emissions with more efficient energy transfer.

Future work should focus primarily on enhancing the TTA-UC system's optical, structural, and mechanical capabilities. One way that the optical capabilities of the system could be enhanced would be through the covalent linkage between the sensitizer-annihilator pair. This modification would ensure constant contact and proximity between the two components, allowing for a more efficient energy transfer between the components. This covalently linked system could form emissive aggregates, that are less prone to trap states formation, leading to enhanced upconversion emission while at the same time promoting a red shift in the absorption closer to the NIR region. Likewise, cellulose acetate polymer films require further analysis of their characteristics to underline the viability of the solid-state material to be used in bioimaging techniques.

5. Experimental section

This section of the work is intended to provide a clear, detailed, and extensive description on how the work presented in this thesis was performed, including the different methodologies used, synthesis routes, purification, and characterization techniques. The chapter is divided into 2 parts, the first, named "Techniques and Purification" that describes the techniques used, and the pre-work-up done on solvent and other compounds. The second, named "Experimental Work" being destined for the synthesis and description of all the products and intermediaries in this work. All the numerical designation for the compounds were maintained the same throughout the work.

5.1. Solvents and Reagents

Reagents were purchased from Sigma-Aldrich, Merck and were used with the purity described by the supplier. All solvents used in the course of this work were purified by distillation or drying according to procedures described in literature.[1]

5.2. Instrumentation and methodology

5.2.1. Chromatography

Two types of chromatography were employed during the work, thin layer chromatography (TLC) using silica plates 60 and silica gel column chromatography using grade 60 silica . The eluent used for each chromatography was considered depending on the compound. A UV250 lamp was used to identify the compounds when its identification was not possible through the naked eye.

5.2.2. Absorption spectra

All spectroscopic data regarding the absorption of light in the Ultraviolet-Visible range were determined using a *Shimadzu U.V.-2100* and a *Hitachi U-2010* spectrophotometer. The spectra were measured using a quartz cell with 10 mm of

optical path. The solvent used for the spectroscopic measurements was 2-MeTHF, except for the free-base TPP data (reference) which was collected in toluene.

5.2.3. Fluorescence Emission/Room Temperature Phosphorescence Emission Spectroscopy

The fluorescence emission and excitation spectra were carried out at room-temperature using a Horiba-Jobin-Ivon SPEX Fluoromax 3.22 spectrofluorometer equipped with a 450 W Xenon lamp, using cells with an optical path of 10 mm. The fluorescence spectra were corrected for the wavelength response of the system.
Two types of methods could be employed for the quantification of the fluorescence the absolute and the relative method. The absolute method consists in the direct quantification of the fluorescence quantum yield by the variation of the number of absorbed/emitted photons requiring the use of an integration sphere to quantify the intensity of the fluorescence emission. While the relative method uses a reference compound with a well established ϕ_F value to which the sample will be compared. Equation 3.8 shows the fluorescence quantum yield equation for the relative method used during this work. For this equation to be correctly applied the solution of both chromophores need to be adjusted so that their absorption would be equal in the excitation wavelength ensuring that the number of absorbed photons is the same in both samples. If the solutions of two chromophores use a different solvent, then the difference in their refractive indexes needs to be quantified. If the same solvent is used in both samples, then this component can be disregarded since they will have a unitary value.

The phosphorescence emission spectra as well as the phosphorescence decays were also quantified using this apparatus but employing a 150W pulsed Xenon lamp. The spectra were obtained by dissolving the compounds in 2-MeTHF in a 10 mm optical path cuvette. The solid-state phosphorescence measurements were made under atmospheric oxygen and temperature conditions using a specialized film holder. As the samples were taken in a solution media and the solvent used was 2-MeTHF one has to consider the effect that the solvent may have on the phosphorescence.[2]

5.2.4. Singlet oxygen photosensitization

Quantification of single oxygen quantum yields, ϕ_Δ, were performed using a modified flash photolysis spectrometer equipped with a Hamamatsu R5509-42 photomultiplier cooled to 193 K in a liquid nitrogen chamber. The phosphorescence emission of singlet oxygen was detected at room-temperature (20°C) with excitation at 355nm (using the third harmonic of a Spectra-Physics Quantaray Nd:YAG laser) and detection at 1270 nm. The first and second harmonic contributions were eliminated with the interposition of a dichroic lens installed in the optical path between the sample and the monochromator used as a harmonic laser separator. The detector was kept at -1600 V.

The samples were prepared by dissolving the porphyrin in 2-MeTHF then determining their absorption at 355nm, the same was performed for the reference sample used was TPP in toluene which had an ϕ_Δ= 0.66.[5] From the equation below the singlet oxygen generation of the sample was quantified by a comparative method of single oxygen quantum yields, ϕ_Δ:

$$\phi_\Delta^{Sample} = \frac{slope^{sample}}{slope^{ref}} * \frac{OD_{ref}(excitation\ \lambda)}{OD_{Sample}(excitation\ \lambda)} * \phi_\Delta^{ref} \qquad \text{Equation 5.1}$$

5.2.5. Transient absorption spectroscopy

The experimental setup used to obtain the triplet-triplet absorption spectra and lifetimes consisted of a nanosecond-millisecond broadband (350-1600 nm) pump-probe Transient Absorption EOS-Fire spectrometer from Ultrafast Systems equipped with an amplified femtosecond Spectra-Physics Solstice-100F laser (1 kHz repetition rate) coupled with a Spectra-Physics TOPAS Prime F optical parametric amplifier (195–22000 nm) for pulse pump generation. In this case the transient absorption data was collected with excitation at 420 nm and probed in the 350-800 nm range. Low laser energy was used to avoid multiphoton and triplet-triplet annihilation effects. The solutions used to collect the transient singlet-triplet difference absorption spectra were bubbled with nitrogen for at least 20 minutes before the experiment and kept bubbling during the experiment. After the first pulse is taken of the sample, a few moments after a second pulse are used to measure the

absorption. The absorption is measured by subtracting the absorption before the second pulse to the absorption after the second pulse, as it can be seen in the following Equation 5.2 :

$$\Delta Abs = Abs(after\ both\ pulses) - Abs(after\ one\ pulse) \qquad \text{Equation 5.2}$$

5.2.6. NMR

All nuclear magnetic resonance spectrums were obtained using a *400 MHz Brucker NMR* belonging to the Chemistry department of the University of Coimbra. All the samples that were characterized through this technique used, the TMS (Tetramethylsilane) or the deuterated solvent in which the sample was assessed in, as a reference. The characterization of the obtained spectra was done with Mestrelab Research S.L. - Analytical Chemistry Software also known as MesTreNova®.

5.3. Porphyrin synthesis (general methods)

5.3.1. Nitrobenzene method for one-pot porphyrin synthesis

The above-mentioned method developed by *Gonsalves e Perreira*[6–8] is one of the main, one-pot synthesis pathways for the synthesis of *meso*-arylporphyrins. The method consists of preheating a mixture nitrobenzene with double the molar amount of acetic acid in aerobic conditions, under temperatures of 120°C up to 140°C. Following the addition of equimolar quantities of aldehyde and pyrrole up to concentrations of 0.2M. The initial condensation step involving acetic acid will promote a sequence of condensation reactions, leading to the production of tetramers. Subsequently, a cyclisation step will result in porphyrinogen formation, after which the nitrobenzene, in the presence of atmospheric oxygen, will oxidize the porphyrinogen yielding the desired porphyrin. After the completion of the reaction the organic solvents are removed under reduced pressure and the mixture is purified by an adequate physical purification technique depending on the characteristics of the product.

5.3.2. Microwave Nitrobenzene method for one-pot porphyrin synthesis

According to this methodology a combination of propionic acid (3.5 mL) and nitrobenzene (1.5 mL) was added to an adequate quantity of aldehyde (10 mmol) and pyrrole (10 mmol) in a 35 mL microwave vial. After that, the reaction vessel was sealed to avoid spills. The vial was inserted in the microwave used to heat the yellowish reaction mixture for five minutes. UV-vis absorption spectrophotometry was used to track the reaction's progress over time. Afterwards by adding methanol, the concentrated crude product combination was readily converted overnight into porphyrins. After filtering the dark purple solid and washing it with methanol we finish by drying and removing the residual solvent under vacuum. The microwave apparatus used was the Microwave synthesizer – CEM Discover SP from CEM Corporation with a 200 W max potency.

5,10,15,20-tetraphenylporphyrin (1)

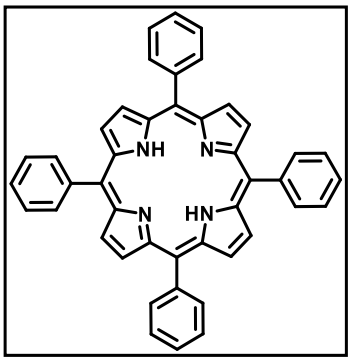

Yield: 8% (batch) 20% (MW)

NMR ^{1}H (400 MHz, $CDCl_3$), δ ppm: 8.84 (s, 8H , β-pyrrolic); 8.23-8.21 (d, J = 7.6 Hz, 8H, o-phenyl); 7.80-7.72 (m, 12H, m,p-phenyl); -2.77 (s, 2H, -NH).

HRMS (ESI-TOF) m/z: calculated for $C_{44}H_{30}N_4$: 614.2543, obtained 615.3421 $[M+H]^+$

5.4. Aldehyde synthesis

5.4.1. Aldehyde synthesis Batch

In a 250mL round bottom flask 41mmol of 4-hydroxybenzaldehyde was dissolved in acetonitrile, then an addition of 210mmol of K_2CO_3 was performed keeping the reaction under medium stirring at room temperature for 30min. After the initial 30min of reaction 61.5mmol of 1-bromo-ethyl-hexane was added and the reaction was put under reflux conditions, with a temperature of 80°C. The reaction was followed by TLC, and the reaction was considered complete after a total of 18h. The reaction mixture was then cooled to room temperature and the K_2CO_3 was filtered out using a funnel and filter paper and by being washed repeatedly with

DCM. Following the filtration of the mixture, the organic solvents were removed under reduced pressure and the product was purified using a C60 grade Silica chromatographic column, with CM as the eluent resulting in pure 4-(2-ethyl-hexiloxy)benzaldehyde.

5.4.2. Microwave

In a 10 mL microwave vial, 60 mg (0.48 mmol) of 4-hydroxybenzaldehyde, 0.1 mL (0.52 mmol) 1-bromo-2-ethylhexane, 0.31 g (0.96 mmol) of Cs2CO3 were dissolved with 1 mL of acetonitrile. It was placed in the microwave (P=200 W) for 10 minutes at 90°C if the solvent was methanol and at 130 °C if the solvent was acetonitrile. The conclusion of the reaction was accessed with the help of TLC and an iodine chamber. Afterwards the reaction solvent evaporated, and the crude was redissolved in dichloromethane and the excess base was extracted with water. The dichloromethane was evaporated obtaining an oil. The microwave apparatus used was the Microwave synthesizer – CEM Discover SP from CEM Corporation with a 200 W max potency.

4-((2-ethylhexyl)oxy)benzaldehyde (2)

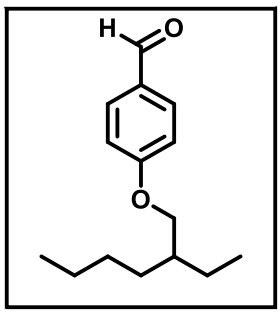

Yield: 88% (batch) 92% (MW)

NMR ^{1}H (400 MHz, $CDCL_3$), δ ppm: 9.87 (s, 1H, CHO); 7.83-7.80 (m, 2H, o-phenyl); 7.01-6.97 (m, 2H, m-phenyl); 3.92 (d, J = 5.8 Hz, 2H, -OCH_2); 1.78-1.72 (m, 1H, -CH); 1.54-1.31 (m, 8H, Alkylics -CH_2); 0.95-0.90 (two t, J = 7.5 Hz, 6H, -CH_3)

NMR ^{13}C (400 MHz, $CDCL_3$), δ ppm: 191.17 (C15); 164.93 (C3); 132.37 (C1+C5); 130.17 (C6); 115.20 (C2+C4); 71.32 (C7); 39.70 (C8); 30.88 (C9); 29.47 (C10); 24.24 (C13); 23.42 (C11); 14.47 (C12); 11.50 (C14).

MS (ESI-TOF): m/z: calculated for $C_{15}H_{22}O_2$=234.162, obtained 235.171 $[M+H]^+$

5.5. Synthesis of 5-(4-hidroxyphenyl)-10,15,20-(4-(2-ethylexyl)oxy)phenyl)porphyrin (3)

The previously synthesized 4-((2-ethylhexyl)oxy)benzaldehyde, is used a reagent for the synthesis of porphyrin (2). The synthesis was carried out through a

one pot nitrobenzene method. For starters, in a round bottom flask 45 mmol of benzaldehyde (2) was mixed with the 15 mmol of 4-hydroxybenzaldehyde both dissolved in 210 mL (1.05 mol) of glacial acetic acid and 105 mL (1.02 mol) of nitrobenzene. 9.1mL (55.6 mmol) of pyrrole was added dropwise to the reaction mixture. The reaction was heated . Afterwards the completion of the reaction was determined by TLC and the mixture was cooled to room temperature and the organic solvents were removed under reduced precure. The resulting bulk of the reaction was purified by column chromatography with ethyl acetate:n-hexane in 1:3 (v:v) as eluent. As the reaction was carried out with different molar quantities of 2 different benzaldehydes different porphyrin will also be formed as product of this reaction. One of the main by-products was the porphyrin (4) produced from the condensation of four 4-((2-ethylhexil)oxy)benzaldehyde groups with pyrrole.

5-(4-hidroxyphenyl)-10,15,20-((4-(2-ethylexyl)oxy)phenyl)porphyrin (3)

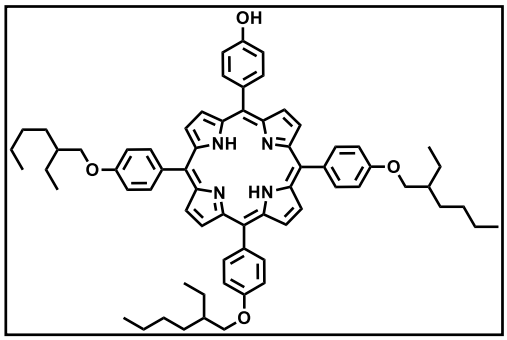

Yield: 6% (batch)

NMR ^{1}H (400 MHz, $CDCL_3$), δ ppm:

9.88 (s, 1H, OH); 8.84-8.87 (s, 8H, β-H); 8.09-8.12 (d, *J* = 8.6 Hz, 6H, m-phenyl); 8.06-8.08 (d, *J* = 8.5 Hz, 2H, m-phenyl); 7.27-7.29 (d, *J* = 8.5 Hz, 6H, o-phenyl); 7.20-7.23 (d, *J* = 8.7 Hz, 2H, o-phenyl); 4.14-4.15 (d, *J* = 5.8 Hz, 6H, -OCH_2); 1.90-1.95 (m, 3H, -CH); 1.42-1.73 (m, 24H,-CH2); 1.06-1.10 (t, *J* = 7.5 Hz, 9H,-CH_3); 0.98-1.01 (t, *J* = 7.0 Hz, 9H, -CH3); -2.74 (s, 2H, -NH).

MS (ESI-TOF): m/z: calculated for $C_{79}H_{95}N_4O_4$=1014.602, obtained 1014.549 $[M+H]^+$

5,10,15,20-tetrakis((4-(2-ethylexyl)oxy)phenyl)porphyrin (4)

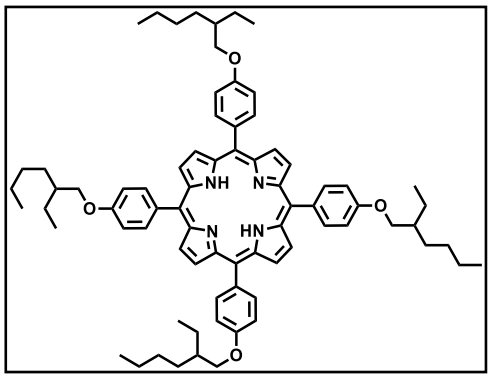

Yield: 8% (batch)

NMR ^{1}H (400 MHz, $CDCL_3$), δ ppm:

8.80 (s, 8H, β-H); 8.02-8.05 (d, *J* = 8.6 Hz, 8H, m-phenyl); 7.20-7.22 (d, *J* = 8.6 Hz, 8H, o-phenyl); 4.07-4.08 (d, *J* = 5.8 Hz, 8H, -OCH_2); 1.83-1.85 (m, 4H, -CH); 1.19-1.66 (m, 32H,-CH_2); 0.99-1.02 (t, *J* = 8.5 Hz, 12H, -CH_3); 0.89-0.93 (t, *J* = 8.5 Hz, 12H, -CH_3); -2.81 (s, 2H, -NH).

HRMS (ESI-TOF): m/z: calculated for $C_{79}H_{95}N_4O_4$=1126.720 obtained 1126.641 $[M+H]^+$

5.6. Palladium porphyrin synthesis

The synthesis of palladium porphyrins was made by two distinct methods.

5.6.1. Method A – (or the modified DMF Method):

In a round bottom flask the porphyrin and an excess of palladium salt were dissolved in DMF. Following this step, the mixture was heated to a temperature of about 120 °C. 2,6-lutidine was then added, dropwise, to the mixture and the reaction was carried out till completion or till no more free-base porphyrin was present. The state of the reaction was followed by TLC. After the completion of the metalation reaction the crude product would be washed with distilled water and from the organic phase the solvents would be extracted under reduced pressure. A silica gel chromatographic column with pure CH_2Cl_2 as eluent was used for the purifications 1Pd while an analogue column with a mixture of 1:1 CH_2Cl_2:n-hexane (v:v) was used in the case of 3Pd to remove any left-over byproduct and/or any unreacted starting materials, yielding the pure palladium porphyrin.

5.6.2. Method B – (or the acetonitrile Method):

In a round bottom flask the 1 equivalent of porphyrin and an excess of palladium acetate (4 or more molar equivalents depending on the porphyrin and its

substituents) would be dissolved in a (80:20; v:v) mixture of chloroform and acetonitrile. The flask was then refluxed at 70 to 80 °C and the reaction was followed till completion, or till no more free-base porphyrin would be detected by TLC. The crude mixture was then purified by chromatographic column with an adequate eluent yielding the palladium porphyrins.

Palladium (II) 5,10,15,20-tetraphenylporphyrinato (1Pd)

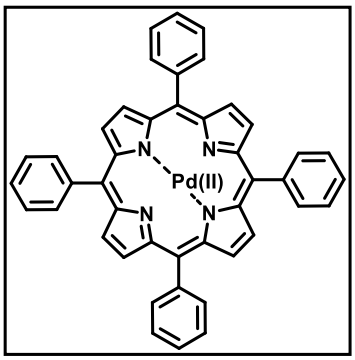

Yield: 97.8%

NMR ^{1}H (400 MHz, CDCL$_3$), δ ppm:

8.81 (s, 8H, β-pyrrole); 7.72-7.77 (m, 12H, m,p-phenyl), 8.16-8.18 (d, *J* =8.4 Hz, 8H, o-phenyl).

Palladium (II) 5-(4-hidroxyphenyl)-10,15,20-((4-(2-ethylexyl)oxy)phenyl)porphyrinato (3Pd)

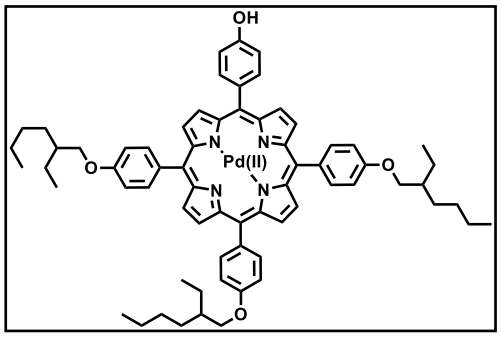

Yield: 88%

NMR ^{1}H (400 MHz, CDCL$_3$), δ ppm:

9.46 (s, 1H, OH); 8.82-8.85 (s, 8H, β-pyrrolic); 8.04-8.06 (m, 6H, m-phenyl); 8.01-8.03 (d, *J* =7.4 Hz 2H, m-phenyl); 7.24-7.27 (m, 6H, o-phenyl); 7.17-7.19 (d, *J* = 8.2 Hz 2H, o-phenyl); 4.11-4.13 (d, *J* = 5.4 Hz 6H, -OCH$_2$); 1.89-1.95 (m, 3H, -CH); 1.42-1.72 (m, 24H,-CH2); 1.05-1.09 (t, *J* = 7.4 Hz 9H, -CH$_3$); 0.98-1.02 (t, *J* =7.2 Hz 9H, -CH3);

5.7. Cellulose Acetate Polymer Blend films

The cellulose acetate (MW 30 000) used in the fabrication process of the films was purchased from Sigma-Aldrich. A solution for each film is prepared by dissolving the components (sensitizer/annihilator) in THF, then 10%wt/v of cellulose acetate (5

mL of solvent are used for 0.5 g of cellulose acetate) is added to the solution and the solution is kept under rigorous steering for 30 min. Afterwards the solution is heated for 3h at 60 to 70 °C till a desired viscosity of the solution is achieved, then the solution is transferred to an ice bath for 1 to 2 min to reduce the presence of air pockets/bubbles. Then the solution is casted into a glass plat with a predetermined thickness of 50 μm. The films are then left to dry for at least 12 to 24h to remove any residual solvent.[7–9]

5.8. References

(1) Williams, D. B. G.; Lawton, M. Drying of Organic Solvents: Quantitative Evaluation of the Efficiency of Several Desiccants. *J. Org. Chem.* **2010**, *75* (24), 8351–8354.

(2) O'Reilly, W. Numerical Data and Functional Relationships in Science and Technology. *Phys. Earth Planet. Inter.* **1987**, *45* (3), 304–305.

s, A. M. d'A. R.; Arnaut, L. G.; Formosinho, S. J. Photoacoustic Measurements of Porphyrin Triplet-State Quantum Yields and Singlet-Oxygen Efficiencies. *Chem. - Eur. J.* **1998**, *4* (11), 2299–2307.

(4) Pinto, S. M. A.; Vinagreiro, C. S.; Tomé, V. A.; Piccirillo, G.; Damas, L.; Pereira, M. M. Nitrobenzene Method: A Keystone in Meso-Substituted Halogenated Porphyrin Synthesis and Applications. *J. Porphyr. Phthalocyanines* **2019**, *23* (04n05), 329–346.

(5) Henriques, C. A.; Gonçalves, N. P. F.; Abreu, A. R.; Calvete, M. J. F.; Pereira, M. M. Unsymmetrical Porphyrins: The Role of Meso-Substituents on Their Physical Properties. *J. Porphyr. Phthalocyanines* **2012**, *16* (03), 290–296.

(6) A. W. Johnstone, R.; Luisa P. G. Nunes, M.; M. Pereira, M.; M. d'A. Rocha Gonsalves, A.; C. Serra, A. Improved Syntheses of 5,10,15,20-Tetrakisaryl- and Tetrakisalkylporphyrins. *HETEROCYCLES* **1996**, *43* (7), 1423.

(7) Vatanpour, V.; Pasaoglu, M. E.; Barzegar, H.; Teber, O. O.; Kaya, R.; Bastug, M.; Khataee, A.; Koyuncu, I. Cellulose Acetate in Fabrication of Polymeric Membranes: A Review. *Chemosphere* **2022**, *295*, 133914.

(8) Monguzzi, A.; Tubino, R.; Meinardi, F. Multicomponent Polymeric Film for Red to Green Low Power Sensitized Up-Conversion. *J. Phys. Chem. A* **2009**, *113* (7), 1171–1174.

(9) Kim, J.-H.; Deng, F.; Castellano, F. N.; Kim, J.-H. High Efficiency Low-Power Upconverting Soft Materials. *Chem. Mater.* **2012**, *24* (12), 2250–2252.

6. Annex

6.1. Molar absorptivity calculation

In this work the UV-Absorption spectra were collected with the previously refereed apparatus (chapter 5.2.2). Porphyrin solutions in 2-MeTHF with concentrations from 10^{-5} M to 10^{-7} M are prepared through the dilution of a stock solution of higher concentration to calculate the molar absorption coefficients. Then, using the law of Beer-Lambert mentioned in chapter 3, the absorption for the maximum of the band under study is accessed and then is graphically represented as a function of the concentration of the various solutions. A linear fit is applied to the obtained values yields resulting in a straight line whose slope value corresponds to the value of the molar absorption coefficient, ε. Figure 6.1 shows the data obtained from the values of maxima absorption of the Q(1,0) band of **1Pd** and its change with concentration.

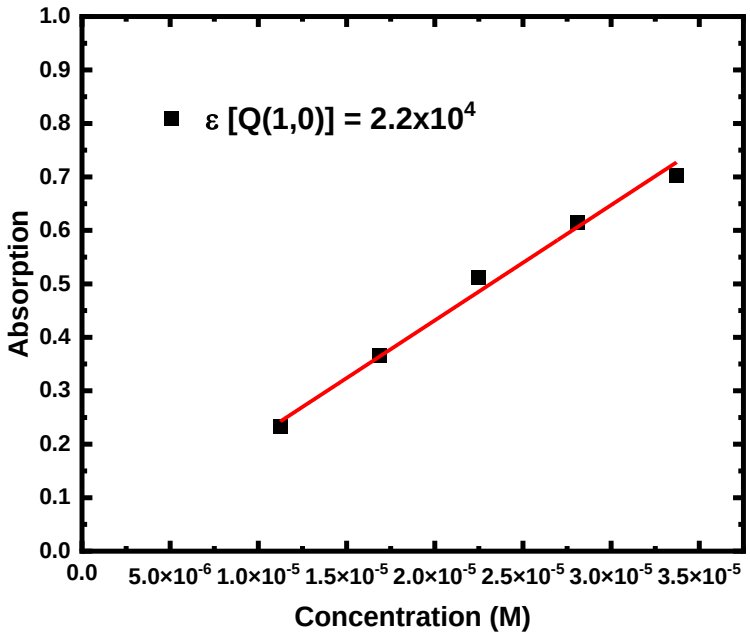

Figure 6.1 – Change in the Q(1,0) bands absorption with concentration, in 2-MeTHF solution of **1Pd**.

6.2. Purity evaluation of the palladium porphyrins/determination of the best metalation method

To determine the effectiveness of each of the metalation methods the **1Pd** (or Pd(II)TPP) were prepared by each method. Both reactions were followed by TLC, UV-Vis, and the ^{1}H-NMR and both reactions seemed to yield pure **1Pd**. After closer examination of the luminescent emission spectrum of the compounds synthesized by the DMF modified method under atmospheric air four bands (two emission pairs with two bands each) were displayed in the spectra, as seen in Figure 6.2. The stronger emission appeared at higher wavelengths with peak maximum at 650 and 717 nm and the lower intensity emission at lower wavelengths with peak maximum at 560 and 608 nm. Luminescent emission of palladium porphyrins is expected to have two band originated from the emission of each Q-band which meant that one of these emission didn´t correspond to the metalated porphyrin. We proceeded with the determination of the excitation spectra of the sample, and by comparing them to the absorption spectrum of **1Pd** we could determine if the compound had promoted this emission or if there were impurities in the sample. The measurements of the same sample were made collecting the emission at 608nm and 650nm, as seen in Figure 6.3 and 6.4 respectively. The first spectrum taken at 608nm has the same spectral profile as the absorption spectrum of **1Pd** with a single Soret band and one Q-band of high intensity. We note that the absorption and excitation spectra are equal so this emission must be related to the **1Pd** species. The second spectrum taken at 650nm has a shape characteristic of a free-base porphyrin. The Soret band has a small shoulder at the left side of the band that may correspond to the metalated porphyrin, also four Q-bands are seen, with the last one being overlapped with the wavelength of emission. In the current case, the sample under study was synthesized using the DMF modified method and was contaminated with the free-base porphyrin which would pose a serious problem in the construction of the TTA-UC. On the other hand, the emissions seen in the Figure 3.4 in Chapter 3, correspond to the emissions of a pure sample of 1Pd and 3Pd obtained with the acetonitrile metalation method.

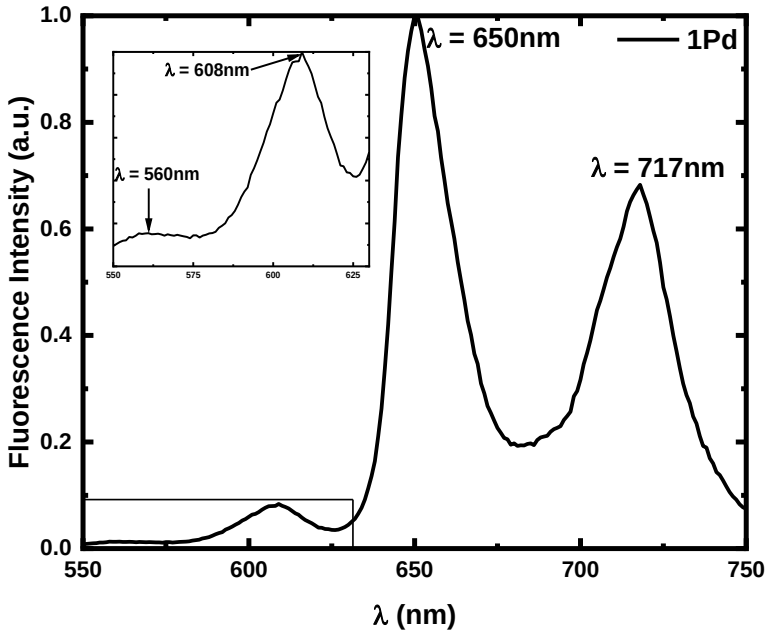

Figure 6.2 – Luminescent emission spectrum of 1Pd, synthesized using the DMF modified method, in 2-Me-THF at RT (A lower intensity first emission is shown in the inset)

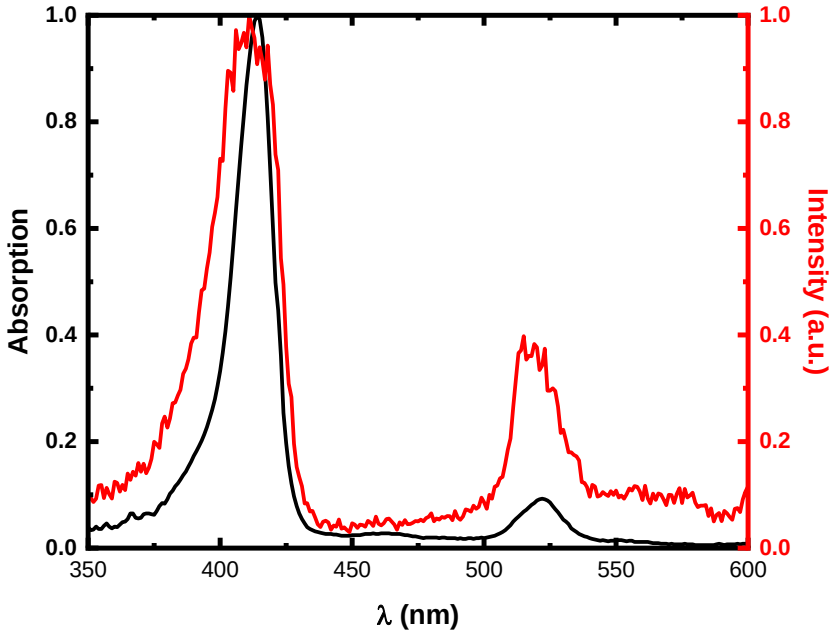

Figure 6.3 – Room temperature absorption (Black) and fluorescence excitation spectra (red) for the 1Pd synthesized using the DMF modified method, in 2-MeTHF solution collected at 608 nm.

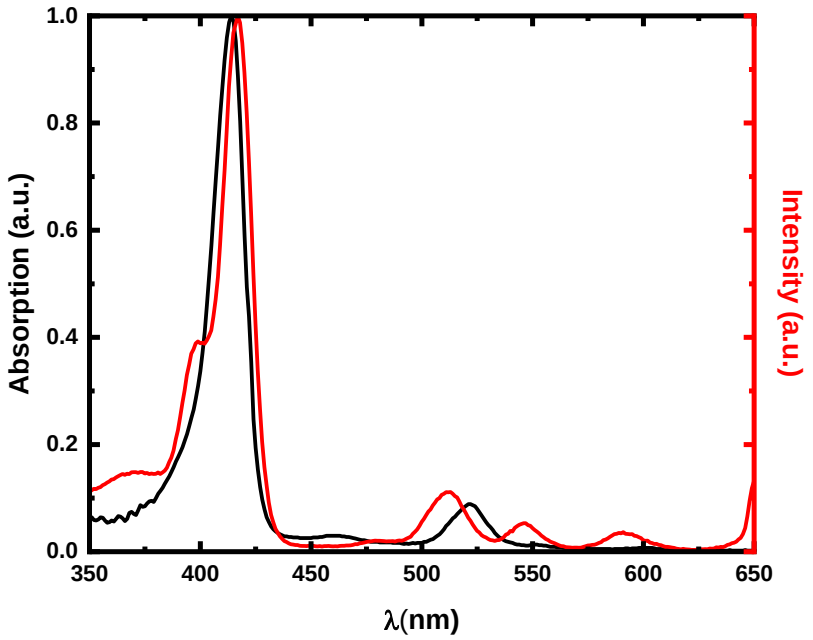

Figure 6.4 – Room temperature absorption (Black) and fluorescence excitation spectra (red) for the 1Pd synthesized using the DMF modified method, in 2-MeTHF solution collected at 650 nm.